

Review

Recent Advances in Electrolyte Engineering for Silicon Anodes

Chenduan Xie ^{1,†}, Tianyang Hong ^{1,†}, Xiaoqin Yi ^{1,†}, Di Liu ¹, Xianting Zhao ^{1,2}, Yunlin Zhu ¹

and Xianhui Zhang ^{1,*} 

¹ Fujian Key Laboratory of Flexible Electronics and Strait Laboratory of Flexible Electronics (SLoFE), Strait Institute of Flexible Electronics (SIFE, Future Technologies), Fujian Normal University, Fuzhou 350117, China; qsx20231441@student.fjnu.edu.cn (C.X.); qsx20231470@student.fjnu.edu.cn (T.H.); qsx20241506@student.fjnu.edu.cn (X.Y.); qbx20240216@yjs.fjnu.edu.cn (D.L.); qsz20231485@student.fjnu.edu.cn (X.Z.); qsz20251502@student.fjnu.edu.cn (Y.Z.)

² College of Chemistry and Materials Science, Fujian Normal University, Fuzhou 350117, China

* Correspondence: ifexhzhang@fjnu.edu.cn; Tel.: +86-183-5013-2818

† These authors contributed equally to this work.

Abstract

Silicon (Si) anodes offer ultrahigh theoretical capacity ($\sim 4200 \text{ mAh g}^{-1}$) for next-generation lithium-ion batteries but suffer from severe mechanical degradation due to repetitive volume expansion ($>300\%$). Conventional electrode-centric strategies face scalability limitations, shifting focus to electrolyte engineering as a critical solution. This review synthesizes recent advances in liquid electrolyte design for stabilizing Si anodes, emphasizing three key pillars: (i) Lithium salts that enable anion-derived inorganic-rich solid electrolyte interphase (SEI) layers with high fracture toughness; (ii) Solvent systems including carbonates, ethers, and phosphonates, where fluorination and steric hindrance tailor SEI elasticity; (iii) Functional additives (F/B/Si-containing) that form mechanically compliant interphases and scavenge detrimental species. Innovative architectures—high-concentration electrolytes (HCEs), localized HCEs (LHCEs), and weakly solvating electrolytes—are critically assessed for their ability to decouple ion transport from volume strain. The perspective highlights the imperative of hybrid solid–liquid interfaces to enable commercially viable Si anodes.



Academic Editor: Diana Golodnitsky

Received: 19 August 2025

Revised: 17 October 2025

Accepted: 27 October 2025

Published: 29 October 2025

Citation: Xie, C.; Hong, T.; Yi, X.; Liu, D.; Zhao, X.; Zhu, Y.; Zhang, X. Recent Advances in Electrolyte Engineering for Silicon Anodes. *Batteries* **2025**, *11*, 399. <https://doi.org/10.3390/batteries11110399>

Copyright: © 2025 by the authors. Licensee MDPI, Basel, Switzerland. This article is an open access article distributed under the terms and conditions of the Creative Commons Attribution (CC BY) license (<https://creativecommons.org/licenses/by/4.0/>).

1. Introduction

The rapid development of portable electronic devices and electric vehicles (EVs) has intensified demand for high-performance energy storage systems. Lithium-ion batteries (LIBs) have dominated this landscape due to the high energy density, wide operational voltage, long cycle life, and absence of memory effect [1,2]. Graphite (Gr), the prevailing commercial anode, delivers a specific capacity near its theoretical maximum (372 mAh g^{-1}) [3,4]. However, its inherent capacity limitations impede further energy density gains, driving the search for alternative anode materials with higher theoretical specific capacity, enhanced cycling stability, improved safety, and scalable manufacturability.

Silicon (Si) emerges as a leading candidate for next-generation LIB anodes, offering compelling advantages: natural abundance, a moderate lithiation potential ($\sim 0.4 \text{ V vs. Li/Li}^+$) that minimizes the risk of lithium (Li) plating, and an exceptional theoretical specific capacity up to 4200 mAh g^{-1} [5–7]. Despite these merits, the substantial volume fluctuations ($>300\%$) of Si during repeated (de)lithiation cycles induce critical mechanical degradation: (i) mechanical pulverization: anisotropic stress evolution (theoretical stress:

1–2 GPa) induces crack propagation through Si particles, culminating in material fragmentation and loss of active mass; (ii) unstable solid electrolyte interphase (SEI): repeated fracture/reformation generates thickened SEI layers, consuming active Li^+ and electrolyte and increasing interfacial resistance; (iii) electronic contact loss: particle disconnection disrupts percolation networks, elevating electrode polarization. These intertwined failure modes ultimately manifest as severely compromised initial Coulombic efficiency (CE) (<70–80%), rapid capacity fading (from ~3000 mAh g⁻¹ to ~1000 mAh g⁻¹ after 10 cycles), and shortened cycle life (<50–100 cycles) [8–13].

To overcome the intrinsic limitations encountered by Si anodes, multifaceted strategies have been pursued, including morphological designs [14], nanoscale architectures (zero- to three-dimension) [15,16], Gr/metal composites [17], self-healing binders [18], pre-lithiation techniques [19], and surface coating technologies [20]. While these approaches demonstrate partial success, each method has its inherent limitations. For instance, nano structuring and pre-lithiation achieve enhanced cyclability, but incur prohibitive costs and intricate manufacturing, impeding commercial viability [21]; surface coatings effectively control the volume fluctuations and passivate the Si surface, while excessive coatings compromise ionic/electronic conductivity, elevating internal resistance and degrading rate capability [22]; and binder optimization further necessitates balancing adhesion resilience, volume change accommodation, cost efficiency, and process scalability [23,24].

Given these persistent limitations of electrode-centric approaches, electrolyte engineering has emerged as a critical frontier for stabilizing Si anodes. As the medium governing interfacial reactions, electrolytes fundamentally dictate the composition, structure, and mechanical properties of the resulting SEI layer. Crucially, designing electrolytes that form mechanically compliant SEI layers capable of accommodating the huge volume expansion of Si anodes represents a transformative strategy to enhance cycling stability. Recent breakthroughs have demonstrated this potential through elevating salt concentration, exploring novel solvents and additives, regulating solvation structures, and developing advanced electrolyte systems [25–28]. These paradigms enable elastic SEI formation via anion-derived inorganic-rich components, dynamic self-adaptation to Si pulverization, and suppressed electrolyte decomposition through solvation sheath control, consequently demonstrating noticeable effects on improving the electrochemical stability of Si-based batteries.

While these electrolyte innovations demonstrate transformative potential, critical knowledge gaps persist in correlating electrolyte design principles with Si anode stabilization mechanisms. This review critically addresses how electrolyte engineering—rather than electrode-centric approaches—can resolve this by designing strain-tolerant SEI architectures. We synthesize recent progress in liquid electrolyte engineering for Si-based anodes, which emphasizes the comparative analysis of electrolyte components (Li salts, solvents, and functional additives) and novel electrolyte systems (high Li salt concentration systems, locally Li salt-enriched systems, and weakly solvating systems) in dictating SEI evolution under volume strain (Figure 1). With the understanding of the roles of electrolyte optimization in improving the electrochemical stability of Si-based batteries, we discuss the design criteria balancing ionic conductivity, SEI elasticity, and scalability. Finally, we present our perspective on the future strategies that are suitable for realizing Si anode commercialization to meet the requirements for EV power sources in view of process and cost.

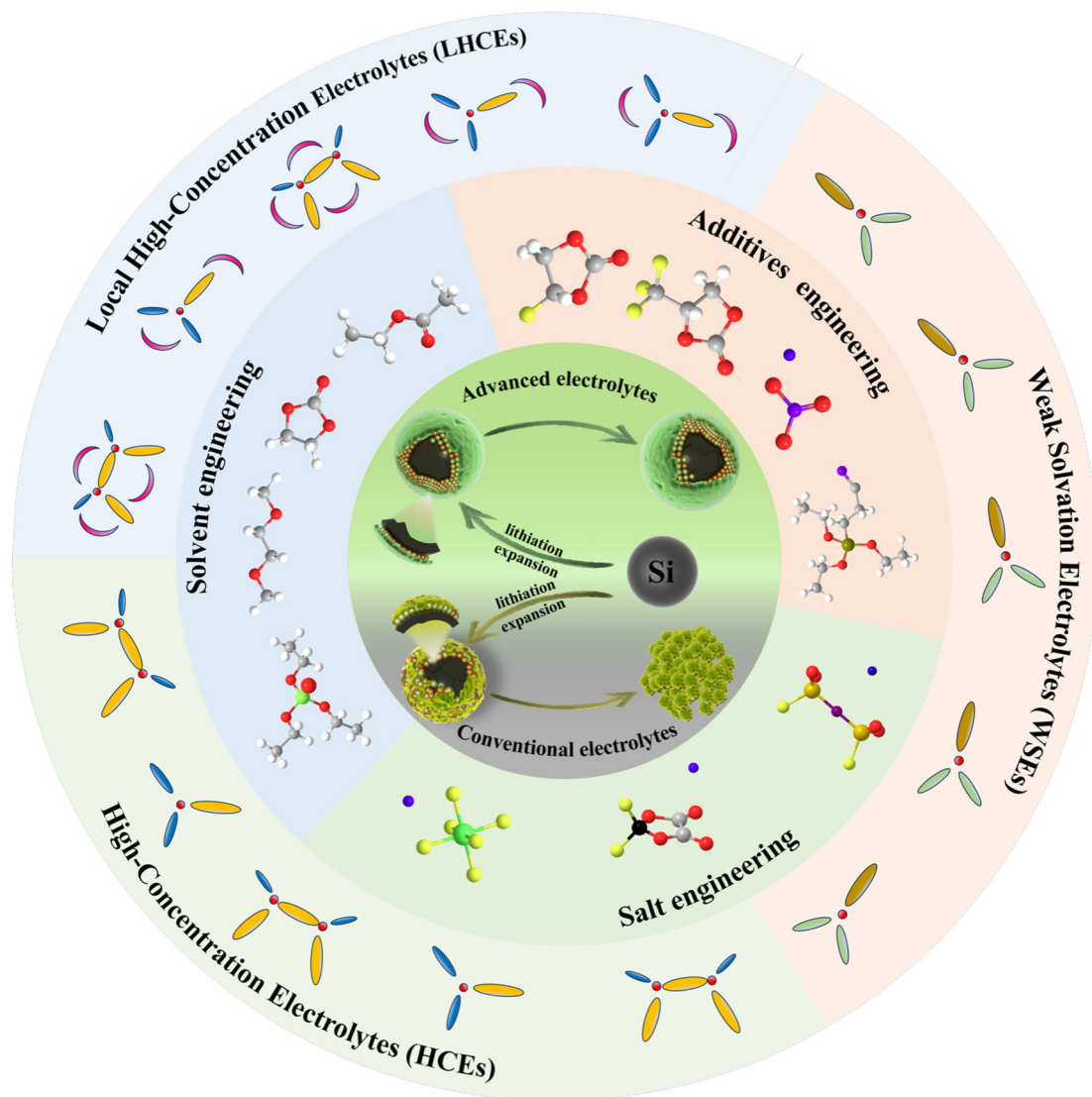


Figure 1. Overview of electrolyte engineering strategies for enhancing the interface stability of Si anodes.

2. Electrolyte Design Strategies

While sharing the core components of conventional electrolytes—Li salts, solvents, and additives—Si-based electrolytes demand fundamentally redesigned formulations. The extreme volume variation and highly active interface necessitate targeted strategies to simultaneously: (i) adapt to volume deformation, (ii) suppress continuous electrolyte decomposition and SEI reformation, (iii) maintain efficient ion transport despite interfacial evolution, and (iv) be compatible with high-voltage cathodes (>4.3 V) [29].

2.1. Li Salts

Li salts primarily perform dual critical functions in LIBs: facilitating Li^+ ion conduction while dictating the chemical composition and mechanical properties of SEI [30]. Commonly employed Li salts in Si-based batteries include lithium hexafluorophosphate (LiPF_6) [31], lithium bis(trifluoromethanesulfonyl)imide (LiTFSI) [32], lithium bis(fluorosulfonyl)imide (LiFSI) [33], lithium bis(oxalato)borate (LiBOB) [34], 4,5-dicyano-2(trifluoromethyl)imidazolium lithium (LiTDI) [35], lithium borohydride (LiBH_4) [36], and lithium perchlorate (LiClO_4) [37].

Among commercial options, LiPF₆ dominates due to its favorable solubility (>1.5 M) and high ionic conductivity (10–12 mS cm⁻¹, measured for 1 M LiPF₆ in ethylene carbonate (EC)/dimethyl carbonate (DMC), 1:1, vol.%) [38,39]. This suppresses the formation of organic by-products and enhances mechanical stability, which are leveraged in recent advances to improve the cycling stability of Si-based batteries. Li et al. strategically employed LiPF₆ as the pivotal Li salt to construct a novel asymmetric electrolyte system, designated as NMEP51. This formulation consists of a custom-synthesized ionic liquid, N-methyl-N-(2-methoxyethoxy)methyl pyrrolidinium hexafluorophosphate (NMEP), and LiPF₆ salt in a precise 5:1 molar ratio. Within this structure, PF₆⁻ anions are strategically positioned within the Li⁺ solvation sheath, enabling their preferential reduction at approximately 0.62 V (vs. Li/Li⁺) during cycling to form a dense LiF-rich SEI layer. Therefore, Li || Si microparticles (μ Si) half cells achieve a high capacity of ~2900 mAh g⁻¹ at C/8 (447 mA g⁻¹) with a high capacity retention of >87% after 400 cycles. Furthermore, under lean electrolyte conditions, NMEP51-based μ Si || LiNi_{0.8}Co_{0.1}Mn_{0.1}O₂ (NCM811) pouch cells (E/C ratio of ~3 g Ah⁻¹ and N/P ratio of ~1.4) achieve a capacity retention of over 72% after 200 cycles [38]. In conclusion, LiPF₆ has become the most widely used Li salt in current electrolyte systems due to its relatively low cost and excellent SEI film-forming ability. Despite its market dominance owing to cost-effectiveness and versatility in SEI engineering, LiPF₆ suffers from intrinsic chemical instability. Studies have shown that even in nearly water-free environments, PF₅ from LiPF₆ decomposition readily reacts with lithium carbonate (Li₂CO₃) on the SEI to produce phosphorus oxyfluoride (POF₃) (Figure 2a). Subsequently, POF₃ further reacts with Li₂CO₃, carbonic acid (H₂CO₃) and lithium bicarbonate (LiHCO₃) to form harmful difluorophosphoric acid (PF₂OOH) and carbon dioxide (CO₂) (Figure 2b) [39]. And it suffers from thermal degradation above 60 °C, leading to poor cycling stability under high temperature [40]. This process may further accelerate the decomposition of the SEI layer and lead to battery capacity degradation. Therefore, future electrolytes can be designed with specific additives to form a SEI richer in organics and poorer in Li₂CO₃, thereby blocking PF₅ access and mitigating LiPF₆ decomposition. Furthermore, in full-cell configurations, the HF generated by LiPF₆ hydrolysis can corrode the transition metal-based cathode (e.g., NCM), leading to metal ion dissolution. These dissolved ions (e.g., Mn²⁺) can migrate to the Si anode and incorporate into the SEI, exacerbating its instability and accelerating capacity fade—a phenomenon known as harmful crosstalk.

LiTFSI and LiFSI have emerged as the most promising alternatives to LiPF₆, offering superior moisture tolerance (<100 ppm H₂O), high solubility (>5 M in carbonate/ether solvents), and exceptional thermal stability (>200 °C decomposition temperature) [41,42]. Cora et al. reported that LiTFSI enables stage-dependent interfacial optimization: during pre-lithiation, they form ultrathin and homogeneous SEI layers through preferential anion adsorption; while in the post-lithiation stage, it generates fluorine (F)/sulfur (S)-rich interfaces via TFSI⁻ decomposition, producing LiF and Li_xS_yO_z compounds that reduce interfacial resistance [32]. This optimized interface structure enables the capacity retention of LiTFSI-based electrolytes to increase by 2.8 times versus LiPF₆ (1627.8 mAh g⁻¹ vs. 583 mAh g⁻¹ after 400 cycles at 0.5 C, Figure 2c) and enhanced SEI elasticity accommodating Si volume strain [30]. While LiFSI and LiTFSI share similar functionalities, LiFSI enables spontaneous formation of a highly stable LiF-rich SEI layer on Si anodes through preferential reduction of FSI⁻ anions (without requiring sulfur-containing additives), thereby significantly reducing interfacial impedance. Critically, LiFSI suppresses detrimental silicon dioxide (SiO₂) fluorination (preventing SiO_xF_y formation) while promoting lithium orthosilicate (Li₄SiO₄) generation that maintains binder-particle cohesion (Figure 2d,e) [33]. The reduced F content in imide salt (<12 wt.% vs. 19 wt.% in LiPF₆) concurrently mitigates

HF-induced safety hazards, establishing a foundation for designing F-minimized Li salts (<5 wt.% F) to enhance cycling stability and safety. In addition, these imide salts have a pivotal advantage in their unique solvation behavior under high concentrations (>3 M). Under such conditions, the solvation structures transition from solvent-dominated to anion-prioritized coordination, characterized by the prevalence of contact ion pairs (CIPs) and aggregates (AGGs) exceeding 80% population. This structural shift redirects decomposition pathways toward anions ($\text{FSI}^-/\text{TFSI}^-$), promoting the formation of inorganic-rich SEI layers comprising LiF , $\text{Li}_x\text{S}_y\text{O}_z$, and $\text{Li}_x\text{N}_y\text{O}_z$. The abundance of these inorganic components endows the SEI with greater mechanical strength than the traditional organic-dominated interface [43,44]. Nevertheless, $\text{LiFSI}/\text{LiTFSI}$ -based electrolytes suffer from severe aluminum (Al) current collector corrosion at potential exceeding 4.0 V vs. Li/Li^+ , constraining their practical deployment in full-cell configurations.

Beyond conventional Li salts, emerging alternatives demonstrate specialized functionalities in Si-based systems. LiBOB forms compact boron (B)-containing polymeric SEI layers with exceptionally high-voltage stability (>4.5 V). Choi et al. added 0.7 M LiBOB into EC/diethyl carbonate (DEC) (3/7, v/v) [34]. The interface layers composed of BOB^- reduction products effectively limit the formation of electrochemically inactive Si phases, markedly improving the discharge capacity retention of a Si thin-film electrode/Li half-cell during cycling. However, the practical application of LiBOB is constrained by low solubility in carbonate solvents (<0.8 M) and relatively high interfacial resistance, limiting deployment to <5 wt.% additive formulations. Notably, LiTDI synergizes with FEC and VC to suppress Si-electrolyte parasitic reactions while enabling progressive SiO_x passivation layer growth that maintains particle integrity. These findings establish its viability as a salt for Si-based systems under these specific conditions [35]. Building on the pursuit of high-solubility and functional salts, LiBH_4 , despite its generally poor solubility in most solvents, has been reported to form a homogeneous 2 M solution in tetrahydrofuran (THF) [45]. Additionally, Li et al. developed a novel fluorine-free 2 M $\text{LiBH}_4/\text{THF}/2\text{-methyltetrahydrofuran}$ (2Me-THF) (1:1, v/v) electrolyte (denoted as LBH) for Si-based anodes [36]. This electrolyte can chemically pre-lithiate the native oxide layer by the reductive LiBH_4 and relieve SEI formation and accumulation to preserve the internal conductive network (Figure 2f). The significance of this F-free electrolyte brings unprecedented F-free interphase that also achieves the high-performance μSi electrode (80 wt.% μSi), including high specific capacity of 2900 mAh g^{-1} , high initial CE of 94.7% and excellent cyclability capacity retention of 84.7% after 400 cycles at 0.2 C. More importantly, the μSi anodes cycled in LiBH_4 -based electrolyte display a high capacity of 2100 mAh g^{-1} even at 3 C (1 C = 4200 mA g^{-1}), retaining 72.4% of the capacity achieved at 0.2 C (Figure 2g). It should be noted, however, that the high moisture sensitivity and handling challenges associated with LiBH_4 pose significant hurdles for its practical industrial application. Furthermore, LiClO_4 can form SEI layers containing highly conductive lithium chloride (LiCl) components. It has been reported that the ionic conductivity of a LiCl-rich interface, measured via electrochemical impedance spectroscopy (EIS) on thin film model electrodes, can be as high as $\sim 10^{-4} \text{ S cm}^{-1}$, significantly greater than that of a typical LiF-rich interface ($\sim 10^{-8} \text{ S cm}^{-1}$) [46]. This enhanced ionic transport underlies the improved rate capability observed in LiClO_4 -based systems [37]. It is important to note, however, that the strong oxidative nature of LiClO_4 raises serious safety concerns in organic electrolytes, which has substantially limited its practical adoption [47].

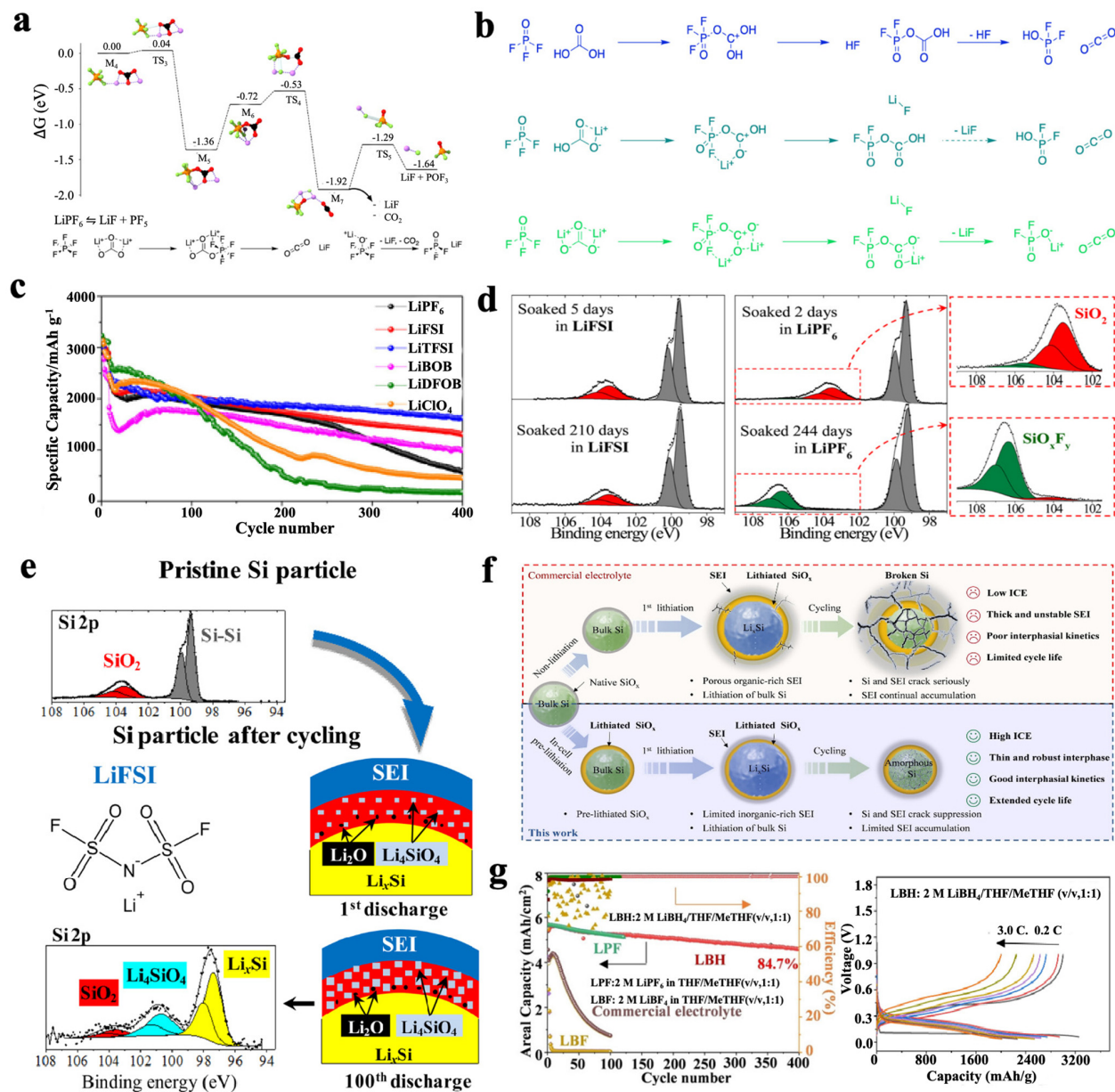


Figure 2. Mechanism of action diagram for Li salts. (a,b) Decomposition pathway of LiPF_6 under nearly anhydrous conditions [39]. Copyright 2023, American Chemical Society. (c) Cycling capabilities of Si anodes with six mono-salt electrolytes [30]. Copyright 2022, Elsevier. (d) Si 2p spectra of the Si electrode after contacting with an electrolyte containing either LiFSI or LiPF_6 salt in EC/DEC (2:1, v/v) [33]. (e) Schematic of SEI formation mechanisms on Si nanoparticle surface upon cycling in $\text{Si} \parallel \text{Li}$ cell with 1 M LiFSI in EC/DEC (2:1, v/v) [33]. Copyright 2013, American Chemical Society. (f) Schematic illustration of the interphase evolution during the cycling of Si anodes in different electrolytes [36]. (g) Electrochemical performance of μSi anodes in LBH (LiBH₄-THF/MeTHF), LBF (LiBF₄-THF/MeTHF) electrolytes [36]. Copyright 2023, Wiley.

In conclusion, while LiPF_6 remains the predominant commercial salt, its inherent thermal and hydrolytic instability has spurred the search for alternatives tailored to Si-based batteries. Salts like LiTFSI and LiFSI offer enhanced chemical and electrochemical stability but introduce new challenges, notably aluminum current collector corrosion at high voltages. Others, including LiBOB , LiBH_4 , and LiClO_4 , exhibit distinct functional advantages such as SEI reinforcement or high ionic conductivity, yet often suffer from limited solubility narrow electrochemical windows, or processing incompatibilities. Future

progress will therefore depend on the strategic development of novel functional salts and synergistic multi-salt electrolytes that balance interfacial stability, conductivity, and manufacturability. Such developments are essential to fully realize the potential of high-capacity Si anodes in next-generation LIBs.

2.2. Solvents

As the core components of LIBs, electrolyte solvents mainly perform two critical functions: dissolving Li salts and facilitating rapid Li^+ transport. In Si-based batteries, solvent selection becomes particularly decisive due to the extreme volume changes of Si compared to conventional Gr anodes (>300% for Si vs. <10% for Gr). These dynamic morphological transformations critically impact interfacial stability, cycle life, rate capability, low-temperature performance, and safety [48,49]. Consequently, solvent design must address more stringent requirements than traditional Gr anode systems, including enhanced SEI elasticity and sustained ion mobility during repeated expansion/contraction cycles.

2.2.1. Carbonate Solvents

During the nascent development of Si-compatible electrolytes, carbonate solvents—namely EC, DMC, and methyl ethyl carbonate (EMC)—are extensively adopted owing to their proven efficacy in Gr systems. These solvents deliver high dielectric constants ($\epsilon > 40$), appropriate viscosity (0.65–2.5 cP), and robust chemical stability, enabling efficient Li^+ solvation and transport. However, compared to the relatively moderate volume expansion of Gr anodes ($\leq 10\%$), Si anodes undergo drastic expansion (300–400%) during charge/discharge cycling. This extreme mechanical strain catastrophically fractures the carbonate-derived SEI, triggering perpetual reformation cycles that deplete active Li and accelerate capacity fade [50].

Conventional carbonate-based electrolytes typically blend high-dielectric cyclic carbonates (e.g., EC, $\epsilon > 89$) and low-viscosity linear carbonates (e.g., EMC, DMC, $\eta \approx 0.65$ cP) to satisfy fundamental ionic transport requirements [51]. While such a formulation (e.g., 1 M LiPF_6 in EC/DMC/EMC, 1:1:1, vol. %) leads to rapid capacity decay in $\text{Li} \parallel \text{Si}$ cells, a representative study reported the capacity plunging from 1545 mAh g^{-1} to 177 mAh g^{-1} within merely 15 cycles [52]. The failure originates from the mechanically inferior SEI layer derived from the reductive decomposition of these carbonate solvents, which primarily consists of lithium alkyl carbonates (ROCO_2Li) and linear poly(ethylene oxide) (PEO)-type oligomers with low elastic modulus (<0.5 GPa) and limited ductility (<5% strain tolerance) [53]. These properties render the SEI incapable of accommodating the substantial volume changes of Si during cycling, triggering mechanical fracture and perpetual reformation. To address these limitations, advanced solvent systems have been engineered. Jin et al. reported that pure FEC or VC electrolytes containing 1 M LiPF_6 can form polymeric SEIs dominated by highly cross-linked PEO and aliphatic chain functionalities on binder-free silicon nanowire (SiNWs)—a model system used to isolate the intrinsic electrolyte-Si interactions [54]. As illustrated in Figure 3a, vinoxy radicals generated from FEC or VC reduction reactions can react with sp^2 -hybridized carbons, forming branched species containing acetal carbons, aldehyde, and alkene terminations. ^{13}C - ^{13}C homonuclear correlation NMR reveals that the acetal carbons connect to PEO-type carbons, creating cross-linking units distinct from the linear PEO-type polymers formed in EC-based electrolytes. The resulting PEO/poly(VC) architectures effectively enhance Li^+ ions conductivity, suppress solvent penetration, and accommodate Si expansion/contraction during cycling, thereby boosting capacity retention to >80% after 100 cycles in this well-defined SiNWs system. However, continuous formation of organosiloxanes and CEs below 99.5% are still observed in pure FEC and VC electrolytes, as the cross-linked polymers are insufficient to form a perfect

protective film on SiNWs surfaces. Critically, it should also be noted that the performance observed in this idealized model may not directly translate to practical electrodes like μ Si or SiO_x , where binders, particle morphologies, and lower conductivity significantly influence SEI formation and cycling stability. Fluorination modification represents another effective approach to enhance the compatibility of carbonate-based solvents with Si-based anodes. Liu et al. developed 2,2,2-trifluoroethyl methyl carbonate (FEMC) by selectively fluorinating conventional solvent EMC, and rationally formulated a LHCE consisting of 2 M LiFSI in FEMC/1H,1H,5H-octafluoroamyl-1,1,2,2-tetrafluoroether (OTE) (FEMC:OTE = 1:1, vol.%) [55]. Compared to EMC, FEMC enables a high-modulus F-rich inorganic inner SEI layer that is beneficial to accommodate μ Si pulverization, and a dense yet pliable F-rich organic outer SEI layer buffering mechanical stress and inhibiting parasitic reactions. This synergistic effect, stemming from the combination of the fluorinated solvent and the LHCE structure, yields a highly robust F-rich inorganic–organic bilayer SEI with 62% capacity retention after 150 cycles at 0.2 C (Figure 3b), significantly outperforming EMC-based electrolytes. Scanning electron microscope (SEM) further validates reduced electrode swelling (22.6 μm thickness) and crack-free morphology in FEMC-cycled μ Si anodes. Collectively, these strategies validate two solvent design paradigms: crosslinked organic matrices for strain accommodation and fluorination-induced inorganic reinforcement for mechanical robustness.

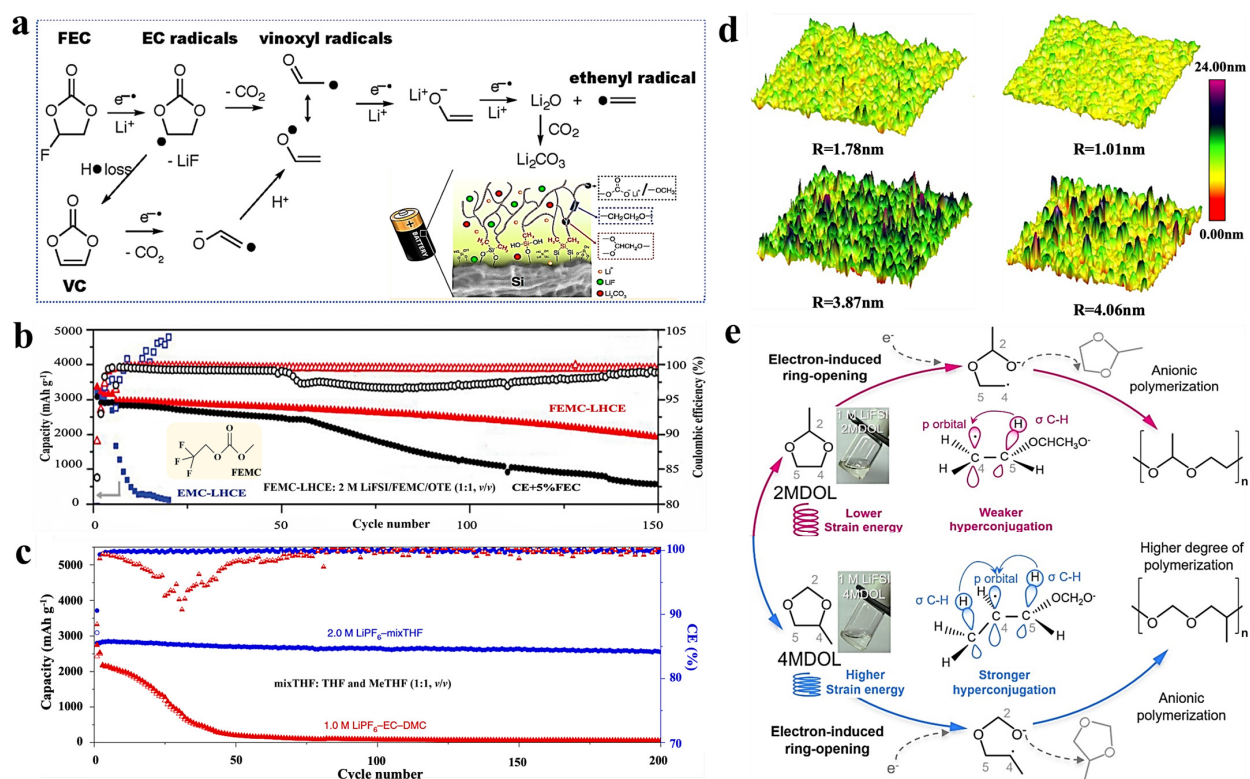


Figure 3. Key properties of carbonate and ether solvents. (a) Decomposition mechanisms of FEC and VC solvents [54]. Copyright 2018, American Chemical Society. (b) Cycling performances of Li⁺||μSi cells in FEMC- and EMC-based electrolytes, respectively [55]. Copyright 2023, Wiley. (c) Cycling stability and CEs of μSi anodes at C/5 rate cycled in 2.0 M LiPF₆-mixTHF and 1.0 M LiPF₆-EC-DMC electrolytes [31]. Copyright 2020, Springer Nature. (d) Typical electrochemical AFM surface roughness (R) comparison of Si anodes cycling in 2.0 M LiPF₆-mixTHF (above) and 1.0 M LiPF₆-EC-DMC (below) at the lithiated (left) and delithiated (right) states, area 2 × 2 μm [31]. Copyright 2020, Springer Nature. (e) Ring-opening polymerization mechanism of methylated dioxolane [56]. Copyright 2024, Wiley.

2.2.2. Ether Solvents

Compared to carbonate solvents, ether-based solvents exhibit unique interfacial stabilization advantages for Si anodes. First, ether solvents possess low reduction potentials (generally < 1.0 V vs. Li/Li⁺), suppressing continuous electrolyte decomposition and minimizing the accumulation of unstable decomposition products [57]. Second, their decomposition yields elastic polyether-rich SEI layers that efficiently buffer the substantial volume strain (300–400%) through reversible polymer chain unfolding. These benefits manifest via tailored solvation engineering. Chen et al. rationally designed a 2 M LiPF₆-based electrolyte with a mixture of THF and 2Me-THF (1:1, v/v) [31]. This THF/2Me-THF (mixTHF) composite solvents system promotes tailored solvation structures dominated by CIPs and AGGs, generating a gradient SEI with a 0.37 nm inner layer with high-modulus LiF for mechanical support and a 0.37 nm outer layer with elastic organic polymer for stress redistribution. Such a LiF-organic bilayer SEI accommodates elastic/plastic deformation of μSi, enabling a high capacity of 2800 mAh g⁻¹ after 200 cycles with an initial CE of 91% and a cycling CE of >99.9% in Li || μSi cells (Figure 3c). Furthermore, the μSi || lithium iron phosphate (LiFePO₄) full cell retained 80% capacity after 100 cycles, whereas only 6.2% and 4.5% capacities remained in the traditional electrolytes with and without FEC additive, respectively. In situ electrochemical atomic force microscopy (AFM) further validates the effectiveness of the SEI. It is shown that the roughness changes from ~1.78 nm (lithiated) to ~1.01 nm (delithiated) in the mixTHF electrolyte, much smaller than the values from the traditional carbonate-based electrolyte, 3.87 and 4.06 nm (Figure 3d). The minimal roughness hysteresis and near-complete reversibility confirm that the bilayer SEI suppresses irregular volume expansion and maintains particle cohesion—unachievable with conventional mixed organic-inorganic SEIs. Similarly, as illustrated in Figure 3e, the ring-opening intermediate formed by 4-methyl-1,3-dioxolane (4MDOL) has a stronger hyperconjugation effect due to the CH₃ group attached at position 4, combined with its larger ring strain, results in a greater propensity for ring-opening and subsequent polymerization at the electrode-electrolyte interface. The designed electrolyte LiFSI/4MDOL/1,1,2,2-tetrafluoroethyl-2,2,3,3-tetrafluoropropyl ether (TTE) (1:2.6:3 by mol) achieves remarkable stability, with 85.4% capacity retention after 400 cycles at 0.5 C without additional additives in Li || Si/graphite (Gr) batteries. Moreover, based on the 4MDOL electrolyte, the Si/Gr || LiNi_{0.6}Co_{0.2}Mn_{0.2}O₂ (NCM622) battery exhibits negligible decay after 250 cycles at 0.5 C [56]. However, the application of ether solvents is constrained by the inherent limitation of high-voltage instability: the strong electron-withdrawing nature of the ether bond renders highly reactive α-hydrogen, triggering oxidative decomposition at potentials that are significantly lower than those of carbonate solvents. For instance, while conventional carbonate-based electrolytes typically exhibit anodic stability up to ~4.5 V vs. Li/Li⁺ (e.g., for EC/DMC), common ethers like 1,2-dimethoxyethane (DME) undergo oxidative decomposition at ~4.0 V [4,58,59]. Recent developments show that molecular fluorination techniques can address this problem in two ways: (i) employing strong electron-withdrawing groups (e.g., -CF₃) to lower the electron density of α-carbon [60]; (ii) utilizing steric hindrance from F atoms to inhibit radical chain reactions [61].

In conclusion, by creating stable interphase layers rich in LiF and improving electrolyte oxidation resistance, fluorinated solvents offer Si-based anode systems an efficient interfacial stabilization option. In order to achieve synergistic optimization of oxidation stability (>4.5 V) and interfacial kinetics, future research should concentrate on: (1) creating new multi-/per-fluorinated solvent design strategies that precisely control the fluorine substitution sites and degree; and (2) using in situ characterization (e.g., Cryo-Transmission Electron Microscopy (cryo-TEM)/X-ray photoelectron spectroscopy (XPS)) to clarify the dynamic

evolution mechanisms of fluorinated solvent-derived SEI, establishing the structure–composition–performance relationships.

2.2.3. Other Solvents

We systematically analyzed the crucial functions of ether and carbonate solvents in Si-based electrolytes in the sections that came before this one. But as knowledge of Si anode interfacial chemistry has grown, researchers have found new solvents that can alleviate particular problems with Si anodes due to their distinct physicochemical characteristics. Through mechanisms like tailored solvation weakening and anion coordination enhancement, these new solvents deliver complete improvements in important performance measures, such as cycling durability, low-temperature operability, and high-voltage stability.

Transcending conventional roles, advanced electrolyte solvents enable unprecedented interfacial control in silicon-based lithium-ion batteries through targeted molecular design. Tian et al. proposed a solvent-induced selective dissolution strategy to *in situ* regulate the mechanical properties of SEI [62]. Through introducing a high donor number (DN) solvent γ -butyrolactone (GBL, DN = 18.0) in a conventional LiPF₆-based electrolyte (1 M LiPF₆ in GBL/DEC/FEC, 45:45:10, vol.-%), SEI components with low modulus (e.g., Li₂CO₃ and lithium ethylene dicarbonate) can be selectively dissolved during cycling. This dissolution process is driven by the strong Lewis basicity of GBL, which effectively coordinates with Li⁺ and disrupts the crystalline structure of these organic carbonate species, leading to their solvation. In contrast, robust components such as LiF and polycarbonates exhibit low solubility in GBL due to their high binding energy and are thus retained. As a result, the SEI is dynamically refined into a mechanically resilient, inorganic-rich framework (Figure 4a). The selective dissolution process, although temporarily removing some SEI components, preserves ionic conductors such as LiF and polycarbonates. Although LiF exhibits relatively low intrinsic ionic conductivity, it enhances interfacial stability and, when uniformly distributed within a polymeric matrix, can provide efficient Li⁺ transport pathways. Meanwhile, the polycarbonates contribute elasticity and help form a continuous ion-conducting network. As a result, the SEI exhibits lower and more stable interfacial resistance, ultimately improving the overall interfacial ionic conductivity. This optimized SEI layer enables 87.5% capacity retention after 100 cycles at 0.2 C (1 C = 3000 mA g⁻¹, 25 °C) in μ Si || Li cells. High capacity can be maintained for 200 cycles, after which the GBL-based cell still delivers a specific capacity of 1804.1 mAh g⁻¹ (Figure 4b). Furthermore, the Si || NCM811 full cells with GBL-based electrolyte retain 83.7% of its capacity over 150 cycles at 0.2 C within a voltage window of 3.0–4.2 V. Thereby, establishing high-DN solvents as design tools to tailor SEI compositions for stabilizing volume-changing anodes. Li et al. leverage the remarkably high-voltage stability and interfacial modification capabilities of sulfolane (SL) to design a high-voltage electrolyte that forms high-modulus (lithium oxide) Li₂O-LiF interphases on μ Si surface, which not only ensures low bonding between SEI and Li_xSi phases (Li_xSi-phobic) but also promotes space charge accumulation along their interfaces (Figure 4c) [63]. The resulting space charge region establishes a highly selective ionic transport pathway, which is quantitatively shown by the theoretical modeling to enhance the local Li⁺ concentration by orders of magnitude while effectively suppressing electron tunneling. These effects suppress cracking of μ Si during cycling and generate a high ionic-to-electronic conductivity ratio, reducing electron leakage and overall SEI thickness resulting in a high reversible capacity of 2175 mAh g⁻¹ after 250 cycles for μ Si anodes (5 μ m, 4.1 mAh cm⁻²) (Figure 4d) and exhibits excellent stability in μ Si || LiNiCoAlO₂ (NCA) full cells, maintaining 81% capacity retention after 200 cycles with a high CE of 99.9%. Moreover, a large-format μ Si || NCA pouch full cell retained 89% of its capacity after 120 cycles, confirming the robust cycling stability of the system.

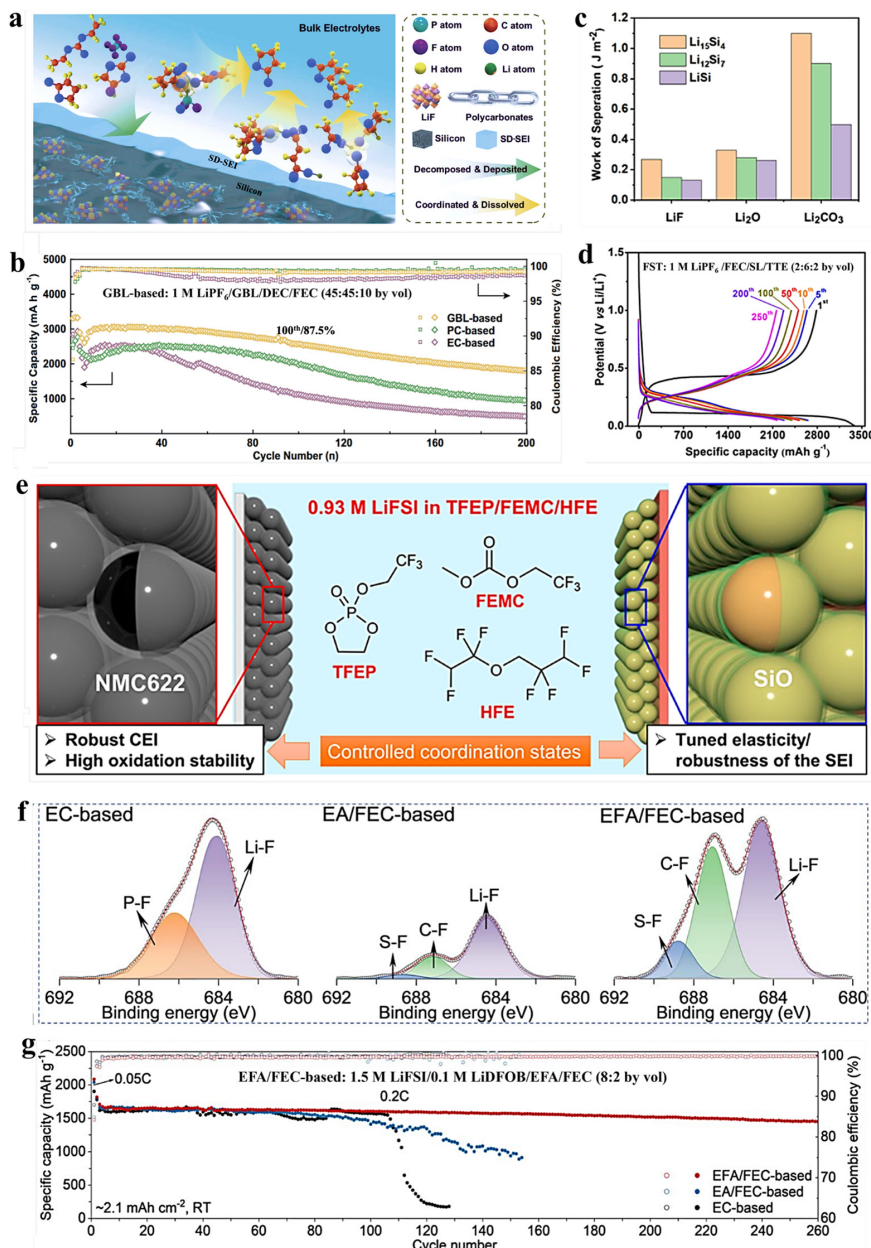


Figure 4. Key properties of advanced electrolyte solvents. **(a)** Schematic of the formation process of the resulting selectively dissolved SEI (SD-SEI) in GBL-based electrolyte [62]. **(b)** Cycling performance and CEs of the μ Si anodes in various electrolytes at 0.2 C [62]. Copyright 2023, Springer Nature. **(c)** Work of separation for LiF | Li_xSi, Li₂O | Li_xSi, and Li₂CO₃ | Li_xSi interfaces [63]. **(d)** Typical charge/discharge profiles of the μ Si electrodes cycled in FST electrolyte [63]. Copyright 2024, Springer Nature. **(e)** Schematic illustration of electrolyte composition of 0.93 M LiFSI in TFEP/FEMC/HFE and the battery configuration [64]. Copyright 2021, American Chemical Society. **(f)** The XPS spectra of F 1s of Si/C anodes after 100 cycles [65]. **(g)** Cycling performance of Li || Si/C half cells at 0.2 C after two activation cycles at 0.05 C [65]. Copyright 2025, Royal Society of Chemistry.

Moreover, organophosphate solvents have emerged as leading candidates for high-voltage electrolytes due to their unique molecular structure: (i) the vacant 3d orbitals of phosphorus (P) atoms enable exceptional oxidation stability (>5 V vs. Li/Li⁺); (ii) the radical quenching capability of phosphorus-based compounds effectively terminates combustion chain reactions, conferring inherent flame retardancy [66]. Representative solvents such as trimethyl phosphate (TMP) maintain stable solvation structures even at ultrahigh voltages (5 V, as confirmed by linear sweep voltammetry) while being com-

pletely non-flammable, as demonstrated by their failure to ignite in a direct flame test (self-extinguishing time < 3 s) [67]. The μ Si anode with 1 M LiDFOB/TMP produces a stable SEI, which effectively prevents capacity loss, delivering a high capacity retention even after 100 cycles with nearly 100% CE. More remarkably, molecularly engineered variants like 2-(2,2,2-trifluoroethoxy)-1,3,2-dioxaphospholane (TFEP) generate elastic polyphosphate-rich SEI layers accommodating Si volume strain (Figure 4e). Notably, the silicon oxide (SiO) || NCM622 full cell with 0.93 M LiFSI in TFEP/FEMC/HFE (1:3:1, vol.%) exhibits a superior cycling stability, with 71.5% capacity retained and 99.9% average CE obtained after 300 cycles at 4.4 V and 0.2 C rate [64]. However, electrolytes containing these solvents face a critical technical bottleneck: the high polarity of phosphate esters results in strong intermolecular forces, which lead to increased viscosity and decreased conductivity at low temperatures. Moreover, for instance, TMP has a melting point of $-46\text{ }^\circ\text{C}$, which can lead to solidification and battery failure at temperatures below $-50\text{ }^\circ\text{C}$. This issue is particularly pronounced when compared to conventional carbonate solvents that form the basis of most commercial electrolytes, many of which have much lower melting points (EMC: $-53\text{ }^\circ\text{C}$, DEC: $-74.3\text{ }^\circ\text{C}$). Therefore, although these solvents successfully address high-voltage tolerance and safety challenges while enabling precise interfacial control, future research must prioritize optimization for low-temperature adaptability. Only by overcoming this limitation can their full application potential be unlocked in wide-temperature-range (from -30 to $60\text{ }^\circ\text{C}$), high-energy-density ($>400\text{ Wh kg}^{-1}$) silicon-based batteries.

Low temperatures can reduce battery capacity and cycle life, primarily due to electrolyte solidification, decreased ion mobility, and increased viscosity [68]. Si-based anodes are further limited by their inherent drawbacks, such as poor conductivity, significant volume expansion, and unstable SEI film formation [69,70]. These issues collectively limit the application of Si-based LIBs across a wide temperature range. Therefore, tailoring new solvent molecules is crucial for enhancing the wide-temperature operation. To address these challenges, the design of new solvent systems is essential. Ester-based solvents such as ethyl acetate (EA) have attracted attention due to their low viscosity and low melting point, which are beneficial for low-temperature performance. However, the use of EA often leads to interfacial instability at the anode, limiting its practical application. Therefore, Sang et al. developed an EA-based electrolyte (0.9 M LiFSI + 0.1 M LiNO₃ in EA/FEC, 9:1 vol.%) that enables μ Si || NCM811 full cells to retain 91.8% capacity after 100 cycles at $-20\text{ }^\circ\text{C}$, attributed to superior low-temperature ion transport properties (0.49 mA cm^{-2} at $-20\text{ }^\circ\text{C}$) [71]. However, the SEI layers formed in pure EA systems are dominated by organic components (e.g., ROCO₂Li) with poor mechanical strength, which are insufficient to accommodate Si volume expansion [72]. To address this limitation, molecular fluorination strategies—exemplified by ethyl fluoroacetate (EFA)—have been employed. These fluorinated ester solvents emerge as optimal candidates due to their intrinsically low viscosity (<1.5 cP) and depressed melting point (< $-60\text{ }^\circ\text{C}$) [27]. The strong electronegativity of F ($\chi = 3.98$) induces σ -inductive effects that reduce the electron density of ester carbonyl carbon, consequently weakening the electron-donating ability of adjacent oxygen atoms. This electronic modulation not only lowers the lowest unoccupied molecular orbital (LUMO) energy level, thus promoting the formation of LiF-rich SEI with high Li⁺ conductivity (Figure 4f), but also moderately reduces solvation capability, thus improving the desolvation kinetics. Comparative studies reveal that EA-based electrolytes (1.5 M LiFSI + 0.1 M LiDFOB in EA/FEC (8:2, vol.%)) in Li || Si/C half-cells suffer rapid capacity decay (56.6% retention after 150 cycles, 941.1 mAh g^{-1} remains), whereas fluorinated EFA electrolyte (1.5 M LiFSI + 0.1 M LiDFOB in EFA/FEC (8:2, vol.%)) enables significant improvement in cycling stability, retaining 84.9% of the initial capacity (1709.1 mAh g^{-1} at 0.2 C) after 260 cycles (Figure 4g). When applied in Si/C || LiFePO₄ full cells, the EFA-

based battery demonstrates outstanding cycling performance, retaining 70.5% of its original capacity after 500 cycles at 0.5 C [65]. These findings demonstrate that targeted molecular fluorination effectively bridges the trade-off between low-temperature ion transport and interfacial stability. Solvent-synergy strategy offers a new pathway to resolve the ionic conductivity-interfacial stability bottleneck of Si anodes at low temperatures. Yang et al. report a rationally designed low-temperature electrolyte comprising 1 M LiFSI in (cyclopentyl methyl ether (CPME)/THF/TTE (1:1:1, v/v/v)) enabling exceptional performance of Si anodes under extreme conditions [73]. The synergistic combination of low-freezing-point CPME and solvation-modulating THF ensures superior ionic conductivity (3.4 S cm^{-1}) and facilitates the formation of a gradient hybrid SEI—characterized by a LiF-rich inner layer for rapid ion transport and an elastic polymer outer layer accommodating volumetric strain. This unique electrolyte empowers a high reversible capacity of 2157 mAh g^{-1} at -40°C (68.5% retention) and sustains over 80% capacity retention after 200 cycles at both -20°C and -35°C . Furthermore, $\text{Si} \parallel \text{LiFePO}_4$ full cells exhibit outstanding cycling stability with negligible capacity decay over 180 cycles at -20°C .

Drawing from the advances discussed, it is proposed that the following design principles for next-generation Si-compatible electrolytes. First, pursue hybrid SEI engineering by combining cross-linking solvents (e.g., FEC) with fluorinated solvents (e.g., FEMC) to synergize elastic organic and rigid inorganic components. Second, leverage weakly solvating systems to promote anion-derived inorganic SEI formation and improve desolvation kinetics. Finally, employ targeted molecular fluorination as a versatile strategy to concurrently enhance oxidation stability, guide the formation of LiF-rich interphases, and reduce electrolyte viscosity. These principles establish a foundational framework for the rational design of next-generation electrolytes that enables high-energy-density, long-lasting Si-based batteries.

2.3. Additives

Electrolyte additives, despite typically being incorporated at low concentrations ($\leq 5 \text{ wt.\%}$), exert a disproportionate influence on Si anode battery performance. These compounds critically enhance safety and cyclability through three critical functions: (i) facilitating the formation of a robust SEI layer on Si surface to mitigate the significant volume changes during cycling; (ii) elevating oxidation stability ($>4.6 \text{ V vs. Li/Li}^+$); (iii) suppressing side reactions and corrosion processes (e.g., gas evolution, HF corrosion). Therefore, given the distinctive challenges of Si—extreme volume expansion ($>300\%$) and interfacial incompatibility—additive engineering emerges as a vital research frontier.

Currently, additive engineering mainly focuses on four functional categories: (i) anode film-forming additives (e.g., VC, FEC) construct elastic SEIs preventing particle isolation [74]; (ii) cathode film-formers (e.g., Tris(trimethylsilyl)phosphite (TTSPi), 1,3-propane sulfonate lactone (PCS)) stabilize high-voltage cathode electrolyte interface (CEI) ($>4.5 \text{ V}$) against transition metal dissolution, which could deposit on anode surface and cause a greater deleterious impact on Si than on Gr [75]; (iii) antioxidants (e.g., Butylhydroxytoluene (BHT), Triphenylphosphine (TPP)) scavenge cathode radicals to extend voltage limits [76]; and (iv) reducing agents (e.g., Li_2S_5 , CO_2) pre-passivate surfaces reducing initial Li^+ loss. Beyond these specialized roles, multifunctional additives such as FEC synergistically encompass multiple functions, integrate multiple functions, serving as a representative parading for multifunctional electrolyte design discussed throughout this review. To systematically understand and design such multifunctional additives, this review correlates elemental composition (F: SEI elasticity; S: Li_2S_x pre-passivation; phosphorus: flame retardancy; B: voltage stabilization with reaction mechanisms), it establishes

structure–property relationships for providing a transformative framework to resolve Si-specific failure modes.

2.3.1. Li Salt Additives

Serve as the primary source of Li^+ for ion conduction, Li salts dominate the bulk properties of electrolytes (e.g., ionic conductivity, viscosity) and decompose to form key inorganic components of SEI (e.g., LiF , lithium nitride (Li_3N), and Li_2O). When acting as an additive, it can further modulate Li^+ solvation structure, ionic transport, and interfacial chemistry. Consequently, they play a critical role in mitigating Si anode degradation at the molecular level through enhanced inorganic SEI formation and optimized interfacial kinetics. Based on their core functions, Li salt additives can be systematically categorized into three primary classes: (i) SEI-forming salts that directly contribute to constructing mechanically stable interphases; (ii) conductive-phase promoters that generate highly ionically conductive SEI components; and (iii) multi-functional/corrosion-inhibiting salts that synergistically address concurrent challenges such as aluminum current collector corrosion and transition metal dissolution. This classification establishes a clear theoretical framework for the rational design of electrolyte formulations tailored for high-performance silicon anodes, allowing for a more comparative and mechanistic understanding of their roles across diverse electrolyte systems.

SEI-forming salt. Salts such as LiBOB, LiDFOB and lithium difluorobutyrate phosphate (LiDFBOP), decompose to form compact, anion-derived interphase layers. Among promising Li salt additives, LiBOB effectively addresses the volume change challenge in the Si anodes by forming an inorganic-rich SEI with high modulus. Dunn et al. demonstrated that incorporating 5 wt.% LiBOB into electrolytes significantly improves capacity retention (87% retention and > 98% CEs after 55 cycles in Li/thin-film Si half cells vs. 59% retention and CEs (93–96%) during the next 54 cycles for using an electrolyte without LiBOB [77]. XPS analysis reveals that LiBOB promotes the formation of a SEI layer rich in lithium oxalate and boron (B)-containing species, while simultaneously reducing the generation of unstable, high-impedance LiF by suppressing the decomposition of the LiPF_6 . Notably, LiBOB works synergistically with flame retardants (TPP/dimethyl methylphosphonate (DMMP)), addressing the issue of flame retardants interfering with SEI formation. Complementary work by Reqzita et al. also confirmed that LiBOB rapidly decomposes to form a stable SEI film. However, its highly sacrificial nature limits capacity utilization in composite anodes [78]. Also, its practical application is constrained by low solubility in carbonate solvents and high interfacial resistance, often limiting its use to additive-level formulations [79]. In contrast, lithium difluoro (oxalato) borate (LiDFOB) has emerged as a more versatile additive. Dalavi et al. demonstrated that the incorporated 1 wt.% LiDFOB in conventional LiPF_6 -based electrolyte enables a SEI layer enriched in oxalate species and $\text{Li}_x\text{PF}_y\text{O}_z$ while reducing LiF content, moderately improving cycling performance for Si thin film electrodes [80]. Extending to practical systems, Lee et al. investigated the effect of LiDFOB additive in $\text{Si}/\text{C} \parallel \text{lithium cobalt oxide} (\text{LiCoO}_2, \text{LCO})$ -lithium nickel manganese cobalt oxide (NCM622) full cells under high-temperature conditions. Studies have shown that LiDFOB may successfully suppress SEI decomposition at high temperatures by forming a LiF -rich SEI layer on Si/C anodes, where the strong thermal stability of LiF is present. Simultaneously, LiDFOB generates a carboxylate-derived SEI on cathode, collectively enhancing electrochemical performance at elevated temperatures [81,82]. Further advancing this approach, LiDFBOP promotes an anion-dominated solvation structure that decomposes into a thin, homogeneous, and inorganic-rich SEI with elevated LiF content, effectively suppressing silicon volume expansion (Figure 5a). Wang et al. demonstrated that adding 2 wt.% LiDFBOP to a commercial electrolyte significantly improved capacity

retention to 62.66% after 100 cycles, compared to 49.28% without it [83]. Overall, the oxalate–borate structure of LiDFOB and the advanced solvation effects of LiDFBOP provide a superior balance between film-forming ability and interfacial kinetics compared to LiBOB. The oxalate–borate structure appears to offer a superior balance between film-forming ability and interfacial kinetics compared to the pure oxalate backbone of LiBOB.

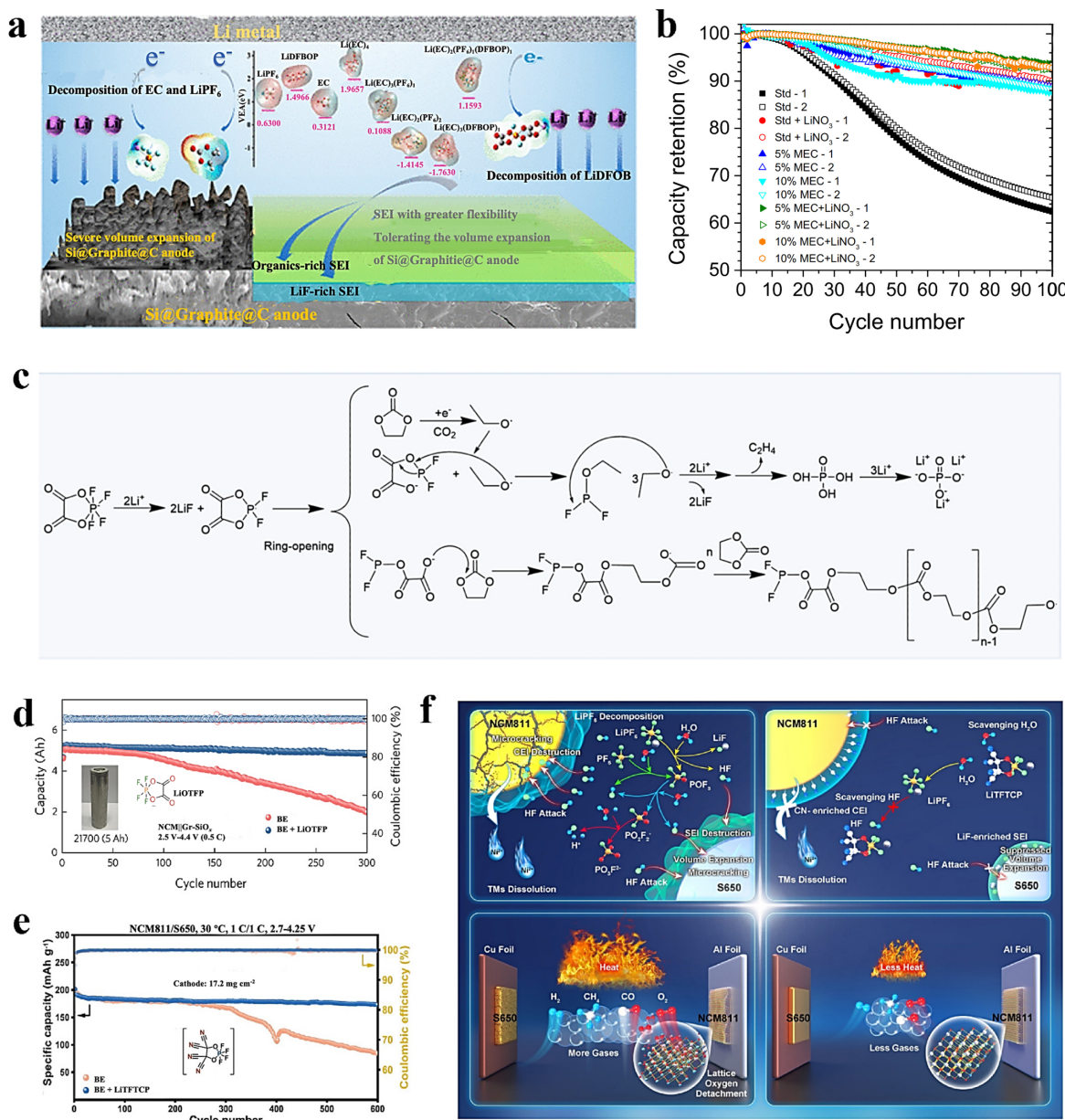


Figure 5. The effects of Li salt additives on Si anodes. **(a)** Mechanism illustration of LiDFBOP-derived SEI films tolerating volume expansion of the Si@Gr/C anode [83]. Copyright 2022, American Chemical Society. **(b)** Capacity retention of Si-Gr/Li cells with different electrolytes [84]. Copyright 2018, Institute of Physics Science. **(c)** The decomposition mechanism of LiOTFP at both cathode and anode sides [85]. **(d)** Cycling performance and CE of LiNi_{0.83}Co_{0.12}Mn_{0.05}O₂ (NCM) || Gr-SiO_x using an electrolyte with LiOTFP additive [85]. Copyright 2024, American Chemical Society. **(e)** Cycling performance of NCM811/S650 full cells using an electrolyte with LiTFTCP additive [86]. **(f)** The multifunctionality of LiTFTCP additive stabilizing electrode/electrolyte interphase layers and enhancing the thermal safety of NCM811/S650 full cells [86]. Copyright 2024, Wiley.

Notably, not all SEI-forming salts rely on extensive decomposition to exert their stabilizing effect. An alternative strategy is exemplified by lithium 4,5-dicyano-2-(n-

heptafluoropropyl)imidazole (LiHDI), a recently developed Hückel-type salt [87]. When used as an additive (2 wt.%) in a conventional carbonate-based electrolyte (LiPF₆ in EC/EMC + 2 wt.% VC), LiHDI significantly enhances the performance of Li||Si cells, increasing the specific capacity at C/10 from 2035 mAh g⁻¹ for the baseline electrolyte to 2250 mAh g⁻¹. Unlike LiBOB, which forms an inorganic-rich SEI via extensive anion decomposition, XPS analysis reveals that LiHDI undergoes minimal decomposition and does not alter the solvent decomposition pathway relative to LiPF₆. Instead, small angle X-ray scattering (SAXS) and SEM characterization confirm that LiHDI induces the formation of a porous SEI architecture that facilitates Li⁺ transport and mechanically accommodates volume changes in Si anodes. This mechanism underscores a new paradigm of “non-sacrificial” interfacial engineering, wherein minimal additive decomposition yields a functionally adaptive SEI for long-life Si anodes.

Conductive-phase promoters. This category is exemplified by lithium nitrate (LiNO₃) in LiTFSI/1,3-dioxolane (DOL)-based electrolytes for SiNW anodes, which are unparalleled in forming high-conductive SEI components such as Li₃N and Li_xNO_y. These species significantly reduce impedance and facilitate rapid Li⁺ transport [88]. Furthermore, the inorganic interface layer synergizes with polymerizable solvents (e.g., DOL) to form an elastic SEI capable of buffer volume expansion for Si anodes. However, the efficacy of LiNO₃ is often limited by its poor solubility in carbonate solvents and low anodic stability. Consequently, its application typically requires synergistic formulations. Nguyen et al. optimized the cycling performance of Si/Gr composite electrodes by combining 0.5 wt.% LiNO₃ with 10 wt.% methylene ethylene carbonate (MEC), achieving a balance between high initial CE (88.4%) and exceptional capacity retention (92.8%), outperforming electrolytes containing any single additive (Figure 5b). Furthermore, Si/Gr||LiNi_{1/3}Co_{1/3}Mn_{1/3}O₂ (NCM111) cells exhibit 79.9% capacity retention after 100 cycles, outperforming electrolytes containing any single additive [84]. This improvement is attributed to LiNO₃, which promotes the transformation of SEI components from unstable organic products (e.g., ROCOOLi) to highly stable inorganic Li₂CO₃ in the inner layer by altering the reduction sequence and providing reactive intermediates. Subsequently, MEC generates a polymeric outer layer (poly-MEC) atop the Li₂CO₃ layer, enhancing the mechanical robustness of the SEI.

Multi-functional and corrosion-inhibiting salts play essential roles in stabilizing Si-based batteries. A critical challenge in full-cells is the corrosion of the aluminum current collector by imide-based salts (LiFSI/LiTFSI) at high voltages (>4.2 V). LiDFOB has demonstrated to be an effective corrosion inhibitor while simultaneously promoting SEI stabilization. Asheim et al. systematically compared LiBF₄ and LiDFOB as additives in 1 M LiFSI-based electrolyte for cells with a high-Si-content anode (60 wt.%) and LiNi_{0.4}Co_{0.4}Mn_{0.2}O₂ (NCM422) cathode [89]. While both additives suppress aluminum corrosion, LiDFOB is markedly more effective, reducing the corrosion current by nearly two orders of magnitude. Furthermore, the electrolyte with 0.2 M LiDFOB delivers the best cycling performance in Si||Gr half-cells (74% capacity retention after 100 cycles), outperforming both LiBF₄ (64%) and the baseline LiFSI electrolyte (71%). XPS analysis reveals that LiDFOB promotes the formation of an SEI rich in organic components while reducing inorganic decomposition products like LiF, which synergizes well with the excellent film-forming properties of LiFSI. After 200 cycles in Si/C||NCM422 full cells, the LiFSI + LiDFOB electrolyte enables 28% capacity retention, comparable to the conventional LiPF₆ electrolyte yet significantly better than pure LiFSI. This study provides a feasible electrolyte design path for high-performance and high-safety Si-based batteries.

Advancing beyond conventional formulations, molecular engineering has yielded novel Li salt additives. Chen et al. synthesized a novel lithium tetrafluorophosphate (LiOTFP) salt as an additive through a combination of LiPF₆ and LiDFOB [85]. Exhibiting

higher HOMO and lower LUMO energy levels than EC and EMC, LiOTFP facilitates the formation of thin yet robust interfacial layers containing LiF, lithium orthophosphate (Li_3PO_4), and P-containing polymers on both cathode and anode surfaces (Figure 5c), which effectively mitigate Si volume expansion and the transition metals dissolution in NCM811. Practical validation in a 4.4 V 21,700 cylindrical battery (5 Ah) demonstrates 92.9% capacity retention after 300 cycles (Figure 5d). Building on targeted molecular design, Zhuang et al. synthesized lithium tetrafluoro(1,2-dihydroxyethane-1,1,2,2-tetracyanate)phosphate (LiTFTCP) by incorporating cyano groups into a difluorophosphate backbone [86]. This innovative salt effectively suppresses HF generation while constructing a thermally resilient cyanide-containing CEI and LiF-rich SEI. These interphases collectively reduce electrode degradation, electrolyte decomposition, heat-triggered gas evolution, and thermal runaway risk. In NCM811/S650 (S650 represents that SiO_x -Gr composite anode possesses a specific capacity of 650 mAh g^{-1}) full cells, electrolyte with 0.5 wt.% LiTFTCP enables 90.24% capacity retention (172.84 vs. 191.53 mAh g^{-1}) and 99.91% average CEs after 600 cycles at 1 °C under 30 °C (Figure 5e,f).

Overall, Li salt additives mainly play three core roles in Si-based LIBs: inducing LiF-rich SEI formation, scavenging reactive species, and enhancing ionic conductivity. Beyond these universal functions, these additives can be functionally categorized to guide targeted electrolyte design. Borate/oxalate salts like LiBOB, LiDFOB and LiDFBOP are ideal for crafting robust, inorganic–organic hybrid SEIs, with LiDFOB offering greater versatility and better compatibility with high-temperature and high-voltage operation. Notably, LiDFOB exemplifies a multi-functional additive, as it also serves as a potent corrosion inhibitor in LiFSI-based electrolytes for high-voltage full cells. Meanwhile, innovative salts like LiHDI demonstrate that modulating SEI morphology (e.g., porosity) is an equally viable pathway to performance enhancement. Nitrate salts remain unmatched for maximizing interfacial ionic conductivity, though their application requires careful electrolyte formulation. Finally, modern multi-functional salts are indispensable for enabling high-voltage compatibility and enhancing safety in systems employing reactive anodes and high-nickel cathodes.

Looking forward, key future research directions should include: (i) the molecular-level design of novel multi-functional salts that integrate, for instance, the stability of borates with the high ionic conductivity of nitrates; (ii) a deeper fundamental understanding of the synergistic decomposition mechanisms in multi-salt systems to precisely control SEI composition and architecture; and (iii) systematic evaluation of the long-term cycling performance and scalability of these advanced electrolyte formulations under realistic high-energy-density battery conditions.

2.3.2. F-Containing Solvent Additives

Since the severe volume expansion during cycling, engineering mechanically resilient SEI architecture is paramount for Si anode viability. Recent breakthroughs reveal F-containing solvent additives as pivotal enablers of SEI stability. Their efficacy originates from the formation of LiF via reductive decomposition, yielding inorganic domains with high elastic modulus and low interfacial energy [28,31]. This allows Si surface passivation, which suppresses continuous electrolyte reduction, and maintains SEI integrity across volume change cycles [90,91].

Among various fluorinated additives used in Si anodes, FEC remains the predominant one due to its ability to generate LiF-rich SEI layers with embedded unsaturated polyenes to enhance mechanical resilience [92]. Combined computational and experimental studies reveal that the FEC-derived LiF domains (elastic modulus $\approx 65 \text{ GPa}$) dissipate mechanical stress during volume changes, and crosslinked polyenes provide elastic buffering. These components synergistically enhance SEI resilience [93–99]. It is widely recognized that

FEC decomposes on Si particle surfaces to form a LiF-rich SEI film, which contributes to interfacial stabilization. However, Li et al. revealed that the role of FEC extends far beyond surface passivation; its more critical function lies in regulating the bulk electrode reaction processes after SEI formation. Their quantitative study demonstrated that adding 10 vol.% FEC to a 1 M LiPF₆ in EC/DMC/EMC (1:1:1, vol.%) electrolyte markedly increases the capacity retention of nano-Si anodes from < 10% to over 70% after 60 cycles. Enhanced gas chromatography analysis reveals that this improvement stems from the suppression of Li trapping. With FEC addition, capacity loss due to Li trapping is significantly reduced by 82.3% (vs. 52.2% without FEC). Complementary X-ray diffraction (XRD) and transmission electron microscopy (TEM) analyses further confirm that FEC promotes bulk LiF doping within the electrode, which inhibits the formation of the high-volume-change crystalline Li₁₅Si₄ phase and stabilizes the low-volume-change amorphous Li_xSi phase (Figure 6a) [100]. This finding reveals that FEC fundamentally mitigates the intrinsic failure mechanism of Si anodes by simultaneously stabilizing both the interface and the bulk structure.

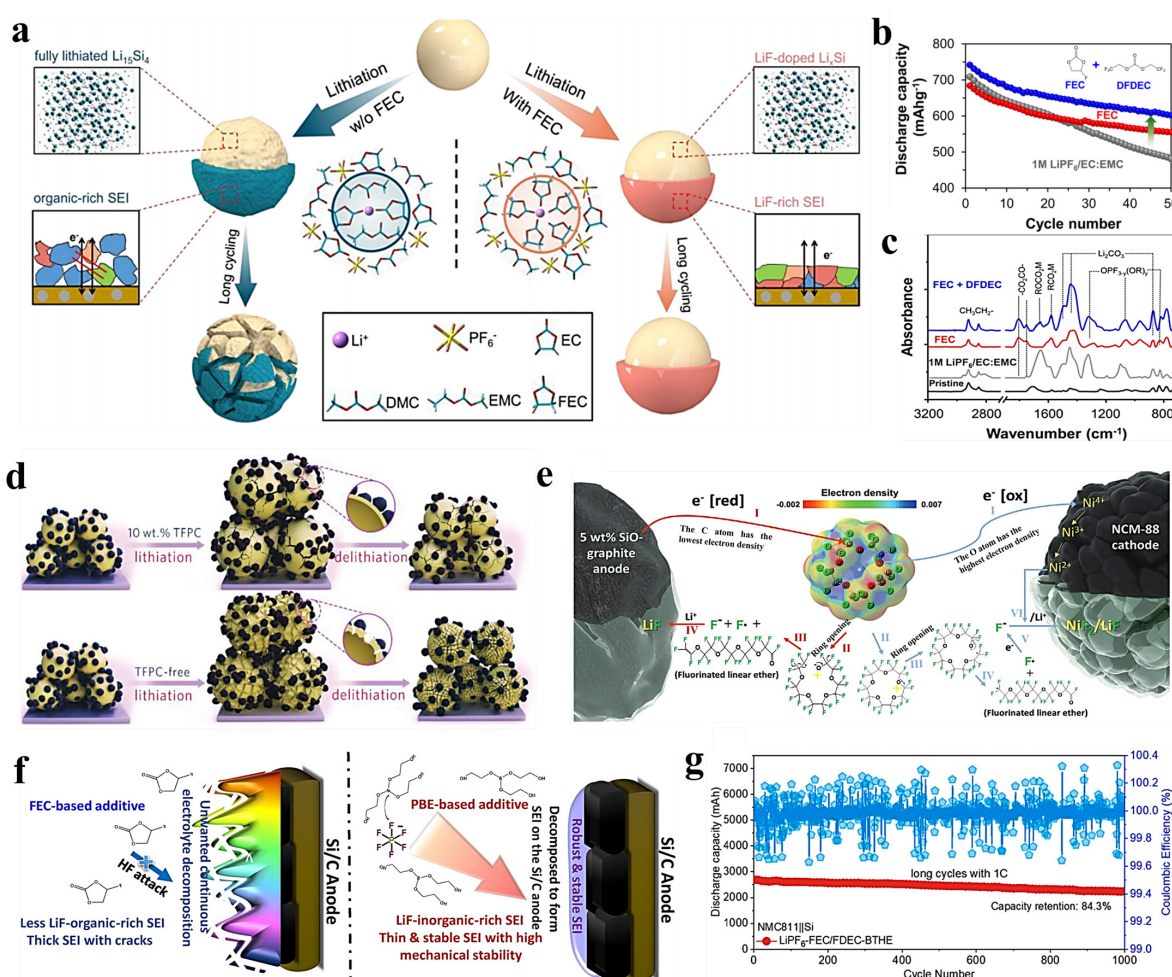


Figure 6. The effects of F-containing additives on Si anodes. (a) Schematic illustration of the role of the FEC additive in suppressing Li-trapping within Si particles [100]. Copyright 2023, American Chemical Society. (b) Cycling performance of Si/Gr anodes in different electrolytes [101]. Copyright 2016, American Chemical Society. (c) Infrared spectroscopy spectral comparison of different electrolytes [101]. Copyright 2016, American Chemical Society. (d) Schematic illustration of TFPC effect on Si-based anodes [102]. Copyright 2019, Wiley. (e) The electrochemical reduction and oxidative decomposition mechanism of IF-CE additives [90]. Copyright 2023, Wiley. (f) The mechanism and morphology of SEI formation on Si/C anode surfaces by PBE and FEC additives [103]. Copyright 2022, American Chemical Society. (g) Cycling properties of the NMC811 || Si pouch cell at 1 C between 3.0 and 4.35 V [104]. Copyright 2024, Elsevier.

However, the performance of FEC is highly concentration-dependent. At moderate concentrations (~10 wt.%), it forms a beneficial SEI, but higher concentrations increase electrolyte viscosity and resistance, leading to deteriorative cycle stability. Moreover, although FEC performs excellently at room temperature, some studies have indicated that at elevated temperatures, FEC undergoes decomposition, which not only leads to gas generation (such as H₂ and CO₂) but also exacerbates side reactions at the electrode/electrolyte interface [99,105]. The continuous decomposition of FEC causes repeated rupture and reconstruction of the SEI and CEI, resulting in a sharp increase in interfacial impedance and significantly shortens the cycle life of LIBs. Moreover, the challenges associated with FEC are not limited to high-temperature cycling. Recent research reveals that the calendar aging issues it triggers during long-term storage are equally detrimental. Multi-scale characterization of Si/Gr || NCM622 full cells (containing 1 M LiPF₆ in EC/DEC/EMC + VC + FEC) stored to 0–13 weeks under open-circuit conditions at 4.1 V reveals distinct degradation mechanisms at different length scales [106]. At the electrode level, FEC undergoes continuous electrochemical reduction on the copper current collector, forming a progressively thickened LiF-rich interphase. This LiF layer originates from the electrochemical reduction of FEC on the copper surface, with its thickness increasing over storage duration and leading to interface delamination and crack formation, thereby significantly increasing interfacial impedance. In stark contrast, at the nanoscale, the SEI on Si particle surfaces remains no significant changes during calendar aging. This finding indicates that while the FEC is essential for improving cycling stability, it may simultaneously become the primary cause of performance degradation during long-term calendar aging due to formation of an insulating LiF layer at the current collector interface. These limitations have catalyzed the exploration of advanced fluorinated additives designed to complement or replace FEC.

An alternative strategy involves using fluorinated co-additives that work synergistically with FEC to construct more robust interphases. The study introduced di(2,2-trifluoroethyl) carbonate (DFDEC) as a co-additive. Leveraging their synergistic effect, an organic–inorganic hybrid solid protective interphase layer was constructed, thereby significantly enhancing the overall performance of silicon-based batteries. Electrochemical tests demonstrated that compared to using FEC alone (1M LiPF₆ in EC:EMC (3:7, vol.%) + 10 wt.% FEC), the binary additive system (FEC-DFDEC) formed by additionally introducing 1 wt.% DFDEC increased the initial discharge capacity of Li || Si/Gr battery from approximately 710 mAh g⁻¹ to 742 mAh g⁻¹ (Figure 6b) [101]. Surface composition analysis revealed that the SEI film predominantly formed by the single FEC additive is primarily composed of organic components (such as anhydride and carboxylate salts), with its inorganic components (such as LiF) being relatively limited. In contrast, the introduction of DFDEC fundamentally optimized the chemical composition of the SEI: acting as an efficient fluorine source and precursor, its decomposition reaction significantly increased the abundance and distribution density of key inorganic components in the SEI—particularly LiF and Li₂CO₃ (Figure 6c). This synergistic combination of an organic framework and inorganic fillers effectively compensate for the deficiencies in mechanical strength and long-term chemical stability of the SEI formed by FEC alone. In conclusion, DFDEC achieves reinforcement of the electrode interface through precise regulation of the SEI chemical composition, fundamentally enhancing the battery's cycle life and interfacial stability.

On the basis of the successful application of FEC, Shen et al. reported 4,5-difluoro-1,3-dioxolan-2-one (DFEC) as a film-forming additive to improve the electrochemical performance of SiO@C || LiNi_{0.8}Co_{0.15}Al_{0.05}O₂ full cells. The dual-F electronegativity in DFEC weakens its LUMO energy level, leading to a lower reductive potential than EC and FEC and consequently accelerating reduction kinetics [107]. XPS indicates increased LiF/C-F content and suppressed SiO_x degradation, leading to superior cycling stability in

Si-based batteries. Similarly, Hu et al. obtained trifluoropropylene carbonate (TFPC) by replacing the F atom in FEC with a fluoromethyl group [102]. TFPC exhibits a lower LUMO energy level than FEC (-0.28 eV for TFPC vs. -0.1 eV for FEC), enabling accelerated reduction kinetics, preferential passivation, and reduced solvent decomposition by >40% versus standard carbonates. Notably, TFPC exhibits a concentration-dependent efficacy. At moderate concentration (10 wt.%), it forms an SEI layer rich in polyolefins and LiF, significantly optimizing the cycling performance of Si nanomaterials (Figure 6d). While a higher concentration (20 wt.%) of TFPC is beneficial for augmenting the LiF content in the SEI layer, it also leads to increased electrolyte viscosity and resistance, ultimately resulting in deteriorative cycle stability.

The fluorinated additive landscape also expands to encompass multifunctional compounds that transcend conventional SEI engineering. The addition of the pentafluoro(phenoxy)cyclotriphosphazene (PhPF₆N) additive enables the detection of 1.6% nitrogen and 2.0% P via XPS analysis. This directly demonstrates that PhPF₆N decomposes and participates in the formation of the SEI. Notably, the P content was significantly higher than expected from LiPF₆ decomposition alone, suggesting ring-opening polymerization of the phosphazene compound, resulting in the formation of linear polyphosphonitrile structures or oligocyclic structures on SiO_x/C surface. Such a pre-coating surface layer is conducive to increasing the elasticity of SEI. In addition, through simultaneous P-F bond cleavage, this F-containing additive generates LiF-rich SEI, improving mechanical stability and thus enhancing capacity retention by >40% in SiO_x-based full cell [108]. Ding et al. systematically investigated the role of the fluorinated phosphazene additive in stabilizing electrode interfaces during high-voltage operation [109]. Incorporating 5 wt.% (ethoxy)-pentafluorocyclotriphosphazene (PF₆N) into a conventional carbonate-based electrolyte not only renders the system non-flammable but also markedly enhances its cycling stability under elevated voltages. The molecular design of PF₆N, characterized by high phosphorus and low hydrogen content and the inclusion of three flame-retardant elements (F, P, and N), endowing it with a synergistic flame-retardant capability. Most importantly, PF₆N undergoes controlled decomposition on both electrodes: it forms a C-N/C = N-enriched CEI on the cathode surface and a nitrogen-containing SEI on the Si-Gr anode. This dual-interphase engineering promotes the construction of uniform, resilient, and ionically conductive protective layers that simultaneously suppress electrolyte oxidation at the cathode and SEI fracture caused by the volume expansion of Si anodes. As a result, a 4.45 V Si/Gr || LiCoO₂ pouch cell cycled at 25 °C achieves 78% capacity retention after 300 cycles at 1 C, with a discharge capacity ratio of ~83% at 6 C/1 C, underscoring the additive's efficacy in enabling high-energy, flame-retardant LIBs. In a parallel development, Oh et al. developed an alternative to FEC, namely icosafluoro-15-crown 5-ether (IF-CE) [90]. By replacing 8 wt.% FEC with 0.4 wt.% IF-CE, these cost-effective additive forms ether-rich dual-electrode passivation layers on both cathode and anode surfaces that mitigate particle cracking and cathode dissolution (Figure 6e), achieving a dramatic improvement of capacity retention to 88% after 100 cycles and high CEs of 99.8% in Si monoxide (SiO)/Gr || LiNi_{0.88}Co_{0.08}Mn_{0.04}O₂ (NCM88) full cells. This study provides valuable insights into the development of cost-effective electrolyte formulations that employ dual-interface stabilization strategies for both Si-based and nickel-rich materials.

In conclusion, F-containing additives have become indispensable in Si-based electrolytes, primarily by engineered stabilization of the anode–electrolyte interface through LiF-dominated SEI formation during initial lithiation (<0.5 V vs. Li/Li⁺). These additives decompose to produce LiF-rich inorganic–organic hybrid layers with exceptional mechanical resilience and high ionic conductivity. They collectively mitigate electrolyte decomposition, reduce active Li⁺ loss, and alleviate the volume strain via elastic recovery. Beyond

SEI enhancement, fluorinated species can secondarily modulate bulk electrolyte properties through wettability optimization (contact angle $\theta < 15^\circ$), which improves electrode coverage [110], oxidation stability elevation (>4.8 V), thus suppressing gas evolution [111], and solvation structure tailoring to enhance Li^+ transference number [112].

Future research should prioritize molecularly targeted fluorination—systematically correlating F atom count (1–6), bonding configuration (C-F, O-F, P-F), and LUMO energy (-3.0 – 0.5 eV) with SEI dynamics and cycling stability (with high Si content and practical electrode loading). Such efforts will accelerate cost-effective and high-energy (>400 Wh kg $^{-1}$) Si batteries beyond conventional Li salt limitations.

2.3.3. B-Containing Solvent Additives

As an electron-deficient element, B shows intrinsic Lewis acidity, which enables dual interfacial enhancements in Si anodes. Firstly, its significant Lewis acidity can coordinate with anions in electrolytes (e.g., PF_6^- , FSI^-), thereby elevating Li^+ transference number by immobilizing counterions. Secondly, the B-O/B-F bond networks facilitate dense SEI formation with mechanical stability. Such a synergistic effect concurrently enhances ionic conductivity and cycling stability in Si anodes.

Building on these mechanistic insights, Han et al. introduced 5 wt.% (pentafluorophenyl)borane (TPFPB) into 1 M LiClO_4 /EC/DEC (1:1, *v/v*) for Si thin film anodes [113]. TPFPB continuously decomposes during cycling. After 100 cycles, F and B contents within the SEI show an increasing trend, indicating that the SEI is continuously repaired through this dynamic decomposition process. Consequently, the Si thin film electrodes attain nearly doubled capacity retention after 100 cycles (87% vs. 46%) compared to the control electrolyte without TPFPB, improved CEs throughout cycling ($>98\%$), and unaltered charge/discharge profiles (the potential range of 0.005–1.5 V vs. Li/Li^+). Extending beyond single-additive systems, comparative analysis reveals the versatile functionality of B-containing additives in Si anodes. An et al. systematically evaluated five additives, 1,3,2-dithiane 2,2-dioxide (DTD), 1-ene-1,3-thione (PES), tris(trimethylsilyl)borate (TMSB), tris(trimethylsilyl)phosphate (TTSP), and methylenedisulfonate (MMDS), in $\text{SiO}_x/\text{C}/\text{Gr} \parallel \text{NCM811}$ full cells with LiPF_6 /carbonate electrolytes [114]. It is revealed that 0.5 wt.% TMSB can reduce transition metal dissolution by $>80\%$ (dissolved $\text{Ni}^{2+} < 0.3$ ppm) and prevent the following metal deposition on the Si surface, consequently achieving 92.4% capacity retention after 200 cycles versus 68.7% for controls. Taking additive design to sophistication, Karkar et al. designed a polymeric borate ester synthesized with diethylene glycol (PBE-DG) for Si/Gr systems [103]. Its strong Lewis acidity and low reduction potential (0.5 V vs. Li/Li^+) facilitate catalytic LiF generation from fluorinated anions (LiF content: 52 at% vs. 38 at% for FEC) and elastic SEI formation (Figure 6f). These attributes reduce the polarization to 43 mV at 1 C versus the 98 mV with FEC additives and deliver 40% higher cycling stability than FEC-based systems at equivalent concentrations. Meanwhile, $\text{Si}/\text{Gr} \parallel \text{LiNi}_{0.5}\text{Co}_{0.3}\text{Mn}_{0.2}\text{O}_2$ (NCM532) full cell exhibit markedly enhanced capacity retention, with only 25% capacity loss after 50 cycles using the PBE-DG electrolyte, versus 63% loss for the FEC-based counterpart.

He et al. incorporated 1 wt.% boric acid tris(hexafluoroisopropyl) ester (BTHE) as a functional additive into a 2 M LiPF_6 in FEC/2,2,2-trifluoroethyl methyl carbonate (FDEC) (3:7, vol.%) [104]. Acting as an anion receptor, the electron-deficient B center of BTHE strongly interacts with PF_6^- anions, promoting the formation of $\text{Li}^+\text{-PF}_6^-$ ion pairs and facilitating the accumulation of more anions in the inner Helmholtz plane (IHP) at the electrode interface. This interfacial rearrangement elevates the anion reduction potential, driving preferential anion decomposition and forming a LiF -rich SEI with superior mechanical strength and interfacial compatibility. Consequently, Si anode volume ex-

pansion is effectively suppressed, enabling a capacity retention of 72.6% after 300 cycles, surpassing those with LiPF₆-FEC/FDEC (29.3%) and LiPF₆-EC/DEC (8.4%) electrolytes. Furthermore, a Si || NCM811 pouch cell employing this BTH-modified electrolyte delivers a high energy density of ~650 Wh kg⁻¹ and retains 2243.9 mAh g⁻¹ after 1000 cycles at 1 C (1 C = 200 mA h g⁻¹), corresponding to 84.3% capacity retention (Figure 6g). This work achieves the perfect integration of the ultra-high energy density characteristics of silicon materials with the flexible and lightweight features of pouch cell structure, leading to a leap forward in battery performance, which marks a significant breakthrough in the field of Si-based pouch batteries.

Collectively, B-containing additives represent a transformative strategy for Si anode enhancement through synergistic interfacial mechanisms. It regulates SEI through catalyzing the formation of uniform, ionically conductive yet electronically insulating layers with high elastic modulus, passivates reactive Si sites to decrease gas evolution and impedance rise by inhibiting solvent decomposition, and modulates interfacial charge distribution to mitigate polarization. Despite these advantages, practical deployment must contend with several inherent limitations, including high viscosity, moderate oxidative stability at high voltage, and potential miscibility issues with carbonate solvents. Given the potential of B-containing additives in regulating interfacial stability and electrochemical behavior, it is necessary to establish quantitative structure–property relationships correlating coordination geometry of B (e.g., trigonal planar vs. tetrahedral), Lewis acidity strength, and reduction potential windows with SEI elastic recovery and Li⁺ diffusivity to enable rational design of next-generation additives for high-energy-density Si-based batteries.

2.3.4. Silane-Containing Additives

Organosilicon compounds exhibit superior oxidative/reductive stability compared to carbon analogues, attributable to the higher bond dissociation energy of the Si-O bond (452 kJ mol⁻¹) versus the C-O bond (358 kJ mol⁻¹) [115]. This inherent stability enables silane additives to function as effective electrolyte stabilizers. Their hydrolysable Si-H bonds can scavenge detrimental species like HF and H₂O. And it enables the consolidation of SEI integrity by suppressing electrolyte decomposition pathways. Consequently, silanes have emerged as promising multifunctional additives for interfacial stability in high-energy Si-based batteries [116–119].

The protective mechanism primarily involves the selective decomposition or adsorption of silanes at the electrode/electrolyte interface, leading to effective passivation of the Si surface. This passivation mitigates the repeated formation and exfoliation of unstable SEI films, facilitating the formation of a more uniform, dense, and ionically conductive interface that significantly reduces impedance growth [118]. For example, dimethoxysilane (DMDOS) forms a dense Si-O-Si cross-linked polymeric network on Si/C surface, which not only suppresses interfacial side reactions but also alleviates volume expansion through its inherent flexibility. Consequently, Si-C anodes exhibit cycling stability, retaining 82% of their capacity after 200 cycles and 85.5% after 100 cycles, with an average CE of ~100% in the Si@C || NCA cell [120]. Notably, adding more than 1 wt.% DMDOS may compromise the mechanical integrity of the SEI layer formed by carbonate solvent redox reactions, leading to inferior long-term stability.

Building upon this fundamental understanding of Si-O reactivity, subsequent research has explored tailored silane structures for enhanced functionality. Aupperle et al. introduced tetraethoxysilane (TEOS) and (2-cyanoethyl)triethoxysilane (TEOSCN) as additives into conventional electrolytes [121]. It is demonstrated that the cyanide group (-C≡N) in TEOSCN, as a strong electron-withdrawing group, significantly lowers the LUMO energy level. This enables its preferential reduction over the decomposition of EC/DEC solvents,

generating highly ionically conductive Li₃N. Simultaneously, the resulting strong nucleophilic intermediates attack fluorine-containing components (e.g., FEC, LiPF₆), promoting LiF formation (Figure 7a). Moreover, the alkoxy groups (-OR) in TEOSCN undergo condensation with surface hydroxyl groups on silicon, forming a covalently anchored layer that further polymerizes into a dense polysiloxane network (Figure 7b). This inorganic network physically blocks direct contact between the electrolyte and silicon, thereby suppressing solvent decomposition and reducing the generation of organic byproducts. Ultimately, TEOSCN significantly increases the proportion of inorganic components within the SEI layer, forming a stable protection layer. This consequently enhances interfacial stability and electrochemical performance. For instance, adding just 1 wt.% TEOSCN to a standard LiPF₆/EC/DEC electrolyte (containing FEC and VC additives) significantly enhances the long-term cycling performance of NCM622/Si-Gr batteries at 45 °C (75.95% capacity retention after 364 cycles) [119]. Further extending this concept, Zhang et al. demonstrated that TEOSCN facilitates the construction of a Li₂CO₃-rich SEI via CO₂ capture and EC ring-opening catalysis triggered by cyano-group reduction, while siloxane groups guide film formation through an anchoring effect [122]. This dual mechanism collaboratively mitigates both cycling degradation and thermal runaway risks, offering a novel strategy for designing high-safety Si-based batteries.

Other functional groups also contribute uniquely. Wang et al. investigated the effect of vinyl tris(2-methoxyethoxy)silane (VTMS) on Si/C anodes, revealing that 5 wt.% VTMS significantly improves initial capacity and CE [123]. This enhancement originates from VTMS participating in forming a composite SEI containing Li₂CO₃, LiF, and organosilicon compounds. Furthermore, through electrochemical polymerization of its vinyl groups and siloxane condensation reactions, VTMS constructs a 3D conductive network (validated by equivalent circuit modeling), which actively suppresses interfacial side reactions. These synergistic processes collaboratively build a thin yet compact SEI, significantly reducing ionic migration resistance (Figure 7c). However, when the VTMS content exceeds 5 wt.%, the electrochemical performance deteriorates again. This decline in cycling capability is attributed to an increase in the resistance of the siloxane network, which impedes the transport of both lithium ions and electrons. Addressing thermal challenges, Tan et al. incorporated 5 wt.% (3-aminopropyl)triethoxysilane (APTES) into conventional carbonate-derived electrolyte, effectively reducing heat output from Si electrodes while maintaining cycling capabilities [116]. On the one hand, the basic -NH₂ group in APTES can form a coordination compound with PF₅, blocking the decomposition chain reaction of LiPF₆. Simultaneously, the cleavage of Si-O-C₂H₅ bonds consumes HF, generating Si-F bonds, thereby preventing HF from corroding the SEI layer (Figure 7d). On the other hand, trace amounts of water in the electrolyte can trigger the hydrolysis and condensation of APTES, forming a cross-linked polymer network that covers the electrode surface (Figure 7e). This isolates the silicon anode from direct contact with the electrolyte. This dual mechanism synergistically enhances thermal resilience with APTES additives. Particularly, regardless of the amount of APTES used, the initial lithiation capacity remains at ~2900 mAh g⁻¹ with a first-cycle CE of ~91%. Batteries employing standard electrolytes exhibit significant capacity decay after 25 cycles, whereas those with 5 wt% APTES additive demonstrate more stable cycling performance. These results collectively highlight the significant potential of functionalized silanes for enhancing both electrochemical performance and safety in Si-anode LIBs.

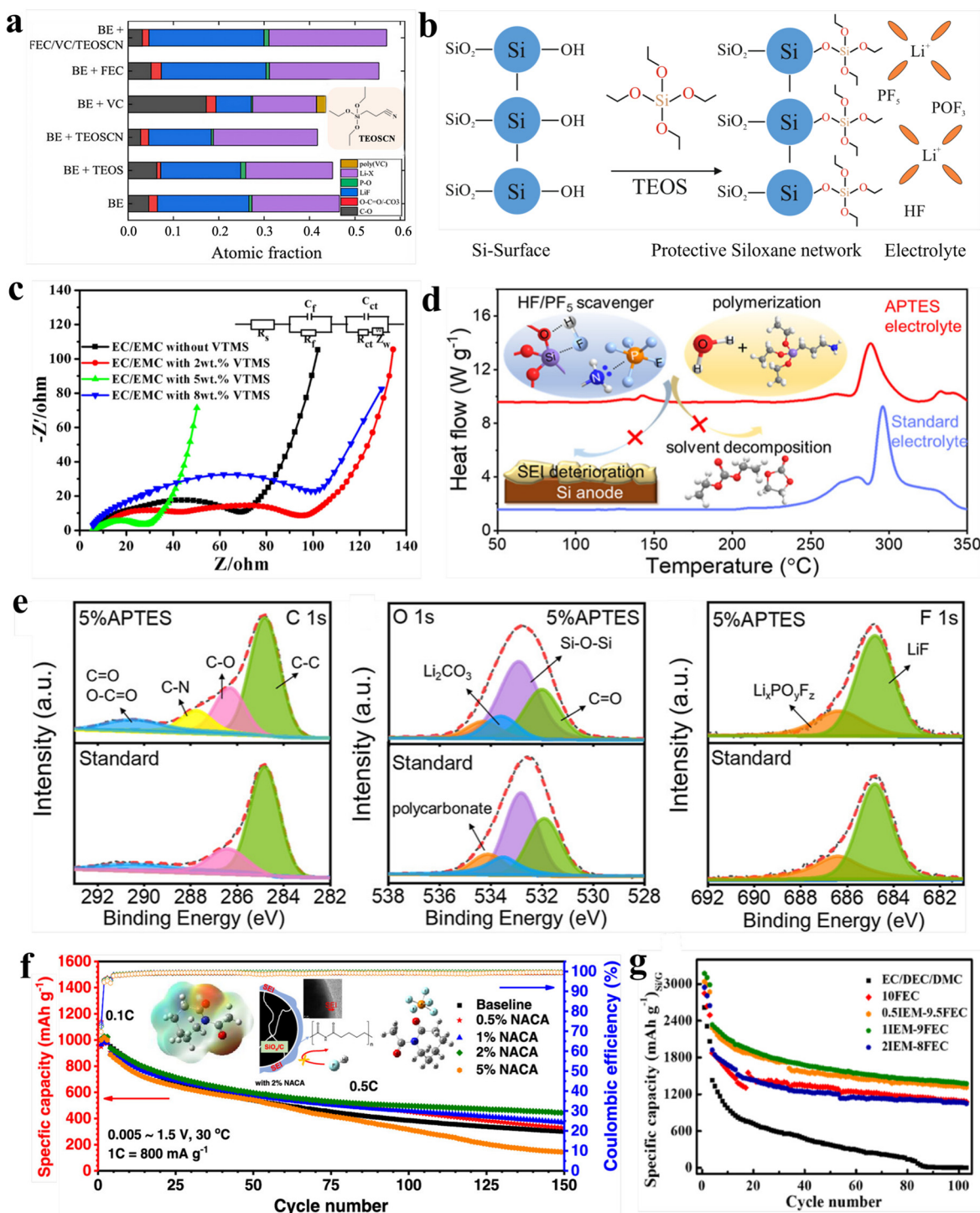


Figure 7. The effects of silane-containing additives on Si anodes. (a) SEI-building species of cycled electrodes with different electrolyte formulations [121]. (b) Schematic diagram of the formation of siloxane network on the surface of TEOS additive [121]. Copyright 2019, American Chemical Society. (c) Nyquist plots of Si/C composite electrodes in electrolytes with different contents of VTMS [123]. Copyright 2018, Springer Nature. (d) Schematic diagram of the possible mechanism of HF removal and PF₅ stabilization with APTES additive [116]. (e) XPS spectra of the Si electrode after first discharge and after annealing with standard and 5 wt.% APTES electrolytes [116]. Copyright 2022, American Chemical Society. (f) Cycling performance of Li||SiO_x/C batteries with electrolytes containing different contents of NACA additive in the voltage range of 0.005–1.5 V [124]. Copyright 2022, American Chemical Society. (g) Cycling performances of Li||Si/G half cells with various electrolytes at 1 A g⁻¹ [125]. Copyright 2023, Elsevier.

Beyond interfacial stabilization on anodes, organosilicon (OS) additives have been shown to effectively mitigate gas generation in full cells. LIBs are prone to gas generation under high-voltage operation or elevated temperatures, which degrades battery performance and poses serious safety risks [126,127]. It is reported that adding only 3 vol.% of OS additives to carbonate-based electrolytes in NMC622/Gr pouch cells can suppress 94–98% of CO₂ generation at 60 °C [128]. The efficacy correlates positively with the degree of fluorination in the silane molecule, with highly fluorinated species offering the greatest suppression. Mechanistically, OS additives scavenge reactive nucleophiles (e.g., O₂^{·-}, O₂²⁻, CO₃²⁻) that initiate solvent decomposition and oligomerize with decomposition products to form a protective interphase, thereby fundamentally reducing gaseous byproducts [129].

In summary, introducing organoSilicon compounds as electrolyte additives demonstrates significant effectiveness in enhancing both battery performance and safety. These additives facilitate the *in situ* formation of stable and uniform SEI films on electrode surfaces, which exhibit enhanced ionic conductivity and electronic insulation. These favorable films effectively suppress the continuous electrolyte decomposition on the anode surface, thereby reducing interface impedance and promoting efficient ion transport. In addition, organosilicon additives provide exceptional thermal stability, delaying electrolyte decomposition at elevated temperatures and thereby enhancing safety under extreme operating conditions. Despite these advantages, practical realization faces intrinsic trade-offs—elevated viscosity and limited miscibility, synthetic and economic challenges associated with silane additives, and the necessity for precise compositional control to avoid forming overly siloxane-rich SEIs that compromise rate performance. Future research should investigate fundamental mechanisms governing structure–property relationships across diverse organosilicon compounds and evaluate their practical viability in various battery systems, thereby providing a theoretical basis and technical support for further optimization of battery performance and safety.

2.3.5. Other Types of Additives

Beyond the aforementioned solvents, additives featuring functional groups like sulfonyl, amide, and isocyanate demonstrate significant potential for Si anodes. Liu et al. reported that allyl phenyl sulfone (APS) facilitates the formation of a compact and durable SEI layer on SiO_x/C anode with enhanced Li⁺ transport kinetics [130]. This is because APS forms a composite SEI structure rich in inorganic species with high lithium-ion conductivity (Li₂SO₃, Li₂S/Li₂S_x) and organic species (ROSO₂Li) that provide good interfacial contact. This composite structure significantly enhances the lithium-ion conductivity of the SEI film, thus reducing interfacial impedance. Eventually, with the addition of 0.5 wt.% APS, the SiO_x/C electrode retains a capacity of 777 mAh g⁻¹ (79.3% retention) after 200 cycles at 0.5 C and 30 °C, significantly outperforming the baseline electrolyte (57.8% retention). More importantly, the SiO_x/C || LiNi_{0.9}Co_{0.05}Mn_{0.05}O₂ (NCM90) cell maintains 135 mAh g⁻¹ with 73.9% retention after 300 cycles, markedly higher than the baseline (124 mAh g⁻¹, 67.4% retention). Extending S chemistry, Liu et al. used Diethyl Sulfite (DES) to modify SEI formation through promoted FEC defluorination and sulfide polymerization [131].

Expanding the scope beyond sulfones to amide functionalities from a lactide structure, Liu et al. explored that N-acetylcaprolactam (NACA) preferentially reduces on SiO_x/C surface, undergoing ring-opening polymerization to form highly flexible SEI films with amide segments [124]. The resulting SEI film effectively adapts to the significant volume changes of SiO_x/C electrodes while maintaining cyclability, inhibits LiPF₆ decomposition through strong Lewis acid–base interactions with PF₅/HF/H₂O, and mitigates electrode corrosion. The incorporation of an appropriate amount of NACA additive significantly enhances the cycling stability of Li || SiO_x/C batteries. At an optimal dosage of 2 wt.%,

the battery delivers a superior delithiation capacity of 444 mAh g^{-1} after 150 cycles, substantially outperforming the baseline electrolyte (300 mAh g^{-1}). This corresponds to a notable 48% improvement in capacity retention (Figure 7f). Further exploring isocyanate functionality, Li et al. utilized isocyanate methacrylate (IEM) synergistically with FEC to construct an organic–inorganic SEI on Si/Gr anodes [125]. Characterized by cross-linked polymers and LiF, this tailored interphase demonstrates exceptional accommodation to Si volume expansion and significantly enhanced cycling stability, remaining the specific capacity of 1373 mAh g^{-1} after 100 cycles in $\text{Li} \parallel \text{Si}/\text{Gr}$ half cells (Figure 7g).

In conclusion, additives with special functional groups play a crucial role in maintaining Si anode stability. Due to the specific chemical structures, they preferentially reduce or adsorb on electrode surfaces to form a uniform, flexible SEI with enhanced ionic conductivity, thereby alleviating volume expansion and enhancing structural stability. At the same time, some of these additives can scavenge trace H_2O , HF, and PF_5 , enhancing chemical stability and interface compatibility of electrolytes. In-depth research on their mechanism of action not only helps understand their multiple functions in film formation but also provides fundamental design principles for next-generation Si anode electrolytes, particularly under practical cycling conditions.

2.3.6. Comparative Summary and Outlook

Li salts lay the fundamental groundwork for interfacial stability by decomposing to form a robust inorganic component within the SEI, whereas solvent additives, through functional group design, fine-tune the chemical composition and mechanical properties of this interphase. The diverse additive families—fluorinated, boron-containing, silane-based, and those featuring sulfonyl, amide, or isocyanate functionalities—employ distinct yet complementary chemical strategies to address the multifaceted degradation pathways of Si anodes. Comparative analysis underscores their synergistic roles: F-containing additives are unparalleled in constructing LiF-rich SEI for superior passivation and mechanical strength. B-containing additives function as Lewis acid mediators, enhancing Li^+ transport and catalytically promoting the formation of elastic, hybrid SEI. Silane-containing additives excel in forming covalently anchored, robust interphases with exceptional thermal and chemical stability. Meanwhile, other functional additives introduce unique mechanisms, such as ring-opening polymerization (e.g., amides) for flexible SEI or radical scavenging (e.g., sulfones) for improved interfacial compatibility. Together, these chemical design strategies highlight a unifying direction for future electrolyte engineering: achieving hierarchically structured, compositionally adaptive SEIs capable of maintaining mechanical resilience and electrochemical integrity across diverse operating conditions.

Ultimately, additive selection represents a multifactorial trade-off among SEI mechanics, ionic conductivity, thermal resilience, and cost-effectiveness. No single additive family can address all challenges; instead, synergistic multi-additive formulations, guided by fundamental understanding of interfacial chemistry, hold greatest promise. Future electrolyte design must pursue hierarchically structured SEI that can simultaneously ensure cycling stability, calendar life, and safety for next-generation Si-based LIBs. The critical importance of calendar life is further underscored by the recent insights into charge-imbalance mechanisms during storage. It is demonstrated that the parasitic reaction rate at the Si anode far exceeds that of common cathodes, leading to spontaneous delithiation and irreversible capacity loss that can contribute 30–38% of the total degradation [132]. This insight elevates the design criterion for additives and SEI: beyond withstanding dynamic volume changes, future SEIs must also be exceptionally passivated under static conditions to suppress parasitic currents and maintain inter-electrode charge balance over time.

2.4. Prelithiation: Compensating Initial Capacity Loss

The formation of the SEI and Li trapping within the bulk Si anode typically leads to low initial Coulombic efficiency (ICE) and substantial active Li loss. To address this issue, researchers have developed various prelithiation strategies, which can be broadly categorized into four types: (i) direct contact with Li foil or stabilized Li metal powder (SLMP), (ii) active-material-assisted prelithiation, (iii) electrochemical prelithiation, and (iv) chemical prelithiation. These techniques compensate for initial Li loss by introducing an additional Li source into the anode prior to cycling, thereby enhancing the energy density of full cells [133,134].

Ou et al. employed biphenyl lithium (Bp-Li) for the chemical prelithiation of SiO [135]. This process not only compensated for lithium loss and enhanced electrode stability by constructing a core-shell structure (nano-Si/Li₂SiO₃@C), increasing the ICE to 91.0%, but also offered benefits far beyond simply providing an additional lithium source. More importantly, the prelithiation treatment fundamentally altered the initial reduction process of the electrolyte at the electrode interface by drastically lowering the silicon anode's open-circuit potential from ~3.20 V to ~0.61 V [136]. This critical change shifted the reduction behavior of various electrolyte components (such as LiTFSI, FEC, and LiBF₄) from a "sequential reduction" to a "synergistic co-reduction." This co-reduction process collaboratively constructed a uniform, robust, and elastic SEI film rich in LiF and boride species. This SEI effectively buffers the substantial volume changes of the silicon anode, inhibits particle pulverization, and significantly reduces interfacial impedance. Ultimately, this ideal interface, triggered by prelithiation and synergistically built with the electrolyte, collectively enabled the full cell to achieve a remarkable performance leap: the ICE surged from 74.8% to 97.2%, and 90.1% capacity retention was maintained after 800 cycles.

Collectively, these studies demonstrate that effective prelithiation strategies not only fundamentally compensate for the initial Li loss in Si anodes but also synergistically promote the formation of stable interphase, thereby comprehensively enhancing the cycle life and rate performance of batteries.

3. Innovative Electrolyte Architecture

Building upon the fundamental roles of Li salts, solvents, and additives, innovative electrolyte systems address persistent challenges in Si anode batteries through advanced solvation engineering. High-concentration electrolytes (HCEs), localized high-concentration electrolytes (LHCEs), and weakly solvating electrolytes (WSEs) represent strategic approaches to engineer SEI with enhanced flexibility and mechanical strength (Figure 8), which are critical for accommodating the significant volume changes of Si anodes during repeated cycling.

3.1. High-Concentration Electrolytes

High-concentration electrolytes (HCEs) refer to an electrolyte design where the Li salt concentration significantly exceeds conventional levels (typically > 3 M, versus 1–1.2 M in commercial cells). This approach fundamentally reconfigures solvation structures from "solvent-dominated coordination" to "anion-involved coordination (CIPs/AGGs)". Such a configuration effectively suppresses solvent decomposition while promoting anion-derived SEI formation dominated by high-modulus components like LiF and Li₃N, enables mechanical stabilization against Si volume changes and electrochemical passivation that maintains interfacial continuity while suppressing parasitic reactions [137–140]. It is important to note that this beneficial structure shift comes with a trade-off: a significant increase in viscosity and a consequent decrease in ionic conductivity. For instance, in model LiTFSI/DMC system, increasing the concentration from 1.1 M, 2.78 M, 5.55 M to 10.11 M causes the viscosity to

surge from 1.81, 6.56, 34.79 to 248.89 mPa·s, while the ionic conductivity drops from 10, 10.54, 4.17 to 1.2 mS cm⁻¹ [141]. This quantitative comparison highlights the fundamental balance between interfacial stability and bulk transport properties and defines the core challenge in HCEs design.

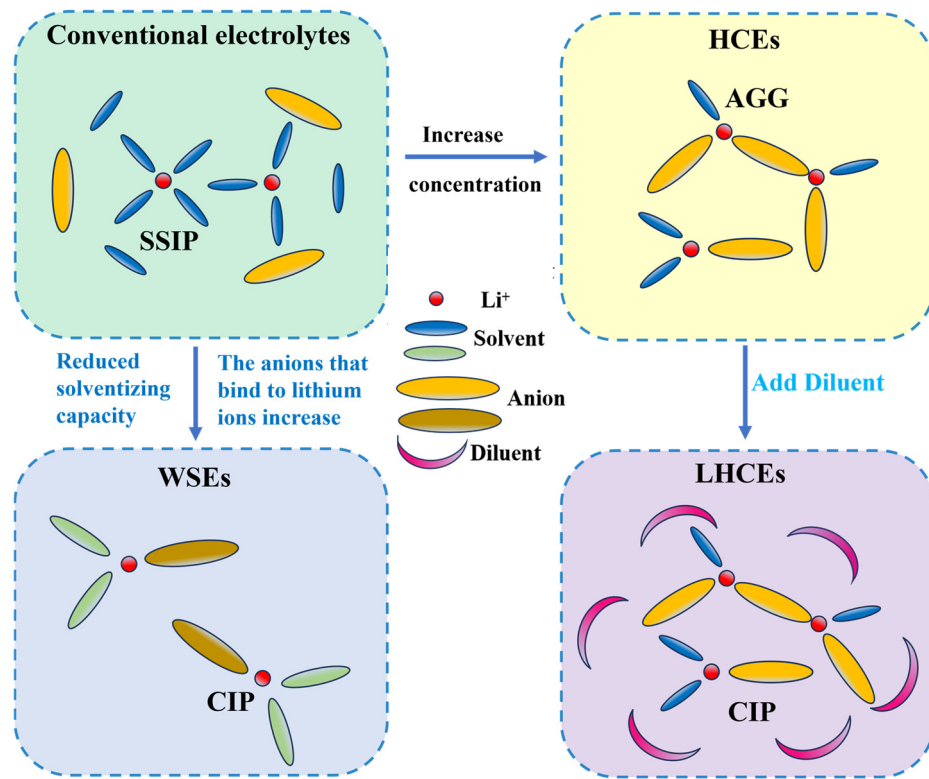


Figure 8. Schematic representation of the solvated configurations of conventional electrolytes, HCEs, LHCEs, and WSEs.

The dominance of CIPs and AGGs in HCEs elevates the LUMO energy level of the solvent while reducing the LUMO energy level of the anion [142]. This orbital energy shift drives preferential anion decomposition, facilitating the formation of mechanically and chemically stable organic–inorganic composite SEI layers. Chang et al. demonstrated this principle using an ultra-high concentration electrolyte by dissolving 7.8 M LiFSI in PC solvents [143]. The coordinated Li⁺-FSI⁻-PC interactions create a fluid polymer-like network. With elevated CIP/AGG concentrations, enhanced FSI⁻ reduction generates a complex SEI layer that effectively suppresses Si particle morphological changes and limits excessive expansion (Figure 9a,b). Consequently, electrodes maintain 63.5% capacity retention after 100 cycles, outperforming the 7.5% capacity retention in low-concentration electrolyte (1.0 M LiFSI/PC) that primarily forms an organic SEI layer dominated by ROCO₂Li. This research offers a novel approach for identifying electrolytes with enhanced cycling stability for Si-based electrode materials. Complementarily, Zhang et al. demonstrated that optimized medium-concentration LiFSI (3 M) with FEC can also yield substantial benefits in SiO_x/C || LiNi_{0.90}Mn_{0.05}Co_{0.05}O₂ (NCM955) full cells [144]. This formulation concurrently establishes LiF-rich SEI layers on both electrodes, accommodating Si anode volume expansion while suppressing transition metal dissolution from the high-nickel cathode, enabling superior cycling stability with a capacity retention of 88.2% after 150 cycles (Figure 9c,d).

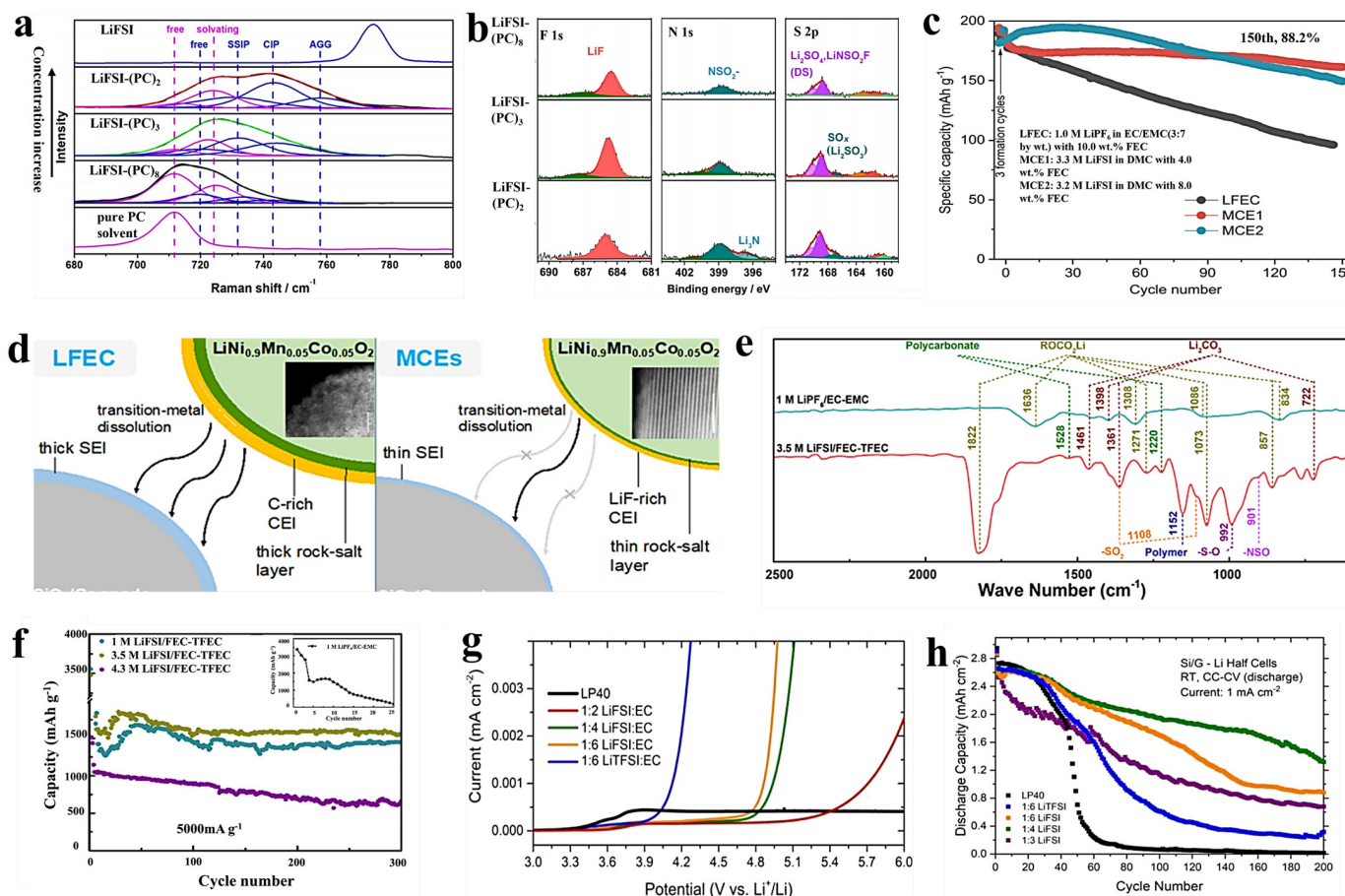


Figure 9. The effects of HCEs on Si anodes. (a) Raman spectra and fitting curves of electrolytes with different LiFSI concentrations [143]. (b) XPS spectra of pristine μ Si electrodes and cycled μ Si electrodes in electrolytes with different LiFSI concentrations [143]. Copyright 2018, Wiley. (c) Cycling stabilities of $\text{SiO}_x/\text{Gr} \parallel \text{NCM955}$ cells with different electrolytes at C/3 rate at 25 $^{\circ}\text{C}$ [144]. (d) SEI is enabled by different electrolytes [144]. Copyright 2023, Elsevier. (e) FTIR pattern of the μ Si electrode in 1 M LiPF₆/EC-EMC and 3.5 M LiFSI/FEC-TFEC electrolytes [145]. (f) Cycling capability of μ Si anodes in TFEC-based electrolytes with different concentrations at 5000 mA g^{-1} (in the first three cycles at 500 mA g^{-1}) [145]. Copyright 2019, American Chemical Society. (g) High voltage stability of different electrolytes as measured with LSV in Al-Li cell configurations at room temperature [137]. (h) Cycling performance of Si/Gr || Li half cells with LiTFSI at various molar concentrations in EC-based electrolytes [137]. Copyright 2022, American Chemical Society.

Building on this understanding of anion-dominated decomposition, Zeng et al. designed a high-concentration fully fluorinated carbonate electrolyte composed of 3.5 M LiFSI dissolved in FEC and di-2,2,2-trifluoroethyl carbonate (TFEC) [145]. In this system, the number of highly reactive free solvent molecules is significantly reduced, which greatly suppresses the reductive decomposition of solvents on the anode surface, prevents excessive growth and thickening of the SEI, and reduces the consumption of active lithium and electrolyte. Simultaneously, both FEC and TFEC decompose at reduction potentials, cooperatively forming a composite-structured SEI characterized by an inorganic LiF skeleton embedded within an elastic polymer matrix (Figure 9e). This electrolyte significantly enhances the cycling stability of μ Si anodes, enabling a high initial reversible capacity of 2644 mAh g^{-1} and an exceptionally low-capacity fading rate of only 0.064% per cycle after 300 cycles (Figure 9f). These findings collectively validate the effectiveness of high-concentration electrolyte systems in stabilizing silicon anodes through interfacial engineering. In addition to the functional advantages of inorganic-rich SEI, HCEs also

show advantages in mitigating corrosion limitations by Li salts like LiFSI and LiTFSI and expanding ether solvents utility at elevated voltages. LiFSI and LiTFSI demonstrate superior thermal/electrochemical stability, but their tendency to corrode aluminum current collectors above 4 V persists. Aktekin et al. demonstrated that increasing LiFSI concentration in EC from conventional (~1 M) to concentrated (>4 M) regimes elevates aluminum corrosion potential from 3.9 V to 5.2 V (Figure 9g) [137]. This corrosion resistance stems from SEI enrichment with stable oxygen-containing inorganic compounds, which concurrently enhance interfacial stability and cycling performance. The electrolyte formulation with an LiFSI/EC (1:4 by mol) exhibits the optimal performance, which is significantly superior to that of other electrolytes (Figure 9h). Notably, the absence of transition metal ions (e.g., Ni²⁺) on the surface of the Si/C anode confirms suppressed cathode dissolution.

HCEs represent a paradigm shift in battery chemistry, leveraging unique solvation science to address degradation mechanisms in Si anodes. The elevated Li salt concentrations enhance electrochemical stability through anion-dominated decomposition pathways, promoting inorganic-rich SEI formation that simultaneously accommodates volume expansion via high-modulus components and reduces interfacial resistance. However, high salt concentration inevitably leads to high viscosity, poor wettability, reduced Li⁺ transference number due to anion crowding, and increased material cost. Future development should address viscosity limitations while extending compatibility to high-voltage cathodes (>4.4 V).

3.2. Localized High-Concentration Electrolytes

Localized High-Concentration Electrolytes (LHCEs) are an advanced electrolyte design that preserves the beneficial solvation structure of HCEs while mitigating their drawbacks by introducing inert, non-solvating but miscible diluents into HCEs. This system maintains microscale high-concentration solvation sheaths around Li⁺ ions while achieving bulk viscosity reduction. More importantly, LHCEs preserve the characteristic CIPs/AGGs configurations critical for inorganic SEI formation while enhancing ionic conductivity due to the chemical inertness of diluents. This architecture retains the electrochemical advantages of HCEs, including Al corrosion resistance (>5.0 V) and transition metal dissolution suppression, while improving rate capability and low-temperature performance [28,31,81,91,93,146].

As the core component in LHCEs, optimal diluents exhibit low Li⁺ solvation energy and high miscibility. The classification of diluents as “inert” or “non-solvating” is principally determined by their minimal coordination with Li⁺, as verified through spectroscopic evidence (e.g., Raman/NMR spectroscopy showing negligible peak shifts) and computational simulations. The most common diluents are fluorinated ethers (e.g., bis(2,2,2-trifluoroethyl)ether (BTFE), TTE, and 2,2,2-trifluoroethyl-1,1,2,2-tetrafluoroethyl ether (HFE), prized for their chemical inertness, low polarity, and compatibility with anion-rich solvation clusters [147]. Recent advances include high-boiling-point 1H,1H,5H-octafluoropentyl 1,1,2,2-tetrafluoroethyl ether (OTE) (133 °C) replacing volatile BTFE. The optimized OTE-based LHCE (1.74 M LiFSI in DMC/OTE, 0.51:0.84:0.84 by mol) not only eliminates solvent evaporation during electrode processing, thus enhancing thermal safety, but also effectively maintains the dense structure of Si/Gr anodes during long-term cycling (Figure 10a) [44]. For Li salts option of LHCEs, LiFSI/LiTFSI dominate due to exceptional solubility (>5 M) and FSI⁻/TFSI⁻-derived LiF nucleation. For solvent selection, carbonates, carboxylates, ethers, nitriles, and sulfones maintain viability. Additionally, since almost all solvent molecules coordinate with Li⁺ in the solvation shell, the HOMO energy of coordinated solvent is lower than that of free solvent molecules, significantly enhancing

the oxidation stability of the electrolyte. Consequently, LHCEs broaden the viable solvent selection beyond conventional electrolytes.

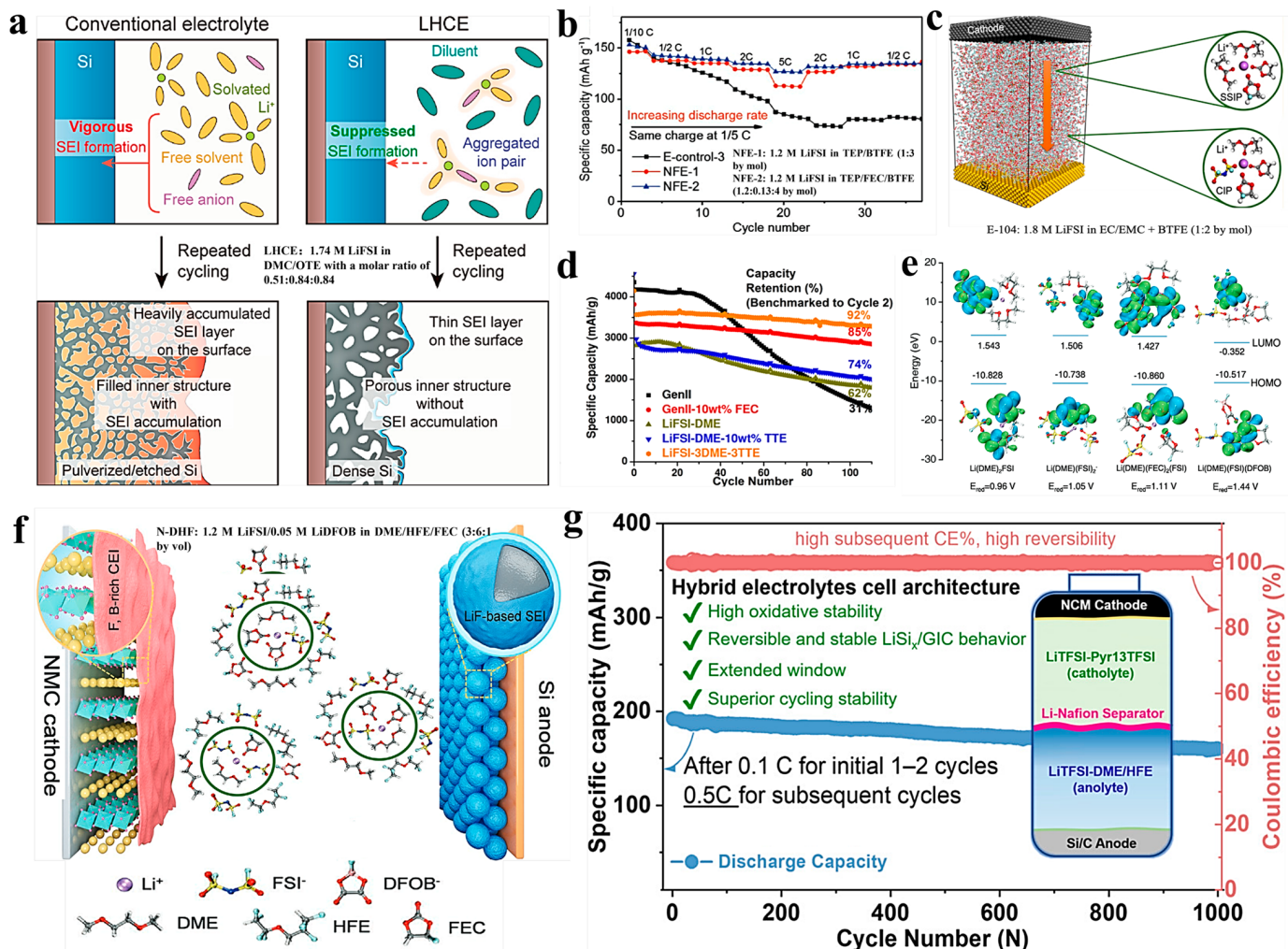


Figure 10. The effects of LHCEs on Si anodes. (a) Si anode degradation in conventional electrolyte vs. LHCE [44]. Copyright 2021, American Chemical Society. (b) Rate capabilities of Si/C || NCM333 cells in different electrolytes [43]. Copyright 2019, Wiley. (c) Schematics of the first shell structure of Li ions in E-104 electrolyte and percentage of CIPs and SSIPs in different electrolyte systems [146]. Copyright 2020, American Chemical Society. (d) Cycling performance comparison of Li/Si half-cells with LHCE and conventional electrolytes [91]. Copyright 2021, American Chemical Society. (e) LUMO and HOMO energy levels of four dominant solvation structures in LHCE [81]. (f) Scheme of the Si || NCM532 battery configuration with LHCE [81]. Copyright 2021, Wiley. (g) Long-term cycling performance of the decoupled Si/C || NCM811 full cell: long-term cycling test and the corresponding CE at 100 mA g⁻¹ [148]. Copyright 2021, American Chemical Society.

Like HCEs, LHCEs enable anion decomposition at electrodes, forming robust LiF-rich SEI/CEI layers critical for stabilizing the electrode/electrolyte interphase. While historically applied to Li metal anodes, LHCEs have recently demonstrated promise for Si-based systems. Jia et al. developed an LHCE for Si/C || LiNi_{0.3}Mn_{0.3}Co_{0.3}O₂ (NMC333) batteries, where LiFSI was dissolved in TEP as the main solvating solvent, with BTFE serving as the inert diluent [43]. It generates locally concentrated Li⁺-TEP coordination clusters and a robust FSI⁻-derived LiF-rich SEI on Si anodes, effectively accommodating volumetric expansion while maintaining electrode integrity. The cells achieve superior cycling stability (92.4% capacity retention after 200 cycles) and rate performance versus

conventional commercial electrolytes (Figure 10b). As one of the earliest adaptations of LHCEs to Si-based anodes, this work advances electrolyte design for Si-dominant LIBs. Building on this initial success, Jia et al. further investigated the influences of solvents on fluorinated diluent molar ratios on the cycling stability of Si/C || LiNi_{0.5}Mn_{0.3}Co_{0.2}O₂ (NMC532) batteries to establish broader applicability and mechanistic insights [146]. By formulating LHCEs with different salt concentrations and carbonate solvents to fluorinated diluent molar ratios, it is revealed that 1.8 M LiFSI in EC/EMC and BTFE (1:2 molar ratio) exhibits the highest proportion of solvent separation of ion pairs (SSIPs) and CIPs and the fastest ion diffusion (Figure 10c), resulting in the most stable electrode–electrolyte interphase and hence shows the best Si anode performance.

The emergent field of Si-compatible electrolytes remains largely unexplored, particularly regarding ether solvents. Ethers offer compelling advantages for Si anodes, as their low reducibility mitigates detrimental side reactions, superior Li salt solubility and low viscosity facilitate high-concentration formulations that promote dense, inorganic-rich SEI layers [149]. Capitalizing on these inherent advantages, Yang et al. compared LiFSI/DME/TTE LHCE with state-of-the-art carbonate electrolytes [91]. It is revealed that the DME-based LHCE enables a functionally graded SEI with an outer elastomeric polyether layer resilient to lithiation-induced stress from Si anodes, and an inner layer domain with reduced carbonates/silicide but enhanced LiF, sulfates, and SiO_xF_y from preferential FSI[−] decomposition. This architecture combining an elastic organic outer buffer with a robust inorganic ion-conducting core reduces internal resistance and maintains 92% capacity retention after 110 cycles (Figure 10d). Although DME predominates LHCE solvents, its tendency toward oligomerization during reduction poses challenges. To address this limitation of DME, Yang et al. focused on innovating the main solvent molecule rather than modifying the diluent. They replaced the linear DME with the cyclic ether, THF, leveraging its reduced ether-oxygen coordination and moderate solvating strength to construct a THF-based LHCE system. In this system, TTE serves as the inert diluent, while THF acts as the main solvent, forming a high-concentration solvation structure with LiFSI. The limited solvation capacity of THF promotes a weakly coordinating environment, lowering desolvation energy and forming a thinner SEI layer enriched with inorganic components. Its unsaturated cyclic nature promotes in situ polymerization, generating a flexible yet durable SEI film. Compared to DME-based LHCE, the THF-based LHCE enables a thinner, more elastic, and LiF-rich SEI that more effectively accommodate Si volumetric expansion. As a result, it delivers a high reversible capacity of 1995.7 mAh g^{−1} after 400 cycles at 1 A g^{−1} for Si anodes and maintains over 80% capacity retention after 600 cycles in Si/Gr || LiFePO₄ full cells. This work confirms the superiority of THF over DME for Si anodes and establishes a molecular design paradigm for high-performance Si anodes [28].

Besides the mono-salt LHCE systems, multi-salt LHCEs demonstrate promising potential in stabilizing Si anodes. Cao et al. engineered a dual-salt system using concentrated LiFSI and LiDFOB in DME/HFE with FEC. Anion decomposition is favored over solvent reduction due to the low reduction potential and strong solvation capability of ether solvents (Figure 10e). Notably, the synergistic introduction of LiDFOB facilitates the formation of ultrathin, F- and B-enriched interfacial layers on both Si anode and NMC532 cathode, improving SEI mechanical stability while suppressing Si particle fragmentation and side reactions (Figure 10f). Consequently, the Si anode achieves 90.2% initial CE and retains a reversible capacity of 2041.9 mAh g^{−1} after 200 cycles at 0.2 C, establishing a scalable interface-engineering strategy for fabricating high-performance Si-based batteries [81].

Rechargeable LIBs pairing Si anodes with Ni-rich cathodes represent a leading high-energy-density configuration. However, conventional electrolytes can hardly simultane-

ously stabilize low-voltage anodes (<0.5 V vs. Li/Li⁺) and high-voltage cathodes (>4.3 V). He et al. resolved this through a hybrid electrolyte system spatially separating the cathode-side and anode-side electrolytes through a Nafion membrane [148]. The cathode-side ionic liquid electrolyte (LiTFSI-Pyr₁₃TFSI) is capable of withstanding high operating potentials of over 4.4 V and promoting the formation of a stable CEI on the NCM811 cathode surface. On the anode side, the LHCE (LiTFSI-DME/HFE) generates a durable SEI. This compartmentalization enables optimal redox kinetics at both electrodes, yielding an Si/C || NCM811 full cell with > 80% capacity retention after 1000 cycles (Figure 10g). This hybrid electrolyte design approach offers a broadly applicable framework for developing high-voltage, high-energy-density LIBs, playing a crucial role in advancing next-generation electrochemical technologies.

Although LHCEs greatly improve Si anode compatibility, there are still important restrictions on the cost and scalability of diluent production, the stability of polymerized SEI over an extended period of time under intense cycling, and compatibility with cathodes with voltages greater than 4.3 V. Future work should prioritize operando SEI characterization and machine learning-guided diluent design to accelerate commercial deployment.

3.3. Weakly Solvating Electrolytes

Weakly solvating electrolytes (WSEs) present a strategic alternative to HCEs and LHCEs, circumventing limitations such as high viscosity/cost and compromised ionic conductivity [110]. WSEs employ low-polarity solvents to reduce Li⁺-solvent binding energy, thereby forming solvation sheaths with looser coordination structures. This design facilitates ion transport by lowering migration resistance and increasing Li⁺ transference number, enabling the formation of a homogeneous inorganic-rich SEI/CEI dominated by anion coordination without requiring high salt concentration. Moreover, compared to LHCEs, it eliminates the reliance on diluents and avoids the viscosity penalties from non-coordinating additives [150]. The weakened Li⁺-solvent interaction additionally streamlines desolvation kinetics, enhancing ionic conductivity and accelerating interfacial ion transfer during battery operation. Therefore, WSEs establish a rational design pathway for high-performance Si anodes by offering the following critical advantages [151]. First, the low Li⁺-solvent binding energy improves rate capability and low-temperature performance [152]. Second, the weakened Li⁺-solvent interactions promote anion-rich solvation sheaths where anions preferentially decompose, promoting robust, inorganic-rich SEI (Figure 11a) [110]. Third, anions within the solvation sheath shield solvent molecules from Li⁺-induced polarization, which inhibits solvent reduction and increases the inorganic content of SEI (Figure 11b) [153].

For Si anode-targeted WSEs design, a solvent engineering strategy could be employed to reduce Li⁺-solvent coordination strength, enabling anion-dominated interfacial chemistry and enhanced electrochemical stability. However, traditional solvents usually have strong solvation capabilities, requiring deliberate modification to meet weak solvation criteria. Methods to reduce the solvent solvation ability include fluorination with electron-withdrawing F atoms to reduce solvent basicity, introducing spatial hindrance at the ends of solvent molecules through the addition of certain groups such as methyl groups to physically block coordination sites, and reducing ionophilic groups (-O-, -S-, and -NH₂, etc.) within the solvent molecules themselves (Figure 11c). Cao et al. demonstrated the fluorinated WSE design principle through engineering electrolytes using 1 M LiFSI in fluorinated FEC/bis(2,2,2-trifluoroethyl)carbonate (BTFC)/ETFA [27]. The trifluoromethyl group (-CF₃) in ETFA exerts a strong electron-withdrawing effect, which reduces the electron density of the carbonyl oxygen. With ultra-low DN (DN = 2.1), low viscosity (0.3 cP), and low freezing point (-78 °C), this system significantly reduced bulk viscosity by more

than 50% in comparison to conventional EC/DEC. It also improved anion participation in solvation sheaths and encouraged preferential FSI^- reduction for the development of LiF-rich SEI. Consequently, the Si-based batteries retain 81.1% capacity after 200 cycles at room temperature (Figure 11d) and exhibits 971.9 mAh g^{-1} after 200 cycles at -20°C , which demonstrates exceptional low-temperature resilience. The $\text{Si} \parallel \text{NCM532}$ full cell also delivers a high reversible capacity of 102.5 mAh g^{-1} at -20°C (66.6% of its room-temperature capacity) while retaining 50.4% of its capacity after 100 cycles. Fluorinated solvents can also be utilized to lower Li^+ -solvent affinity for optimized WSE compatible with Si anodes. Yang et al. use FEC and DMC to take advantage of differential solvent binding energies [26]. Reduced Li^+ -solvent affinity, rapid Li^+ desolvation kinetics, preferential PF_6^- reduction, and improved PF_6^- coordination in primary solvation shells are all made possible by FEC's lower Li^+ affinity (binding energy: $\sim 35 \text{ kJ mol}^{-1}$ compared to $\sim 50 \text{ kJ mol}^{-1}$ for DMC). These synergistically result in a stable and inorganic-dominant SEI layer with improved protective properties, suppressing parasitic reactions and improving the cycling performance of micro-sized SiO_x electrode (Figure 11e). The $\text{SiO}_x \parallel \text{LiFePO}_4$ full cell delivers a specific discharge capacity of 135.6 mAh g^{-1} and a high energy density of 365 Wh kg^{-1} , while exhibiting outstanding cycling stability with a capacity retention of 83.5% after 300 cycles and an average CE of 99.92% at 0.5 C ($1 \text{ C} = 170 \text{ mA g}^{-1}$).

Building on the strategy of steric engineering for anion-derived SEI, Peng et al. engineered a WSE using ethylene glycol dibutyl ether (EGDE), a linear ether with sterically hindered terminal butyl groups [25]. This steric bulk significantly reduces Li^+ coordination strength, promoting CIPs and AGGs in 2 M $\text{LiPF}_6/\text{EGDE}$. The PF_6^- -rich solvation structures preferentially decompose on μSi anodes, forming a stratified inorganic-rich SEI (Figure 11f,g). The EGDE-based WSE enables a high capacity $> 1800 \text{ mAh g}^{-1}$ after 200 cycles and $> 99.8\%$ CEs after 100 cycles at a current density of 1.0 A g^{-1} for μSi anodes. More importantly, the $\mu\text{Si} \parallel \text{LiFePO}_4$ full cell shows an initial capacity of 130.3 mAh g^{-1} and retains 101.2 mAh g^{-1} after 80 cycles at 0.2 C ($1 \text{ C} = 150 \text{ mA g}^{-1}$), demonstrating performance markedly superior to the baseline system ($134.8 \rightarrow 54.7 \text{ mAh g}^{-1}$). This highlights the exceptional ability of electrolyte to sustain reversible Li^+ storage and maintain interfacial integrity during prolonged cycling. Building upon their exploration of solvent properties for weak solvation and anion-derived SEI, Sang et al. developed a temperature-inert WSE (TIWSE) for μSi anodes by formulating a $\text{LiFSI-LiNO}_3/\text{EA-FEC}$ system that precisely balances ion-ion and ion-dipole interactions [71]. This innovative electrolyte stabilizes the Li^+ solvation sheath to form a temperature-insensitive SEI on μSi anodes, where the high-donor-number NO_3^- anions play a critical role in maintaining anion-enriched solvation structures and mitigating temperature-induced structural degradation (Figure 11h,i). Consequently, $\mu\text{Si} \parallel \text{NCM811}$ full cells employing TIWSE exhibited excellent capacity retention—91.8% at -20°C and 80.8% at 30°C after 100 cycles (Figure 11j)—with a specific capacity of 137.4 mAh g^{-1} at a 6 C . This study provides valuable insights into the rational design of electrolytes for low-temperature Si-based LIBs, thereby advancing the development of high-energy-density LIBs.

Collectively, these studies establish WSEs as a versatile design paradigm for Si anode. Through strategic molecular engineering—fluorination, steric hindrance, solvent affinity tuning, or cyclic architecture—researchers have systematically weakened Li^+ solvation while promoting anion-derived interphase formation. This approach directly addresses the interfacial degradation challenges of Si anodes, enabling exceptional cycling stability and rate capability across multiple electrolyte systems.

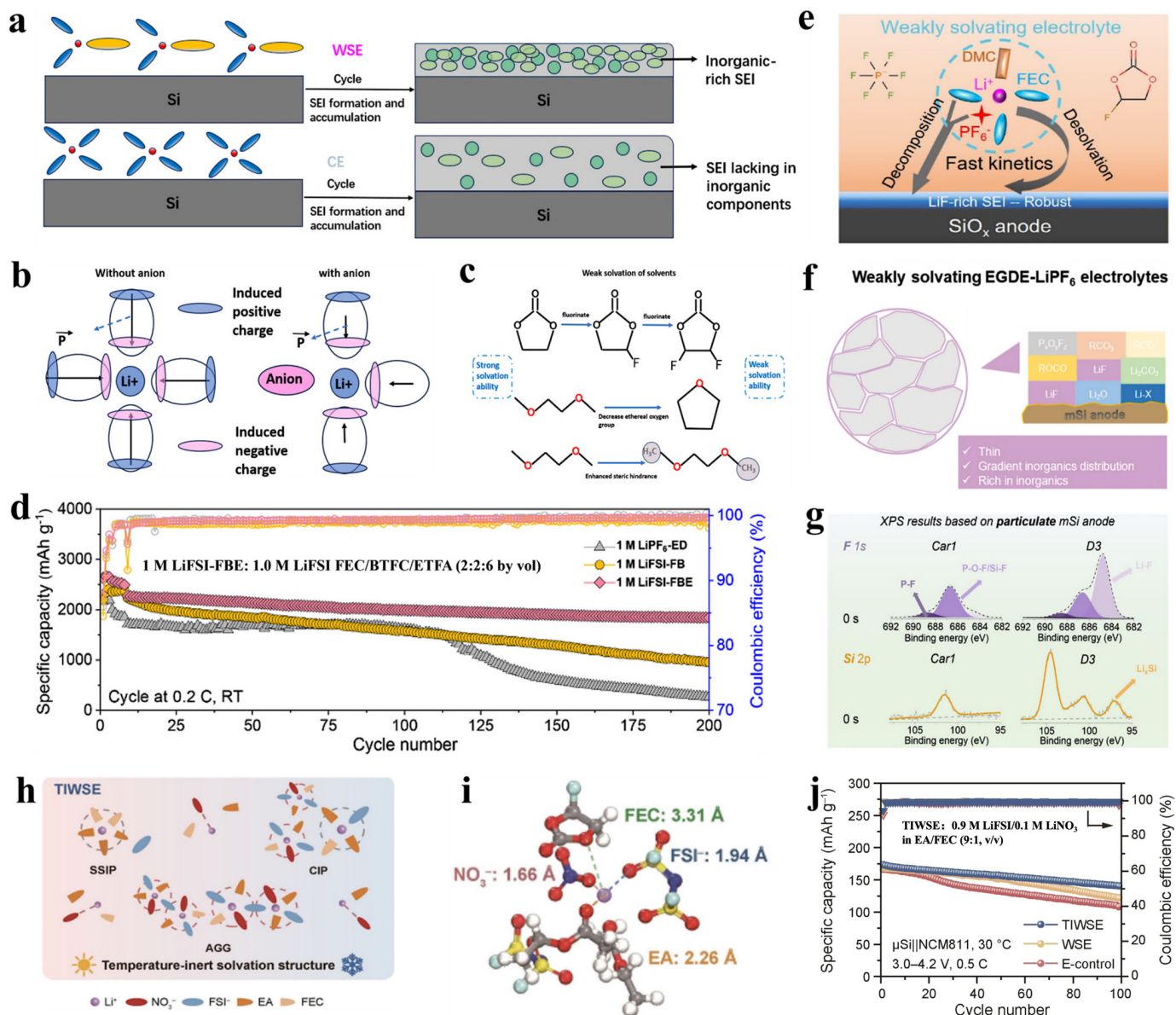


Figure 11. The effects of WSEs on Si anodes. (a) Comparison of SEI layers formed by WSEs and conventional electrolytes [110]. Copyright 2023, Tsinghua University Press. (b) Schematic of Li^+ solvation structure and polarization effects of solvent molecules [153]. Copyright 2022, Wiley. (c) Molecular design strategies for weakly solvating solvents. (d) Long-term cycling capability and CE values of $\text{Li} \parallel \text{Si}$ cells at 0.2 C [27]. Copyright 2022, American Chemical Society. (e) Schematic illustration of Li^+ solvation sheath structure and SEI composition in WSEs system [26]. Copyright 2023, Elsevier. (f) Characteristics of SEI formed in EGDE-LiPF₆-based electrolyte [25]. (g) F 1s and Si 2p XPS spectra of Si anodes cycled in different electrolytes without etching [25]. Copyright 2023, American Chemical Society. (h) Schematic of temperature-inert solvation structure in TIWSE as the temperature decreases [71]. (i) Representative solvation structure of TIWSE and the distances between Li^+ and coordinated components [71]. (j) Cycling performance of $\mu\text{Si} \parallel \text{NCM811}$ full cells with different electrolytes [71]. Copyright 2025, Wiley.

Despite promising results, the development of WSEs remains nascent. Current research mainly focuses on specific solvent and Li salt combinations, with insufficient understanding of the structure–property relationships and an absence of unified design principles. Further efforts on machine learning-guided solvent screening, polymerization-controlled SEI engineering, and decoupled electrolyte systems are encouraged to resolve the current

challenges. Such fundamental advances will transform WSEs from exploratory solutions into rationally designed electrolyte platforms for next-generation batteries.

3.4. In Situ Gel Polymer Electrolytes

While the study demonstrates the efficacy of advanced liquid electrolytes through solvation structure engineering, alternative strategies such as in situ polymerized gel polymer electrolytes (GPEs) have emerged as a promising integrated approach to address the interfacial instability issues of both Si anodes and high-voltage cathodes. Unlike conventional liquid electrolytes (LEs) that struggle to simultaneously meet requirements for mechanical strength, ionic conductivity, and interfacial stability, GPEs offer a unique combination of these attributes.

Recently, Bai et al. reported a fluorine-free GPE (PVCM-GPE) constructed via in situ polymerization of cyclic poly(vinylene carbonate) (PVCM) and LiDFOB. The highly elastic PVCM matrix (tensile strength ~39.5 MPa), coupled with a spatially hierarchical structured Si/C@C anode, effectively dissipates the enormous stress of Si during cycling [154]. Furthermore, this GPE achieves an ionic conductivity comparable to that of LEs (8.61×10^{-4} S cm⁻¹ at 25 °C) and increases the Li⁺ transference number to 0.45 (compared to 0.33 in LEs), which helps reduce polarization and suppress dendrite growth. A 2.7 Ah Si/C@C-Gr || NMC811 pouch full cell employing this GPE retained 88.7% capacity retention after 2000 cycles at 0.5 C, delivering a high gravimetric energy density of 325.9 Wh kg⁻¹. Similarly, Liu et al. reported a quasi-solid GPE (QSGPE) based on in situ copolymerization of *N,N'*-methylenebis(acrylamide) (NMBA) and nanosized silica resin (NR) [69]. After polymerization within the electrode, the resulting polymer chains (PNMBA) chains interact with pre-existing polyacrylic acid (PAA) binder through multiple hydrogen bonds, significantly enhancing the overall strength, toughness, and adhesion of the electrode. Stress-strain tests show that the fracture strain of the PAA-PNMBA composite film reaches 667%, far exceeding that of pure PAA film (320%), enabling effective adaptation to the large volume changes of Si particles.

Collectively, the works by Bai and Liu et al. underscore the design flexibility and immense potential of in situ polymerization for creating integrated GPE systems. This approach represents a paradigm shift toward structurally robust and intrinsically safe batteries. Meanwhile, the liquid-electrolyte strategy explored in this review offers a complementary, yet equally vital route that achieves ultra-stable interphases through precise solvation structure control, prioritizing exceptional rate capability and manufacturing simplicity. Both strategies are indispensable and likely to converge in the pursuit of practical, high-energy-density batteries.

3.5. Comparative Analysis and Outlook

The exploration of HCEs, LHCEs, WSEs, and in situ GPEs represents a multifaceted effort to overcome the interfacial instability of Si anodes, each adopting distinct mechanistic principles and exhibiting characteristic trade-offs.

HCEs establish the fundamental principle of using high salt concentration to promote anion-derived, inorganic-rich SEI. However, their benefits are counterbalanced by high viscosity, limited wettability, and elevated cost, which impedes large-scale implementation. LHCEs ingeniously mitigate these drawbacks by employing inert diluents to create a locally concentrated environment while maintaining bulk transport properties. This strategy preserves the interfacial advantages of HCEs yet introduces new challenges, including formulation complexity and high diluent cost. WSEs achieve similar interfacial outcomes through molecular-level solvent design, wherein low donor-number solvents facilitate anion participation even at moderate concentrations. While avoiding the severe

viscosity penalties of HCEs and the diluent dependency of LHCEs, WSEs suffer from moderate ionic conductivity due to poor salt dissociation, synthetic complexity, environmental concerns, and limited stability against high-voltage cathodes. In situ GPEs represent an integrated structural–interfacial strategy. By forming a solid-like polymer network within the cell, they simultaneously provide superior mechanical strength to suppress electrode pulverization and maintain intimate interfacial contact. While potentially sacrificing some rate performance compared to advanced liquid systems and facing challenges in uniform polymerization, GPEs are unparalleled in enhancing safety and electrode integrity.

In conclusion, the current landscape of electrolyte and interphase engineering is diverging yet complementary, encompassing two converging paradigms: (i) advanced liquid-state electrolytes (HCEs, LHCEs, WSEs), which prioritize ultra-stable interphases and fast ion transport through precise solvation control; and (ii) integrated polymer systems (in situ GPEs), which emphasizes structural robustness, interfacial cohesion, and intrinsic safety. The optimal electrolyte strategy ultimately depends on targeted performance metrics regarding energy density, power density, cycle life, and safety. Looking forward, the integration of weakly solvating concepts into polymer matrices represents a promising direction toward next-generation hybrid electrolytes capable of meeting the multifaceted demands of high-energy-density Si-based batteries.

4. Summary and Outlook

Compared with the well-established Gr anodes, Si anodes remain an emerging technology facing significant challenges. The core issue lies in severe volume expansion during cycling, which induces repeated rupture of the SEI, leading to rapid capacity degradation. While strategies such as binder optimization, artificial SEI construction, and Si-C composites offer partial solutions electrolyte engineering emerges as a critical pathway to stabilize Si interfaces. This review systematically analyzes mechanism of electrolyte components—Li salts, solvents, and additives—in mitigating Si anode degradation. Key findings reveal that ether-based solvents exhibit excellent performance in HCEs and LHCEs due to their low reduction potential. However, high costs and excessive Li salt consumption limit their practicality. Additives in Si-based electrolytes have the potential to significantly enhance cycling stability by forming mechanically robust SEI layers or scavenging harmful species. More importantly, WSEs achieve high performance in Si-based batteries at conventional concentrations, presenting a promising direction for future electrolyte design. To advance commercially viable Si anodes, six key research priorities are outlined:

1. Lithium salt innovation

The limited repertoire of commercially viable salts (LiPF_6 , LiFSI , LiTFSI , LiDFOB) restricts anion-derived SEI design. Novel salts must overcome intrinsic limitations—low solubility (<0.5 M), inadequate oxidation stability (<4.3 V), and poor thermal resilience—while enabling anion-enriched solvation sheaths. The target is to develop salts with oxidative stability > 4.5 V and solubility over 2 M [155,156].

2. Additive mechanism elucidation

While additives enhance SEI stability, their decomposition pathways and interactions with Si interfaces remain poorly understood. Fundamental studies on functional group breakdown (e.g., C-F, B-O, Si-O) at electrode surfaces are essential to design next-generation additives. The target is to establish structure–property relationships linking molecular motifs to SEI elasticity (modulus > 1 GPa) and ionic conductivity [81].

3. Toward cost-effective electrolyte systems

While HCE, LHCE, WSE strategies significantly improve electrochemical performance, they currently rely on high salts loadings or costly fluorinated solvents (e.g.,

BTFE/TTE > \$500 kg⁻¹), which hinder large-scale deployment. Future research should prioritize formulations that deliver high energy density (>400 Wh kg⁻¹) at conventional concentrations (1–1.5 M). The ultimate goal is to achieve > 90% capacity retention after 500 cycles with electrolyte costs lower than \$50 kg⁻¹.

4. Environmental sustainability

Current electrolytes contain ecotoxic solvents (e.g., cyclic carbonates) and fluorinated compounds. Developing bio-derived solvents (e.g., γ -valerolactone), halogen-free additives, and recyclable electrolytes is imperative. The target is to replace > 90% of fluorinated components with green alternatives while maintaining electrochemical performance [157].

5. AI-driven electrolyte design

Machine learning (ML) can accelerate the discovery of novel components by predicting key parameters such as LUMO energy, viscosity, and SEI formation tendency. Cross-disciplinary collaboration across material science, computational chemistry, and AI is required to build ML models trained on multi-scale datasets. The target is to enable high-throughput screening of $\sim 10^6$ candidate molecules with >95% prediction accuracy [158,159].

6. Integrated material-electrolyte optimization

Combining electrolyte engineering with advanced Si material design—nanostructuring, porous architectures, and self-healing binders—will provide synergistic improvements [14]. Emphasis should be placed on scalable manufacturing processes to bridge lab-scale innovations with industrial implementation. The target is to deliver full cells with Si-dominant anodes (>80% Si) achieving 1000 stable cycles under wide-temperature operation.

Author Contributions: Conceptualization, C.X., T.H. and X.Y.; data curation, D.L., X.Z. (Xianting Zhao) and Y.Z.; writing—original draft preparation, T.H.; writing—review and writing, C.X. and X.Y.; supervision, X.Z. (Xianhui Zhang); project administration, X.Z. (Xianhui Zhang); funding acquisition, X.Z. (Xianhui Zhang). All authors have read and agreed to the published version of the manuscript.

Funding: This work was financially supported by the Natural Science Foundation of Fujian Province (2024J01301), the Award Program for Fujian Minjiang Scholar Professorship and the Hundred Talents Plan of Fujian Province.

Data Availability Statement: No new data were created or analyzed in this study. Data sharing is not applicable to this article.

Conflicts of Interest: The authors declare no conflicts of interest.

Abbreviations

The following abbreviations are used in this manuscript:

AFM	Atomic Force Microscopy
BHT	Butylhydroxytoluene
CEI	Cathode Electrolyte Interface
CPI	Cyclopentyl Isocyanate
DMC	Dimethyl Carbonate
DMDOS	Dimethoxysilane
DN	Donor Number
EVs	Electric Vehicles
Gr	Graphite
HOMO	Highest Occupied Molecular Orbital
IEM	Isocyanate Methacrylate
LIBs	Lithium-ion batteries

LUMO	Lowest Unoccupied Molecular Orbital
MEC	Methylene Ethylene Carbonate
NCM811	$\text{LiNi}_{0.8}\text{Co}_{0.1}\text{Mn}_{0.1}\text{O}_2$
SEM	Scanning Electron Microscope
SL	Sulfolane
μSi	Si Microparticles
SiNWs	Si Nanowires
TEOS	Tetraethoxysilane
TEP	Triethyl Phosphate
TMP	Trimethyl Phosphate
TPP	Triphenylphosphine
VC	Vinylene Carbonate
XPS	X-ray photoelectron spectroscopy

References

- Winter, M.; Barnett, B.; Xu, K. Before Li Ion Batteries. *Chem. Rev.* **2018**, *118*, 11433–11456. [[CrossRef](#)] [[PubMed](#)]
- Durmus, Y.E.; Zhang, H.; Baakes, F.; Desmaizieres, G.; Hayun, H.; Yang, L.; Kolek, M.; Küpers, V.; Janek, J.; Mandler, D.; et al. Side by Side Battery Technologies with Lithium-Ion Based Batteries. *Adv. Energy Mater.* **2020**, *10*, 2000089. [[CrossRef](#)]
- Li, P.; Zhang, Z.; Zhao, Z.; Zhang, X.; Zhang, H.; Li, G. Localized Medium Concentration Electrolyte with Fast Kinetics for Lithium Metal Batteries. *Angew. Chem. Int. Ed.* **2024**, *63*, e202319090. [[CrossRef](#)] [[PubMed](#)]
- Xu, K. Electrolytes and Interphases in Li-Ion Batteries and Beyond. *Chem. Rev.* **2014**, *114*, 11503–11618. [[CrossRef](#)]
- Oznam, F.; Rosso, M. Silicon as Anode Material for Li-Ion Batteries. *Mater. Sci. Eng. B* **2016**, *213*, 2–11. [[CrossRef](#)]
- Jin, Y.; Zhu, B.; Lu, Z.; Liu, N.; Zhu, J. Challenges and Recent Progress in the Development of Si Anodes for Lithium-Ion Battery. *Adv. Energy Mater.* **2017**, *7*, 1700715. [[CrossRef](#)]
- Ge, M.; Cao, C.; Biesold, G.M.; Sewell, C.D.; Hao, S.-M.; Huang, J.; Zhang, W.; Lai, Y.; Lin, Z. Recent Advances in Silicon-Based Electrodes: From Fundamental Research toward Practical Applications. *Adv. Mater.* **2021**, *33*, 2004577. [[CrossRef](#)]
- Heine, J.; Hilbig, P.; Qi, X.; Niehoff, P.; Winter, M.; Bieker, P. Fluoroethylene Carbonate as Electrolyte Additive in Tetraethylene Glycol Dimethyl Ether Based Electrolytes for Application in Lithium Ion and Lithium Metal Batteries. *J. Electrochem. Soc.* **2015**, *162*, A1094–A1101. [[CrossRef](#)]
- Winter, M. The Solid Electrolyte Interphase—The Most Important and the Least Understood Solid Electrolyte in Rechargeable Li Batteries. *Z. Phys. Chem.* **2009**, *223*, 1395–1406. [[CrossRef](#)]
- Winter, M.; Appel, W.K.; Evers, B.; Hodal, T.; MoÈller, K.-C.; Schneider, I.; Wachtler, M.; Wagner, M.R.; Wrodnigg, G.H. Studies on the Anode/Electrolyte Interface in Lithium Ion Batteries. *Monatsh. Chem.* **2001**, *132*, 473–486. [[CrossRef](#)]
- Holtstiege, F.; Wilken, A.; Winter, M.; Placke, T. Running out of Lithium? A Route to Differentiate between Capacity Losses and Active Lithium Losses in Lithium-Ion Batteries. *Phys. Chem. Chem. Phys.* **2017**, *19*, 25905–25918. [[CrossRef](#)] [[PubMed](#)]
- Feng, K.; Li, M.; Liu, W.; Kashkooli, A.G.; Xiao, X.; Cai, M.; Chen, Z. Silicon-Based Anodes for Lithium-Ion Batteries: From Fundamentals to Practical Applications. *Small* **2018**, *14*, 1702737. [[CrossRef](#)] [[PubMed](#)]
- Schmuck, R.; Wagner, R.; Höpel, G.; Placke, T.; Winter, M. Performance and Cost of Materials for Lithium-Based Rechargeable Automotive Batteries. *Nat. Energy* **2018**, *3*, 267–278. [[CrossRef](#)]
- He, J. Sieving Pore Design Enables Stable and Fast Alloying Chemistry of Silicon Negative Electrodes in Li-Ion Batteries. *Nat. Commun.* **2025**, *16*, 4858. [[CrossRef](#)]
- Chan, C.K.; Peng, H.; Liu, G.; McIlwrath, K.; Zhang, X.F.; Huggins, R.A.; Cui, Y. High-Performance Lithium Battery Anodes Using Silicon Nanowires. *Nat. Nanotechnol.* **2008**, *3*, 31–35. [[CrossRef](#)]
- An, W.; Gao, B.; Mei, S.; Xiang, B.; Fu, J.; Wang, L.; Zhang, Q.; Chu, P.K.; Huo, K. Scalable Synthesis of Ant-Nest-like Bulk Porous Silicon for High-Performance Lithium-Ion Battery Anodes. *Nat. Commun.* **2019**, *10*, 1447. [[CrossRef](#)]
- Dou, F.; Chang, Y.; Zhang, Y.; Li, Q.; Chen, T.-Y.; Yan, Y.; Sun, Y.; Guo, X.; Yin, C.; Zhou, H.; et al. Improving Electron and Ion Transport in Nano-Si Anodes through Integration with Conductive Nano-Metal–Organic Frameworks. *Nano Lett.* **2025**, *25*, 8915–8922. [[CrossRef](#)]
- Tong, Y.; Jin, S.; Xu, H.; Li, J.; Kong, Z.; Jin, H.; Xu, H. An Energy Dissipative Binder for Self-Tuning Silicon Anodes in Lithium-Ion Batteries. *Adv. Sci.* **2023**, *10*, 2205443. [[CrossRef](#)]
- Yang, Y.; Wang, J.; Kim, S.C.; Zhang, W.; Peng, Y.; Zhang, P.; Vilá, R.A.; Ma, Y.; Jeong, Y.K.; Cui, Y. In Situ Prelithiation by Direct Integration of Lithium Mesh into Battery Cells. *Nano Lett.* **2023**, *23*, 5042–5047. [[CrossRef](#)]
- Mu, T.; Zhao, Y.; Zhao, C.; Holmes, N.G.; Lou, S.; Li, J.; Li, W.; He, M.; Sun, Y.; Du, C.; et al. Stable Silicon Anodes by Molecular Layer Deposited Artificial Zirconia Coatings. *Adv. Funct. Mater.* **2021**, *31*, 2010526. [[CrossRef](#)]

21. Szczech, J.R.; Jin, S. Nanostructured Silicon for High Capacity Lithium Battery Anodes. *Energy Environ. Sci.* **2011**, *4*, 56–72. [[CrossRef](#)]
22. Song, W.; Chae, O.B. Surface-Coating Strategies of Si-Negative Electrode Materials in Lithium-Ion Batteries. *Batteries* **2024**, *10*, 327. [[CrossRef](#)]
23. Wang, X.; Li, Y.; Wang, X.; Gan, Q.; Wang, Z.; Liao, K.; Wu, S.; Guo, H.; Li, J.; Huang, B.; et al. Carbon-Coating Strengthens the Solid Electrolyte Interphase to Inhibit Si Pulverization. *J. Mater. Chem. A* **2023**, *11*, 9807–9815. [[CrossRef](#)]
24. Li, L.; Du, B.; Yang, Y.; Ye, S.; Huang, T.; Huang, S.; Ren, X.; Hu, J.; Zhang, Q.; Liu, J. Ionic/Electronic Dual-Conductor Coating Layer Fabrication Enabling High-Performance Silicon Anode. *Small Struct.* **2023**, *4*, 2200296. [[CrossRef](#)]
25. Peng, X.; Liu, B.; Chen, J.; Jian, Q.; Li, Y.; Zhao, T. A Steric-Hindrance-Induced Weakly Solvating Electrolyte Boosting the Cycling Performance of a Micrometer-Sized Silicon Anode. *ACS Energy Lett.* **2023**, *8*, 3586–3594. [[CrossRef](#)]
26. Yang, Y.; Li, Z.; Xu, Y.; Yang, Z.; Zhang, Y.; Wang, J.; Xu, H.; He, X.; Zhao, H. Boosting Fast Electrode Reaction Kinetics of Silicon Suboxide Anodes by Fluoroethylene Carbonate-Based Electrolyte. *J. Power Sources* **2023**, *577*, 233261. [[CrossRef](#)]
27. Cao, Z.; Zheng, X.; Zhou, M.; Zhao, T.; Lv, L.; Li, Y.; Wang, Z.; Luo, W.; Zheng, H. Electrolyte Solvation Engineering toward High-Rate and Low-Temperature Silicon-Based Batteries. *ACS Energy Lett.* **2022**, *7*, 3581–3592. [[CrossRef](#)]
28. Yang, Y.; Yang, Z.; Li, Z.; Wang, J.; He, X.; Zhao, H. Rational Electrolyte Design for Interfacial Chemistry Modulation to Enable Long-Term Cycling Si Anode. *Adv. Energy Mater.* **2023**, *13*, 2302068. [[CrossRef](#)]
29. Seo, H.; Kim, D.; Park, S.; Seo, E.; Kim, P.; Choi, J.; Yoo, J. A Comprehensive Review of Liquid Electrolytes for Silicon Anodes in Lithium-Ion Batteries. *Adv. Ind. Eng. Chem.* **2025**, *1*, 3. [[CrossRef](#)]
30. Lv, L.; Wang, Y.; Huang, W.; Wang, Y.; Zhu, G.; Zheng, H. Effect of Lithium Salt Type on Silicon Anode for Lithium-Ion Batteries. *Electrochim. Acta* **2022**, *413*, 140159. [[CrossRef](#)]
31. Chen, J.; Fan, X.; Li, Q.; Yang, H.; Khoshi, M.R.; Xu, Y.; Hwang, S.; Chen, L.; Ji, X.; Yang, C.; et al. Electrolyte Design for LiF-Rich Solid-Electrolyte Interfaces to Enable High-Performance Microsized Alloy Anodes for Batteries. *Nat. Energy* **2020**, *5*, 386–397. [[CrossRef](#)]
32. Cora, S.; Key, B.; Vaughey, J.; Sa, N. Electrolyte Role in SEI Evolution at Si in the Pre-Lithiation Stage vs the Post-Lithiation Stage. *J. Electrochem. Soc.* **2023**, *170*, 020507. [[CrossRef](#)]
33. Philippe, B.; Dedryvère, R.; Gorgoi, M.; Rensmo, H.; Gonbeau, D.; Edström, K. Improved Performances of Nanosilicon Electrodes Using the Salt LiFSI: A Photoelectron Spectroscopy Study. *J. Am. Chem. Soc.* **2013**, *135*, 9829–9842. [[CrossRef](#)]
34. Choi, N.-S.; Yew, K.H.; Kim, H.; Kim, S.-S.; Choi, W.-U. Surface Layer Formed on Silicon Thin-Film Electrode in Lithium Bis(Oxalato) Borate-Based Electrolyte. *J. Power Sources* **2007**, *172*, 404–409. [[CrossRef](#)]
35. Lindgren, F.; Xu, C.; Niedzicki, L.; Marcinek, M.; Gustafsson, T.; Björefors, F.; Edström, K.; Younesi, R. SEI Formation and Interfacial Stability of a Si Electrode in a LiTDI-Salt Based Electrolyte with FEC and VC Additives for Li-Ion Batteries. *ACS Appl. Mater. Interfaces* **2016**, *8*, 15758–15766. [[CrossRef](#)]
36. Li, Q.; Ruan, J.; Weng, S.; Zhang, X.; Hu, J.; Li, H.; Sun, D.; Wang, X.; Fang, F.; Wang, F. Interphasial Pre-Lithiation and Reinforcement of Micro-Si Anode through Fluorine-Free Electrolytes. *Angew. Chem. Int. Ed.* **2023**, *62*, e202310297. [[CrossRef](#)]
37. Wu, B.; Chen, C.; Danilov, D.L.; Jiang, M.; Raijmakers, L.H.J.; Eichel, R.-A.; Notten, P.H.L. Influence of the SEI Formation on the Stability and Lithium Diffusion in Si Electrodes. *ACS Omega* **2022**, *7*, 32740–32748. [[CrossRef](#)]
38. Li, A.-M. Asymmetric Electrolyte Design for High-Energy Lithium-Ion Batteries with Micro-Sized Alloying Anodes. *Nat. Energy* **2024**, *9*, 1551–1560. [[CrossRef](#)]
39. Spotte-Smith, E.W.C.; Petrocelli, T.B.; Patel, H.D.; Blau, S.M.; Persson, K.A. Elementary Decomposition Mechanisms of Lithium Hexafluorophosphate in Battery Electrolytes and Interphases. *ACS Energy Lett.* **2023**, *8*, 347–355. [[CrossRef](#)]
40. Wang, J.; Zheng, Q.; Fang, M.; Ko, S.; Yamada, Y.; Yamada, A. Concentrated Electrolytes Widen the Operating Temperature Range of Lithium-Ion Batteries. *Adv. Sci.* **2021**, *8*, 2101646. [[CrossRef](#)] [[PubMed](#)]
41. Xu, G.; Shangguan, X.; Dong, S.; Zhou, X.; Cui, G. Formulierung von Elektrolyten mit gemischten Lithiumsalzen für Lithium-Batterien. *Angew. Chem. Int. Ed.* **2020**, *132*, 3426–3442. [[CrossRef](#)]
42. Zhang, S.S. A Review on Electrolyte Additives for Lithium-Ion Batteries. *J. Power Sources* **2006**, *162*, 1379–1394. [[CrossRef](#)]
43. Jia, H.; Zou, L.; Gao, P.; Cao, X.; Zhao, W.; He, Y.; Engelhard, M.H.; Burton, S.D.; Wang, H.; Ren, X.; et al. High-Performance Silicon Anodes Enabled By Nonflammable Localized High-Concentration Electrolytes. *Adv. Energy Mater.* **2019**, *9*, 1900784. [[CrossRef](#)]
44. Chae, S.; Kwak, W.-J.; Han, K.S.; Li, S.; Engelhard, M.H.; Hu, J.; Wang, C.; Li, X.; Zhang, J.-G. Rational Design of Electrolytes for Long-Term Cycling of Si Anodes over a Wide Temperature Range. *ACS Energy Lett.* **2021**, *6*, 387–394. [[CrossRef](#)]
45. Kaur, U.; Jaiswal, S.; Cordier, M.; Fokwa, B.P.T.; Ghosh, S. Bridging Bis(Boryl) and Borylene Species Stabilized in the Coordination Sphere of Ruthenium Metals. *Organometallics* **2024**, *43*, 617–625. [[CrossRef](#)]
46. Liu, X. Probing the Heterogeneous Nature of LiF in Solid-Electrolyte Interphases. *Nature* **2025**, *646*, 102–107. [[CrossRef](#)]
47. Hernández, G.; Mogensen, R.; Younesi, R.; Mindemark, J. Fluorine-Free Electrolytes for Lithium and Sodium Batteries. *Batter. Supercaps* **2022**, *5*, e202100373. [[CrossRef](#)]

48. Martinez De La Hoz, J.M.; Soto, F.A.; Balbuena, P.B. Effect of the Electrolyte Composition on SEI Reactions at Si Anodes of Li-Ion Batteries. *J. Phys. Chem. C* **2015**, *119*, 7060–7068. [[CrossRef](#)]
49. McDowell, M.T.; Lee, S.W.; Nix, W.D.; Cui, Y. 25th Anniversary Article: Understanding the Lithiation of Silicon and Other Alloying Anodes for Lithium-Ion Batteries. *Adv. Mater.* **2013**, *25*, 4966–4985. [[CrossRef](#)]
50. Takata, K. In-Situ Imaging of Li Intercalation in Graphite Particles in an Li-ion Battery. *J. Microsc.* **2017**, *266*, 249–252. [[CrossRef](#)]
51. Borodin, O.; Olguin, M.; Ganesh, P.; Kent, P.R.C.; Allen, J.L.; Henderson, W.A. Competitive Lithium Solvation of Linear and Cyclic Carbonates from Quantum Chemistry. *Phys. Chem. Chem. Phys.* **2016**, *18*, 164–175. [[CrossRef](#)]
52. Yu, R.; Pan, Y.; Jiang, Y.; Zhou, L.; Zhao, D.; Van Tendeloo, G.; Wu, J.; Mai, L. Regulating Lithium Transfer Pathway to Avoid Capacity Fading of Nano Si Through Sub-Nano Scale Interfused SiO_x/C Coating. *Adv. Mater.* **2023**, *35*, 2306504. [[CrossRef](#)] [[PubMed](#)]
53. Shin, H.; Park, J.; Han, S.; Sastry, A.M.; Lu, W. Component-/Structure-Dependent Elasticity of Solid Electrolyte Interphase Layer in Li-Ion Batteries: Experimental and Computational Studies. *J. Power Sources* **2015**, *277*, 169–179. [[CrossRef](#)]
54. Jin, Y.; Kneusels, N.-J.H.; Marbella, L.E.; Castillo-Martínez, E.; Magusin, P.C.M.M.; Weatherup, R.S.; Jónsson, E.; Liu, T.; Paul, S.; Grey, C.P. Understanding Fluoroethylene Carbonate and Vinylene Carbonate Based Electrolytes for Si Anodes in Lithium Ion Batteries with NMR Spectroscopy. *J. Am. Chem. Soc.* **2018**, *140*, 9854–9867. [[CrossRef](#)] [[PubMed](#)]
55. Liu, Y.; Huang, Y.; Xu, X.; Liu, Y.; Yang, J.; Lai, J.; Shi, J.; Wang, S.; Fan, W.; Cai, Y.; et al. Fluorinated Solvent-Coupled Anion-Derived Interphase to Stabilize Silicon Microparticle Anodes for High-Energy-Density Batteries. *Adv. Funct. Mater.* **2023**, *33*, 2303667. [[CrossRef](#)]
56. Ma, Z.; Ruan, D.; Wang, D.; Lu, Z.; He, Z.; Guo, J.; Fan, J.; Jiang, J.; Wang, Z.; Luo, X.; et al. Selective Methylation of Cyclic Ether Towards Highly Elastic Solid Electrolyte Interphase for Silicon-based Anodes. *Angew. Chem. Int. Ed.* **2024**, *137*, e202414859. [[CrossRef](#)]
57. Liu, J.; Ihuaenyi, S.; Kuphal, R.; Salinas, J.; Xie, L.; Yang, L.; Janakiraman, U.; Fortier, M.E.; Fang, C. A Comparison of Carbonate-Based and Ether-Based Electrolyte Systems for Lithium Metal Batteries. *J. Electrochem. Soc.* **2023**, *170*, 010535. [[CrossRef](#)]
58. Wang, Z.; Chen, C.; Wang, D.; Zhu, Y.; Zhang, B. Stabilizing Interfaces in High-Temperature NCM811-Li Batteries via Tuning Terminal Alkyl Chains of Ether Solvents. *Angew. Chem. Int. Ed.* **2023**, *62*, e202303950. [[CrossRef](#)]
59. Yamada, Y.; Furukawa, K.; Sodeyama, K.; Kikuchi, K.; Yaegashi, M.; Tateyama, Y.; Yamada, A. Unusual Stability of Acetonitrile-Based Superconcentrated Electrolytes for Fast-Charging Lithium-Ion Batteries. *J. Am. Chem. Soc.* **2014**, *136*, 5039–5046. [[CrossRef](#)]
60. Xue, Y.; Wang, Y.; Zhang, H.; Kong, W.; Zhou, Y.; Kang, B.; Huang, Z.; Xiang, H. Molecular Design of Mono-Fluorinated Ether-Based Electrolyte for All-Climate Lithium-Ion Batteries and Lithium-Metal Batteries. *Angew. Chem. Int. Ed.* **2025**, *64*, e202414201. [[CrossRef](#)]
61. Feng, Y.-H.; Lin, C.; Qin, H.; Wei, G.-X.; Yang, C.; Tang, Y.; Zhu, X.; Sun, S.; Chen, T.-L.; Liu, M.; et al. Cation–Anion Regulation Engineering in a Flame-Retardant Electrolyte toward Safe Na-Ion Batteries with Appealing Stability. *J. Am. Chem. Soc.* **2025**, *147*, 16107–16118. [[CrossRef](#)] [[PubMed](#)]
62. Tian, Y.-F.; Tan, S.-J.; Yang, C.; Zhao, Y.-M.; Xu, D.-X.; Lu, Z.-Y.; Li, G.; Li, J.-Y.; Zhang, X.-S.; Zhang, C.-H.; et al. Tailoring Chemical Composition of Solid Electrolyte Interphase by Selective Dissolution for Long-Life Micron-Sized Silicon Anode. *Nat. Commun.* **2023**, *14*, 7247. [[CrossRef](#)] [[PubMed](#)]
63. Li, A.-M.; Wang, Z.; Pollard, T.P.; Zhang, W.; Tan, S.; Li, T.; Jayawardana, C.; Liou, S.-C.; Rao, J.; Lucht, B.L.; et al. High Voltage Electrolytes for Lithium-Ion Batteries with Micro-Sized Silicon Anodes. *Nat. Commun.* **2024**, *15*, 1206. [[CrossRef](#)] [[PubMed](#)]
64. Yang, S.; Zhang, Y.; Li, Z.; Takenaka, N.; Liu, Y.; Zou, H.; Chen, W.; Du, M.; Hong, X.-J.; Shang, R.; et al. Rational Electrolyte Design to Form Inorganic–Polymeric Interphase on Silicon-Based Anodes. *ACS Energy Lett.* **2021**, *6*, 1811–1820. [[CrossRef](#)]
65. Li, M.; Li, S.; Yan, D.; Ma, Y.; Niu, X.; Wang, L. Electrolyte Design Weakens Lithium-Ion Solvation for a Fast-Charging and Long-Cycling Si Anode. *Chem. Sci.* **2025**, *16*, 2609–2618. [[CrossRef](#)]
66. Kim, J.; Hyun, J.; Kim, S.; Park, W.H.; Yu, S. Phosphorus-Based Flame-Retardant Electrolytes for Lithium Batteries. *Adv. Energy Mater.* **2025**, *15*, 2500587. [[CrossRef](#)]
67. Zhang, K.; Tian, Y.; Wei, C.; An, Y.; Feng, J. Building Stable Solid Electrolyte Interphases (SEI) for Microsized Silicon Anode and 5V-Class Cathode with Salt Engineered Nonflammable Phosphate-Based Lithium-Ion Battery Electrolyte. *Appl. Surf. Sci.* **2021**, *553*, 149566. [[CrossRef](#)]
68. Jing, K.; Wang, W.; Wang, S.; Ma, H.; Song, R.; Liang, K.; Cai, S.; Ren, Y.; Li, J.; Ding, Z. High Solid and Conductivity Solid Electrolyte Interface Regulated by Novel Silane Additive for High-Performance Si/C Anode at -20°C 2025. *Electrochim. Acta* **2025**, *536*, 146696. [[CrossRef](#)]
69. Liu, Q.; Feng, Y.; Liu, J.; Liu, Y.; Cui, X.; He, Y.-J.; Nuli, Y.; Wang, J.; Yang, J. In Situ Integration of a Flame Retardant Quasisolid Gel Polymer Electrolyte with a Si-Based Anode for High-Energy Li-Ion Batteries. *ACS Nano* **2024**, *18*, 13384–13396. [[CrossRef](#)]
70. Huang, X.; Shea, J.; Liu, J.; Hagh, N.M.; Nageswaran, S.; Wang, J.; Wu, X.; Kwon, G.; Son, S.-B.; Liu, T.; et al. Comparative Study of Vinylene Carbonate and Lithium Difluoro(Oxalate)Borate Additives in a $\text{SiO}_x/\text{Graphite}$ Anode Lithium-Ion Battery in the Presence of Fluoroethylene Carbonate. *ACS Appl. Mater. Interfaces* **2025**, *17*, 7648–7656. [[CrossRef](#)]

71. Sang, X.; Hu, K.; Chen, J.; Wang, Z.; Xu, H.; Huang, Y.; Hu, X. Temperature-Inert Weakly Solvating Electrolytes for Low-Temperature Lithium-Ion Batteries with Micro-Sized Silicon Anodes. *Angew. Chem. Int. Ed.* **2025**, *64*, e202500367. [CrossRef]
72. Park, S.; Kim, S.; Lee, J.-A.; Ue, M.; Choi, N.-S. Liquid Electrolyte Chemistries for Solid Electrolyte Interphase Construction on Silicon and Lithium-Metal Anodes. *Chem. Sci.* **2023**, *14*, 9996–10024. [CrossRef] [PubMed]
73. Yang, Y.; Li, Z.; Zhang, M.; Wang, J.; Wang, Y.; Qiu, J.; Zhao, H. Electrolyte Chemistry Modulation Toward High-Performance and Ultralow-Temperature Silicon Anode. *Adv. Mater.* **2025**, *37*, 2417981. [CrossRef] [PubMed]
74. Wagner-Henke, J.; Kuai, D.; Balbuena, P.B.; Kreuer, U. Understanding the Effect of Vinylene Carbonate on SEI Formation, Morphology and Stability on Lithium Metal Anodes. *ESM* **2025**, *81*, 104434. [CrossRef]
75. Zhang, X.; Cui, Z.; Manthiram, A. Insights into the Crossover Effects in Cells with High-Nickel Layered Oxide Cathodes and Silicon/Graphite Composite Anodes. *Adv. Energy Mater.* **2022**, *12*, 2103611. [CrossRef]
76. Yehye, W.A.; Rahman, N.A.; Ariffin, A.; Abd Hamid, S.B.; Alhadi, A.A.; Kadir, F.A.; Yaeghoobi, M. Understanding the Chemistry behind the Antioxidant Activities of Butylated Hydroxytoluene (BHT): A Review. *Eur. J. Med. Chem.* **2015**, *101*, 295–312. [CrossRef]
77. Dunn, R.P.; Nadimpalli, S.P.V.; Guduru, P.; Lucht, B.L. Flame Retardant Co-Solvent Incorporation into Lithium-Ion Coin Cells with Thin-Film Si Anodes. *J. Electrochem. Soc.* **2014**, *161*, A176–A182. [CrossRef]
78. Rezqita, A.; Sauer, M.; Foelske, A.; Kronberger, H.; Trifonova, A. The Effect of Electrolyte Additives on Electrochemical Performance of Silicon/Mesoporous Carbon (Si/MC) for Anode Materials for Lithium-Ion Batteries. *Electrochim. Acta* **2017**, *247*, 600–609. [CrossRef]
79. Arifiadi, A.; Wichmann, L.; Brake, T.; Lechtenfeld, C.; Buchmann, J.; Demelash, F.; Yan, P.; Brunklaus, G.; Cekic-Laskovic, I.; Wiemers-Meyer, S.; et al. Evaluation of Alternative Lithium Salts for High-Voltage Lithium Ion Batteries: Higher Relevance of Plated Li Morphology Than the Amount of Electrode Crosstalk. *Small* **2025**, *21*, 2410762. [CrossRef]
80. Dalavi, S.; Guduru, P.; Lucht, B.L. Performance Enhancing Electrolyte Additives for Lithium Ion Batteries with Silicon Anodes. *J. Electrochem. Soc.* **2012**, *159*, A642–A646. [CrossRef]
81. Cao, Z.; Zheng, X.; Qu, Q.; Huang, Y.; Zheng, H. Electrolyte Design Enabling a High-Safety and High-Performance Si Anode with a Tailored Electrode–Electrolyte Interphase. *Adv. Mater.* **2021**, *33*, 2103178. [CrossRef]
82. Lee, S.J.; Han, J.-G.; Lee, Y.; Jeong, M.-H.; Shin, W.C.; Ue, M.; Choi, N.-S. A Bi-Functional Lithium Difluoro(Oxalato)Borate Additive for Lithium Cobalt Oxide/Lithium Nickel Manganese Cobalt Oxide Cathodes and Silicon/Graphite Anodes in Lithium-Ion Batteries at Elevated Temperatures. *Electrochim. Acta* **2014**, *137*, 1–8. [CrossRef]
83. Wang, J.; Li, S.; Zhang, J.; Song, L.; Dong, H.; Zhang, N.; Wang, P.; Zhao, D.; Zhang, L.; Cui, X. Improving Toleration of Volume Expansion of Silicon-Based Anode by Constructing a Flexible Solid-Electrolyte Interface Film via Lithium Difluoro(Bisoxalato) Phosphate Electrolyte Additive. *ACS Sustain. Chem. Eng.* **2022**, *10*, 15199–15210. [CrossRef]
84. Nguyen, C.C.; Lucht, B.L. Development of Electrolytes for Si-Graphite Composite Electrodes. *J. Electrochem. Soc.* **2018**, *165*, A2154–A2161. [CrossRef]
85. Chen, S.; Zheng, G.; Yao, X.; Xiao, J.; Zhao, W.; Li, K.; Fang, J.; Jiang, Z.; Huang, Y.; Ji, Y.; et al. Constructing Matching Cathode–Anode Interphases with Improved Chemo-Mechanical Stability for High-Energy Batteries. *ACS Nano* **2024**, *18*, 6600–6611. [CrossRef]
86. Zhuang, X.; Zhang, S.; Cui, Z.; Xie, B.; Gong, T.; Zhang, X.; Li, J.; Wu, R.; Wang, S.; Qiao, L.; et al. Interphase Regulation by Multifunctional Additive Empowering High Energy Lithium-Ion Batteries with Enhanced Cycle Life and Thermal Safety. *Angew. Chem. Int. Ed.* **2024**, *63*, e202315710. [CrossRef]
87. Jagodziński, K.; Cid, R.; Saurel, D.; Bonilla, F.; López Del Amo, J.M.; Gomez Castresana, K.; Asres, N.E.; Mikus-Ostrowska, A.; Casado, N.; Wieczorek, W.; et al. Imidazole-Based LiHDI Salt for SEI Optimization in Silicon Anodes. *J. Power Sources* **2025**, *658*, 238289. [CrossRef]
88. Etacheri, V.; Geiger, U.; Gofer, Y.; Roberts, G.A.; Stefan, I.C.; Fasching, R.; Aurbach, D. Exceptional Electrochemical Performance of Si-Nanowires in 1,3-Dioxolane Solutions: A Surface Chemical Investigation. *Langmuir* **2012**, *28*, 6175–6184. [CrossRef]
89. Asheim, K.; Holsen, I.F.; Renmann, V.; Blanco, M.V.; Vullum, P.E.; Wagner, N.P.; Mæhlen, J.P.; Svensson, A.M. Enabling the Use of Lithium Bis(Trifluoromethanesulfonyl)Imide as Electrolyte Salt for Li-ion Batteries Based on Silicon Anodes and Li(Ni_{0.4}Co_{0.4}Mn_{0.2})O₂ Cathodes by Salt Additives. *Batter. Supercaps* **2024**, *7*, e202300541. [CrossRef]
90. Oh, M.; Kwak, S.; An, K.; Tran, Y.H.T.; Kang, D.G.; Park, S.J.; Lim, G.; Kim, K.; Lee, Y.S.; Song, S. Perfluoro Macroyclic Ether as an Ambifunctional Additive for High-Performance SiO and Nickel 88%-Based High-Energy Li-ion Battery. *Adv. Funct. Mater.* **2023**, *33*, 2212890. [CrossRef]
91. Yang, G.; Frisco, S.; Tao, R.; Philip, N.; Bennett, T.H.; Stetson, C.; Zhang, J.-G.; Han, S.-D.; Teeter, G.; Harvey, S.P.; et al. Robust Solid/Electrolyte Interphase (SEI) Formation on Si Anodes Using Glyme-Based Electrolytes. *ACS Energy Lett.* **2021**, *6*, 1684–1693. [CrossRef]

92. Markevich, E.; Fridman, K.; Sharabi, R.; Elazari, R.; Salitra, G.; Gottlieb, H.E.; Gershinsky, G.; Garsuch, A.; Semrau, G.; Schmidt, M.A.; et al. Amorphous Columnar Silicon Anodes for Advanced High Voltage Lithium Ion Full Cells: Dominant Factors Governing Cycling Performance. *J. Electrochem. Soc.* **2013**, *160*, A1824–A1833. [[CrossRef](#)]
93. Zhang, Y.; Wu, B.; Bi, J.; Zhang, X.; Mu, D.; Zhang, X.; Zhang, L.; Xiao, Y.; Wu, F. Facilitating Prelithiation of Silicon Carbon Anode by Localized High-concentration Electrolyte for High-rate and Long-cycle Lithium Storage. *Carbon Energy* **2024**, *6*, e480. [[CrossRef](#)]
94. Etacheri, V.; Haik, O.; Goffer, Y.; Roberts, G.A.; Stefan, I.C.; Fasching, R.; Aurbach, D. Effect of Fluoroethylene Carbonate (FEC) on the Performance and Surface Chemistry of Si-Nanowire Li-Ion Battery Anodes. *Langmuir* **2012**, *28*, 965–976. [[CrossRef](#)] [[PubMed](#)]
95. Xu, C.; Lindgren, F.; Philippe, B.; Gorgoi, M.; Björefors, F.; Edström, K.; Gustafsson, T. Improved Performance of the Silicon Anode for Li-Ion Batteries: Understanding the Surface Modification Mechanism of Fluoroethylene Carbonate as an Effective Electrolyte Additive. *Chem. Mater.* **2015**, *27*, 2591–2599. [[CrossRef](#)]
96. Nakai, H.; Kubota, T.; Kita, A.; Kawashima, A. Investigation of the Solid Electrolyte Interphase Formed by Fluoroethylene Carbonate on Si Electrodes. *J. Electrochem. Soc.* **2011**, *158*, A798–A801. [[CrossRef](#)]
97. Chen, X.; Li, X.; Mei, D.; Feng, J.; Hu, M.Y.; Hu, J.; Engelhard, M.; Zheng, J.; Xu, W.; Xiao, J.; et al. Reduction Mechanism of Fluoroethylene Carbonate for Stable Solid-Electrolyte Interphase Film on Silicon Anode. *ChemSusChem* **2014**, *7*, 549–554. [[CrossRef](#)]
98. Nie, M.; Abraham, D.P.; Chen, Y.; Bose, A.; Lucht, B.L. Silicon Solid Electrolyte Interphase (SEI) of Lithium Ion Battery Characterized by Microscopy and Spectroscopy. *J. Phys. Chem. C* **2013**, *117*, 13403–13412. [[CrossRef](#)]
99. Schiele, A.; Breitung, B.; Hatsukade, T.; Berkes, B.B.; Hartmann, P.; Janek, J.; Brezesinski, T. The Critical Role of Fluoroethylene Carbonate in the Gassing of Silicon Anodes for Lithium-Ion Batteries. *ACS Energy Lett.* **2017**, *2*, 2228–2233. [[CrossRef](#)]
100. Li, Y.; Cao, Z.; Wang, Y.; Lv, L.; Sun, J.; Xiong, W.; Qu, Q.; Zheng, H. New Insight into the Role of Fluoro-Ethylene Carbonate in Suppressing Li-Trapping for Si Anodes in Lithium-Ion Batteries. *ACS Energy Lett.* **2023**, *8*, 4193–4203. [[CrossRef](#)]
101. Jo, H.; Kim, J.; Nguyen, D.-T.; Kang, K.K.; Jeon, D.-M.; Yang, A.-R.; Song, S.-W. Stabilizing the Solid Electrolyte Interphase Layer and Cycling Performance of Silicon–Graphite Battery Anode by Using a Binary Additive of Fluorinated Carbonates. *J. Phys. Chem. C* **2016**, *120*, 22466–22475. [[CrossRef](#)]
102. Hu, Z.; Zhao, L.; Jiang, T.; Liu, J.; Rashid, A.; Sun, P.; Wang, G.; Yan, C.; Zhang, L. Trifluoropropylene Carbonate-Driven Interface Regulation Enabling Greatly Enhanced Lithium Storage Durability of Silicon-Based Anodes. *Adv. Funct. Mater.* **2019**, *29*, 1906548. [[CrossRef](#)]
103. Karkar, Z.; Houache, M.S.E.; Niketic, S.; Yim, C.-H.; Abu-Lebdeh, Y. Use of Polymeric Borate-Ester Electrolyte Additives to Stabilize the Interface and Enhance the Cycling Performance of Silicon/Graphite Composites in Lithium-Ion Batteries. *ACS Appl. Energy Mater.* **2022**, *5*, 14081–14091. [[CrossRef](#)]
104. He, S.; Huang, S.; Liu, X.; Zeng, X.; Chen, H.; Zhao, L.; Noor, H.; Hou, X. Electrolyte Design for Robust Gradient Solid-Electrolyte Interfaces to Enable High-Performance Silicon Anodes for Pouch Batteries. *CEJ* **2024**, *489*, 150620. [[CrossRef](#)]
105. Kim, J.-M.; Yi, R.; Cao, X.; Xu, Y.; Engelhard, M.; Tripathi, S.; Wang, C.; Zhang, J.-G. Extending Calendar Life of Si-Based Lithium-Ion Batteries by a Localized High Concentration Electrolyte. *ACS Energy Lett.* **2024**, *9*, 2318–2325. [[CrossRef](#)]
106. Quinn, J.; Kim, J.; Yi, R.; Zhang, J.; Xiao, J.; Wang, C. Fluoro-Ethylene-Carbonate Plays a Double-Edged Role on the Stability of Si Anode-Based Rechargeable Batteries During Cycling and Calendar Aging. *Adv. Mater.* **2024**, *36*, 2402625. [[CrossRef](#)]
107. Shen, J.; Chen, H.; Yu, L.; Huang, D.; Luo, Z. 4,5-difluoro-1,3-dioxolan-2-one as an Film Forming Additive on $\text{LiNi}_{0.8}\text{Co}_{0.15}\text{Al}_{0.05}\text{O}_2/\text{SiO}@C$ Full Cells. *J. Electroanal. Chem.* **2019**, *834*, 1–7. [[CrossRef](#)]
108. Ghaur, A.; Peschel, C.; Dienwiebel, I.; Haneke, L.; Du, L.; Profanter, L.; Gomez-Martin, A.; Winter, M.; Nowak, S.; Placke, T. Effective SEI Formation via Phosphazene-Based Electrolyte Additives for Stabilizing Silicon-Based Lithium-Ion Batteries. *Adv. Energy Mater.* **2023**, *13*, 2203503. [[CrossRef](#)]
109. Ding, T.; Wang, Z.; Dong, J.; Chen, G.; Zhao, S.; Wang, Z.; Fang, S. Maleic Anhydride and (Ethoxy)Pentafluorocyclotriphosphazene as Electrolyte Additives for High-Voltage LiCoO_2/Si -Graphite Lithium-Ion Batteries. *ACS Appl. Mater. Interfaces* **2024**, *16*, 38101–38110. [[CrossRef](#)]
110. Wang, Z.; Zhang, B. Weakly Solvating Electrolytes for Next-Generation Lithium Batteries: Design Principles and Recent Advances. *EMD* **2023**, *1*, 9370003. [[CrossRef](#)]
111. Amanchukwu, C.V.; Yu, Z.; Kong, X.; Qin, J.; Cui, Y.; Bao, Z. A New Class of Ionically Conducting Fluorinated Ether Electrolytes with High Electrochemical Stability. *J. Am. Chem. Soc.* **2020**, *142*, 7393–7403. [[CrossRef](#)]
112. Zou, Y.; Cheng, F.; Lu, Y.; Xu, Y.; Fang, C.; Han, J. High Performance Low-Temperature Lithium Metal Batteries Enabled by Tailored Electrolyte Solvation Structure. *Small* **2023**, *19*, 2203394. [[CrossRef](#)] [[PubMed](#)]
113. Han, G.-B.; Lee, J.-N.; Choi, J.W.; Park, J.-K. Tris(Pentafluorophenyl) Borane as an Electrolyte Additive for High Performance Silicon Thin Film Electrodes in Lithium Ion Batteries. *Electrochim. Acta* **2011**, *56*, 8997–9003. [[CrossRef](#)]
114. An, F.; Zhao, H.; Zhou, W.; Ma, Y.; Li, P. S-Containing and Si-Containing Compounds as Highly Effective Electrolyte Additives for SiO_x -Based Anodes/NCM 811 Cathodes in Lithium Ion Cells. *Sci. Rep.* **2019**, *9*, 14108. [[CrossRef](#)] [[PubMed](#)]

115. Huang, Y.; Li, R.; Weng, S.; Zhang, H.; Zhu, C.; Lu, D.; Sun, C.; Huang, X.; Deng, T.; Fan, L.; et al. Eco-Friendly Electrolytes via a Robust Bond Design for High-Energy Li Metal Batteries. *Energy Environ. Sci.* **2022**, *15*, 4349–4361. [[CrossRef](#)]
116. Tan, T.; Lee, P.-K.; Marium, M.; Zettsu, N.; Yu, D.Y.W. (3-Aminopropyl)Triethoxysilane as an Electrolyte Additive for Enhancing the Thermal Stability of Silicon Anode in Lithium-Ion Batteries. *ACS Appl. Energy Mater.* **2022**, *5*, 11254–11262. [[CrossRef](#)]
117. Wu, J.; Zhou, T.; Zhong, B.; Wang, Q.; Liu, W.; Zhou, H. Designing Anion-Derived Solid Electrolyte Interphase in a Siloxane-Based Electrolyte for Lithium-Metal Batteries. *ACS Appl. Mater. Interfaces* **2022**, *14*, 27873–27881. [[CrossRef](#)]
118. Ryu, Y.-G.; Lee, S.; Mah, S.; Lee, D.J.; Kwon, K.; Hwang, S.; Doo, S. Electrochemical Behaviors of Silicon Electrode in Lithium Salt Solution Containing Alkoxy Silane Additives. *J. Electrochem. Soc.* **2008**, *155*, A583. [[CrossRef](#)]
119. Aupperle, F.; Eshetu, G.G.; Eberman, K.W.; Xia, A.; Bridel, J.-S.; Figgemeier, E. Realizing a High-Performance $\text{LiNi}_{0.6}\text{Mn}_{0.2}\text{Co}_{0.2}\text{O}_2$ /Silicon–Graphite Full Lithium Ion Battery Cell via a Designer Electrolyte Additive. *J. Mater. Chem. A* **2020**, *8*, 19573–19587. [[CrossRef](#)]
120. Wang, E.; Liu, Y.; Dong, J.; Zhang, L.; Liu, J.; Qin, P.; Liu, F. Construction of Stable SEI Film on Si@C High-Loading Electrodes by Dimethoxydimethylsilane Electrolyte Additives. *Ionics* **2022**, *28*, 1625–1634. [[CrossRef](#)]
121. Aupperle, F.; Von Aspern, N.; Berghus, D.; Weber, F.; Eshetu, G.G.; Winter, M.; Figgemeier, E. The Role of Electrolyte Additives on the Interfacial Chemistry and Thermal Reactivity of Si-Anode-Based Li-Ion Battery. *ACS Appl. Energy Mater.* **2019**, *2*, 6513–6527. [[CrossRef](#)]
122. Zhang, C.-Z.; Xie, L.-J.; Tang, Y.; Li, Y.; Jiang, J.-C.; Huang, A.-C. Thermal Safety Evaluation of Silane Polymer Compounds as Electrolyte Additives for Silicon-Based Anode Lithium-Ion Batteries. *Processes* **2022**, *10*, 1581. [[CrossRef](#)]
123. Wang, J.; Zhang, L.; Zhang, H. Effects of Electrolyte Additive on the Electrochemical Performance of Si/C Anode for Lithium-Ion Batteries. *Ionics* **2018**, *24*, 3691–3698. [[CrossRef](#)]
124. Liu, G.; Jiao, T.; Cheng, Y.; Zhou, K.; Zou, Y.; Wang, M.; Yang, Y.; Zheng, J. Interfacial Enhancement of Silicon-Based Anode by a Lactam-Type Electrolyte Additive. *ACS Appl. Energy Mater.* **2021**, *4*, 10323–10332. [[CrossRef](#)]
125. Li, R.; Fu, C.; Cui, B.; Cui, C.; Mu, X.; Gao, Y.; Yin, G.; Zuo, P. Constructing Highly Stable Solid Electrolyte Interphase for Si@Graphene Anodes by Coupling 2-Isocyanatoethyl Methacrylate and Fluoroethylene Carbonate. *J. Power Sources* **2023**, *554*, 232337. [[CrossRef](#)]
126. Azam, S.; Alter, E.; Black, W.; Ingham, H.; Dressler, R.; Aiken, C.P.; Dahn, J.R. Impact of Pyrocarbonate Additives and Salt Chemistries (LiFSI and LiPF₆) on Gassing and Performance in Silicon-Containing Pouch Cells. *J. Electrochem. Soc.* **2025**, *172*, 090529. [[CrossRef](#)]
127. Cheng, J.; Huang, Z.; Lu, A.; He, A.; Shao, Y.; Fan, Y.; Huang, Y. Synergistic Functional Additives on Cycling Performance of Silicon-Carbon Composite Anode in Pouch Cells. *J. Mater.* **2025**, *11*, 100941. [[CrossRef](#)]
128. Wang, J.; Guillot, S.L.; Usrey, M.L.; Hou, T.; Persson, K.A. Elucidating Gas Reduction Effects of Organosilicon Additives in Lithium-Ion Batteries. *J. Am. Chem. Soc.* **2025**, *147*, 8841–8851. [[CrossRef](#)]
129. Guillot, S.L.; Usrey, M.L.; Peña-Hueso, A.; Kerber, B.M.; Zhou, L.; Du, P.; Johnson, T. Reduced Gassing In Lithium-Ion Batteries With Organosilicon Additives. *J. Electrochem. Soc.* **2021**, *168*, 030533. [[CrossRef](#)]
130. Liu, G.; Gao, J.; Xia, M.; Cheng, Y.; Wang, M.; Hong, W.; Yang, Y.; Zheng, J. Strengthening the Interfacial Stability of the Silicon-Based Electrode via an Electrolyte Additive—Allyl Phenyl Sulfone. *ACS Appl. Mater. Interfaces* **2022**, *14*, 38281–38290. [[CrossRef](#)]
131. Liu, X.; Sun, X.; Shi, X.; Song, D.; Zhang, H.; Li, C.; Wang, K.-Y.; Xiao, C.; Liu, X.; Zhang, L. Low-Temperature and High-Performance Si/Graphite Composite Anodes Enabled by Sulfite Additive. *CEJ* **2021**, *421*, 127782. [[CrossRef](#)]
132. Cai, J.; Zhou, X.; Li, T.; Nguyen, H.T.; Veith, G.M.; Qin, Y.; Lu, W.; Trask, S.E.; Fonseca Rodrigues, M.-T.; Liu, Y.; et al. Critical Contribution of Imbalanced Charge Loss to Performance Deterioration of Si-Based Lithium-Ion Cells during Calendar Aging. *ACS Appl. Mater. Interfaces* **2023**, *15*, 48085–48095. [[CrossRef](#)]
133. Zhang, Y.; Wu, B.; Mu, G.; Ma, C.; Mu, D.; Wu, F. Recent Progress and Perspectives on Silicon Anode: Synthesis and Prelithiation for LIBs Energy Storage. *J. Energy Chem.* **2022**, *64*, 615–650. [[CrossRef](#)]
134. Tian, Y.; Li, G.; Xu, D.; Lu, Z.; Yan, M.; Wan, J.; Li, J.; Xu, Q.; Xin, S.; Wen, R.; et al. Micrometer-Sized SiMg_yO_x with Stable Internal Structure Evolution for High-Performance Li-Ion Battery Anodes. *Adv. Mater.* **2022**, *34*, 2200672. [[CrossRef](#)] [[PubMed](#)]
135. Ou, Y.; Chang, Z.; Yang, S.; Shu, Y.; Zhang, J.; Tan, R.; Zhang, Q.; Ai, X.; Huo, K.; Qian, J. Mild Chemical Lithiation Strategy for Achieving Synergistic Lithium-Compensation and Carbon-Coating on SiO Anodes. *Adv. Funct. Mater.* **2025**, *35*, 2423538. [[CrossRef](#)]
136. Quan, L.; Su, Q.; Lei, H.; Zhang, W.; Deng, Y.; He, J.; Lu, Y.; Li, Z.; Liu, H.; Xing, L.; et al. Integrated Prelithiation and SEI Engineering for High-Performance Silicon Anodes in Lithium-Ion Batteries. *Natl. Sci. Rev.* **2025**, *12*, nwaf084. [[CrossRef](#)] [[PubMed](#)]
137. Aktekin, B.; Hernández, G.; Younesi, R.; Brandell, D.; Edström, K. Concentrated LiFSI–Ethylene Carbonate Electrolytes and Their Compatibility with High-Capacity and High-Voltage Electrodes. *ACS Appl. Energy Mater.* **2022**, *5*, 585–595. [[CrossRef](#)]

138. Yamada, Y.; Wang, J.; Ko, S.; Watanabe, E.; Yamada, A. Advances and Issues in Developing Salt-Concentrated Battery Electrolytes. *Nat. Energy* **2019**, *4*, 269–280. [[CrossRef](#)]
139. Chang, Z.; Li, X.; Yun, F.; Shao, Z.; Wu, Z.; Wang, J.; Lu, S. Effect of Dual-Salt Concentrated Electrolytes on the Electrochemical Performance of Silicon Nanoparticles. *ChemElectroChem* **2020**, *7*, 1135–1141. [[CrossRef](#)]
140. Wang, J.; Yamada, Y.; Sodeyama, K.; Chiang, C.H.; Tateyama, Y.; Yamada, A. Superconcentrated Electrolytes for a High-Voltage Lithium-Ion Battery. *Nat. Commun.* **2016**, *7*, 12032. [[CrossRef](#)]
141. Bergstrom, H.K.; McCloskey, B.D. Ion Transport in (Localized) High Concentration Electrolytes for Li-Based Batteries. *ACS Energy Lett.* **2024**, *9*, 373–380. [[CrossRef](#)] [[PubMed](#)]
142. Hai, F.; Ban, Y.; Huang, Z.; Xue, W.; Yang, Y.; Yan, W.; Hua, W.; Li, M.; Tang, W.; Zhang, S. A Review on Localized High Concentration Electrolytes for Advanced Li Metal Batteries. *ESM* **2025**, *81*, 104534. [[CrossRef](#)]
143. Chang, Z.; Wang, J.; Wu, Z.; Gao, M.; Wu, S.; Lu, S. The Electrochemical Performance of Silicon Nanoparticles in Concentrated Electrolyte. *ChemSusChem* **2018**, *11*, 1787–1796. [[CrossRef](#)] [[PubMed](#)]
144. Zhang, X.; Cui, Z.; Jo, E.; Manthiram, A. Inhibition of Transition-Metal Dissolution with Advanced Electrolytes in Batteries with Silicon-Graphite Anodes and High-Nickel Cathodes. *ESM* **2023**, *56*, 562–571. [[CrossRef](#)]
145. Zeng, G.; An, Y.; Xiong, S.; Feng, J. Nonflammable Fluorinated Carbonate Electrolyte with High Salt-to-Solvent Ratios Enables Stable Silicon-Based Anode for Next-Generation Lithium-Ion Batteries. *ACS Appl. Mater. Interfaces* **2019**, *11*, 23229–23235. [[CrossRef](#)]
146. Jia, H.; Gao, P.; Zou, L.; Han, K.S.; Engelhard, M.H.; He, Y.; Zhang, X.; Zhao, W.; Yi, R.; Wang, H.; et al. Controlling Ion Coordination Structure and Diffusion Kinetics for Optimized Electrode-Electrolyte Interphases and High-Performance Si Anodes. *Chem. Mater.* **2020**, *32*, 8956–8964. [[CrossRef](#)]
147. Gao, W.; Peng, Y.; Lu, Y.; Liu, X.; Xu, Y.; Yang, K.; Wu, Y.; He, J. Localized High-Concentration Electrolytes for Rechargeable Batteries. *Energy Storage Mater.* **2025**, *80*, 104378. [[CrossRef](#)]
148. He, S.; Huang, S.; Zhao, Y.; Qin, H.; Shan, Y.; Hou, X. Design of a Dual-Electrolyte Battery System Based on a High-Energy NCM811-Si/C Full Battery Electrode-Compatible Electrolyte. *ACS Appl. Mater. Interfaces* **2021**, *13*, 54069–54078. [[CrossRef](#)]
149. Wang, S.; Shi, J.; Liu, Z.; Xia, Y. Advanced Ether-Based Electrolytes for Lithium-ion Batteries. *Adv. Energy Mater.* **2024**, *14*, 2401526. [[CrossRef](#)]
150. Li, X.; Luo, F.; Zhou, N.; Adenusi, H.; Fang, S.; Wu, F.; Passerini, S. Weakly Solvating Electrolytes for Lithium and Post-Lithium Rechargeable Batteries: Progress and Outlook. *Adv. Energy Mater.* **2025**, *15*, 2501272. [[CrossRef](#)]
151. Xiao, P.; Yun, X.; Chen, Y.; Guo, X.; Gao, P.; Zhou, G.; Zheng, C. Insights into the Solvation Chemistry in Liquid Electrolytes for Lithium-Based Rechargeable Batteries. *Chem. Soc. Rev.* **2023**, *52*, 5255–5316. [[CrossRef](#)] [[PubMed](#)]
152. Song, G.; Yi, Z.; Su, F.; Xie, L.; Wang, Z.; Wei, X.-X.; Xu, G.; Chen, C.-M. Boosting the Low-Temperature Performance for Li-Ion Batteries in LiPF₆-Based Local High-Concentration Electrolyte. *ACS Energy Lett.* **2023**, *8*, 1336–1343. [[CrossRef](#)]
153. Wang, Z.; Wang, Y.; Li, B.; Bouwer, J.C.; Davey, K.; Lu, J.; Guo, Z. Non-Flammable Ester Electrolyte with Boosted Stability Against Li for High-Performance Li Metal Batteries. *Angew. Chem. Int. Ed.* **2022**, *61*, e202206682. [[CrossRef](#)] [[PubMed](#)]
154. Bai, M.; Tang, X.; Zhang, M.; Wang, H.; Wang, Z.; Shao, A.; Ma, Y. An In-Situ Polymerization Strategy for Gel Polymer Electrolyte Si || Ni-Rich Lithium-Ion Batteries. *Nat. Commun.* **2024**, *15*, 5375. [[CrossRef](#)]
155. Jiang, Z.; Mo, J.; Li, C.; Li, H.; Zhang, Q.; Zeng, Z.; Xie, J.; Li, Y. Anion-Regulated Weakly Solvating Electrolytes for High-Voltage Lithium Metal Batteries. *Energy Environ. Mater.* **2023**, *6*, e12440. [[CrossRef](#)]
156. Kang, D.W.; Moon, J.; Choi, H.-Y.; Shin, H.-C.; Kim, B.G. Stable Cycling and Uniform Lithium Deposition in Anode-Free Lithium-Metal Batteries Enabled by a High-Concentration Dual-Salt Electrolyte with High LiNO₃ Content. *J. Power Sources* **2021**, *490*, 229504. [[CrossRef](#)]
157. Ma, X.; Zhang, D.; Wen, J.; Fan, L.; Rao, A.M.; Lu, B. Sustainable Electrolytes: Design Principles and Recent Advances. *Chem. Eur. J.* **2024**, *30*, e202400332. [[CrossRef](#)]
158. Gong, S.; Zhang, Y.; Mu, Z.; Pu, Z.; Wang, H.; Han, X.; Yu, Z.; Chen, M.; Zheng, T.; Wang, Z.; et al. A Predictive Machine Learning Force-Field Framework for Liquid Electrolyte Development. *Nat. Mach. Intell.* **2025**, *7*, 543–552. [[CrossRef](#)]
159. Gao, X.; Yang, A.; Yu, W.; Zhou, J.; Pei, M.; Chen, J.; Yan, W.; Luo, G.; Liu, Y.; Xiao, J.; et al. Generative Artificial Intelligence Navigated Development of Solvents for Next Generation High-Performance Magnesium Batteries. *Adv. Mater.* **2025**, e10083. [[CrossRef](#)]